PION-NUCLEON SCATTERING AND DEUTERON PHOTODISINTEGRATION AT INTERMEDIATE ENERGIES

David Bofinger

A thesis submitted for the degree of Doctor of Philosophy of The Australian National University

25 July 1994

Except where reference is made to the work of others, the research described in this thesis is the product of my collaboration with Dr. W. S. Woolcock and Professor W. Jaus.

Chapter 1 contains introductory material from the literature which is generally known, except for section 1.1 which describes a philosophy of effective lagrangian models evolved jointly with Dr. Woolcock and Professor Jaus. The model of pion-nucleon scattering described in Chapter 2 is due to Dr. Woolcock and me: numerous debts to earlier models of this type and workers in related fields have been referenced. Many of the results in section 2.2 can easily be and have earlier been obtained from basic principles, and these have not been referenced. The fit to experiment described in Chapter 3 was performed by me with the advice of Dr. Woolcock. This includes the discussion in section 3.1 and the writing of the necessary computer programs. The conclusions in that chapter were drawn jointly by Dr. Woolcock and me.

Chapter 4 contains introductory material. Section 4.1 is a description of the work of others which I compiled. Section 4.2 describes a formalism evolved by Dr. Woolcock and Professor Jaus. Section 4.3 is mostly well-known material common to models of deuteron photodisintegration. The model of deuteron photodisintegration described in Chapter 5 is an evolutionary modification of one due to Dr. Woolcock and Professor Jaus. The numerical implementation similarly required a program by Professor Jaus to be modified, which I performed. The fitting procedure described in section 6.1 was evolved jointly with Dr. Woolcock, but I conducted the fits themselves. The remainder of Chapter 6 is the joint responsibility of Dr. Woolcock, Professor Jaus and myself.

I would like to extend my heartfelt thanks to my supervisor Bill Woolcock. I am also grateful for the advice and encouragement of my advisers, Brian Robson and Ray Spear. My final thanks go to those who gave the earliest assistance – my parents.

It is the mark of an educated mind to rest satisfied with the degree of precision which the nature of the subject admits, and not to seek exactness when only an approximation is possible.

– Aristotle (384 – 323 B.C.)

Abstract

This thesis falls naturally into two parts, in each of which we consider a few-nucleon reaction at intermediate energies. Pion-nucleon scattering is discussed in the first three chapters, and deuteron photodisintegration in the last three. The first chapter of each part contains material concerning the interaction generally. In the second chapter we describe our model of the process. In the last chapter of each part the predictions of this model are compared with the experimental results available in the literature.

An effective lagrangian model is found to be quite successful at describing pion-nucleon scattering, although it was not possible to determine all the tunable parameters of our model. This difficulty was exacerbated by ambiguities in the method by which unitarity was imposed on the partial wave amplitudes. The large values of K_ρ implied by the vector meson dominance model of $\rho(770)$ exchange could not be reproduced. A suggestion by Williams [1] for the spin-$\frac{3}{2}$ propagator was found to be unsuitable for describing $\Delta(1232)$ exchange in pion-nucleon scattering, as compared with the unitary propagator, however the propagator can be salvaged to some extent if an *ad hoc* modification is made to the invariant amplitudes obtained from it.

For energies below about 75 MeV we are able to fit the experimental data on deuteron photodisintegration quite well, provided we perform our calculations using one of the coordinate space forms of the Bonn potential [2]. We are unable to fit the forward and total cross-sections in this energy range using the parameterised Paris [3] or Moscow [4] potentials, or without using the 1πE mismatch correction arising from the modified current conservation method we discuss in section 5.1. At higher energies the global fit obtained using the Bonn potential is rather good, and much better than previous attempts. The data again underdetermine the model's tunable parameter set.

Contents

PART I: PION-NUCLEON SCATTERING

PART II: DEUTERON PHOTODISINTEGRATION

List of Figures

List of Tables

Chapter 1

Introduction

This first part of the thesis concerns the theory and results of an effective lagrangian model of low energy pion-nucleon scattering, which was published in Bofinger and Woolcock [5]. Chapter 2 describes the theoretical basis for the model, and compares it with several of the better known models of this kind in the literature. Chapter 3 describes the procedure and results of our attempt to fit the predictions of the model to phase shift analyses of experimental data, and some conclusions which can be drawn from them.

In section 1.1, we discuss what we hope to achieve with our model, and the philosophy behind some of its features. The remaining sections of this chapter concern the formalism of pion-nucleon scattering, and general theoretical concepts such as isospin and the partial wave expansion which apply to any model of the process.

1.1 Motivation

Although it has long been well-established that hadrons possess a quark and gluon substructure, such structure tends to manifest itself explicitly only at very high energies. At present, little can be done to use this substructure to predict the behaviour of hadrons at low and intermediate energies.

In an effective lagrangian model of pion-nucleon scattering hadrons are treated as fundamental, usually pointlike objects with known quantum numbers. This is a low energy expansion, in the same way that a free quark model is a high energy expansion. We truncate the expansion by considering all the hadrons with quantum numbers of interest to our reaction and with masses up to some reasonable limit, and by limiting ourselves to tree diagrams.

A disadvantage of such an approach is that one tends to inherit a large number of tunable parameters in the form of particle masses and coupling constants. Some of these (most obviously, the nucleon mass) can be fixed by appealing to the results of other experiments. Others, however, must be fixed by comparing the model predictions with experimental results, or nearly experimental results such as phase shift analyses. If the model is to have any predictive value it is essential that the number of such parameters be kept to a minimum. If these parameters can be well determined then they can eventually serve as data for comparison with the results of calculations using QCD, and for fixing parameters in effective lagrangian models of other processes, such as deuteron photodisintegration.

Our model is similar to that of Olsson and Osypowski [6], and our principal motive in evolving our model was to correct several perceived deficiencies in theirs. The most obvious weaknesses in the Olsson and Osypowski model are the parameterised diffractive and σ contributions to the isospin-even invariant amplitudes. We discuss in subsection 2.5.2 why we do not regard the diffractive contribution as necessary.

The σ contribution is a consequence of the strong attraction between two pions in a scalar isoscalar state. It cannot be ignored, but neither we nor Olsson and Osypowski have attempted to model it in a manner that could be given a field theoretical justification. We have replaced Olsson and Osypowski's functional form with one which adheres more closely to the form such a near-resonance would produce.

The most important motivation for this model was the suggestion by Williams [1] of an alternative spin-$\frac{3}{2}$ propagator. Preliminary calculations by Jaus and Woolcock [7] had suggested that in the absence of the diffractive contribution the alternative propagator gave much better results at threshold than did the unitary propagator. As we shall show in subsection 2.2.3, however, the alternative propagator contains a serious flaw which requires an *ad hoc* correction.

In addition, we attempt to test the theory of vector meson dominance. Unfortunately, doing so requires the introduction of new parameters in the vector-isovector t-channel exchanges, whereas in Olsson and Osypowski's model vector meson dominance is used to determine them.

One might hope for a such a model of pion-nucleon scattering to remain a good quantitative description for laboratory pion energies up to 250 MeV.

1.2 Kinematics

We consider the reaction

$$\mathrm{N}(p') + \pi(q') \rightarrow \mathrm{N}(p'') + \pi(q''), \tag{1.1}$$

where p', p'', q', q'' are 4-momenta. The sixteen components of p', p'', q', q'' are not, of course, all independent. Energy and momentum conservation $p' + q' = p'' + q''$ removes four degrees of freedom, and requiring the incoming and outgoing particles to be on the mass shell $p'^2 = p''^2 = m^2$, $q'^2 = q''^2 = m_\pi^2$ removes another four. Invariance under "boost" (rotationless Lorentz) transformations removes another three degrees of freedom. We can see this from the centre-of-mass reference frame, in which $p' + q' = p'' + q'' = (W, \mathbf{0})$, where W is the centre of mass energy of the system. We can remove two degrees of freedom from the incoming particles by fixing an axis at the (centre of mass) direction in which the pion enters the reaction, and one degree of freedom from the outgoing particles by fixing another axis normal to the scattering plane. The scattering event is thus completely described by two kinematic quantities, for instance the centre of mass energy of the system and the angle between the incoming and outgoing pions in that frame.

It is convenient and conventional to describe scattering events in terms of the Mandelstam invariants

$$\begin{aligned} s &= (p' + q')^2 = (p'' + q'')^2 \\ t &= (p' - p'')^2 = (q'' - q')^2 \\ u &= (p' - q'')^2 = (p'' - q')^2. \end{aligned} \tag{1.2}$$

It is not hard to show that

$$\begin{aligned} s + t + u &= q'^2 + q''^2 + p'^2 + p''^2 \\ &= 2(m^2 + m_\pi^2), \end{aligned} \tag{1.3}$$

so there are only two independent invariants. At the πN threshold $s = (m + m_\pi)^2$, $u = (m - m_\pi)^2$ and $t = 0$.

We will find it useful to relate the Mandelstam invariant s to the magnitude q

of the centre of mass momentum of any particle by

$$q^2 = \frac{(s-(m+m_\pi)^2)(s-(m-m_\pi)^2)}{4s} \tag{1.4}$$

and to the laboratory frame pion kinetic energy by

$$T_\pi^{\text{lab}} = \frac{(s-(m+m_\pi)^2)}{2m}. \tag{1.5}$$

The other Mandelstam invariants can be related to the centre-of-mass angle θ between the momenta of the incoming and outgoing nucleons using (1.3) and

$$t = -2q^2(1-\cos\theta). \tag{1.6}$$

1.3 Partial Wave Decomposition

Derivations for the formulae in this section can be found in Pilkuhn [8]. Throughout this section we omit isospin indices.

The fundamental description of pion-nucleon scattering is via the S-operator, which takes an incoming state $|\text{in}\rangle$ to an outgoing state $|\text{out}\rangle = S\,|\text{in}\rangle$. Since the trivial case $|\text{out}\rangle = |\text{in}\rangle$ corresponds to $S = \mathbb{1}$, the identity operator, it is usual to separate the S-matrix into scattering and non-scattering components by defining the T-matrix through

$$\langle f|\,S\,|i\rangle = \langle f|i\rangle + i(2\pi)^4\delta^{(4)}(p'+q'-p''-q'')\frac{m}{2\sqrt{m^2+q^2}\sqrt{m_\pi^2+q^2}}\overline{u}(\boldsymbol{p}'')Tu(\boldsymbol{p}'), \tag{1.7}$$

where $|f\rangle, |i\rangle$ are the final and initial states. The kinematic factor after the δ-function makes the factor $\overline{u}Tu$ Lorentz invariant by compensating for our normalisation

$$\overline{u}(\boldsymbol{p}'')u(\boldsymbol{p}') = \frac{2\sqrt{m^2+q^2}}{m}\delta^{(3)}(\boldsymbol{p}''-\boldsymbol{p}'). \tag{1.8}$$

The T-matrix is a 4 by 4 matrix function of state momenta. For plane wave states, Lorentz invariance and the Dirac equation allow us to reduce this to an expression containing just two scalar functions of any two of the Mandelstam variables s,t,u. It is usual to write

$$T = -A(s,t,u) - B(s,t,u)\gamma\cdot Q, \tag{1.9}$$

where $Q = \frac{1}{2}(q'+q'')$ and it is understood that only two of s,t,u are independent. The functions A,B are known as invariant amplitudes and are free of kinematic singularities (see Bransden and Moorhouse [9]).

The two invariant amplitudes A and B can be related to the spin flip and non-flip amplitudes f and g by

$$f_1(s,t,u) = \frac{E+m}{8\pi W}\left[+A(s,t,u) + (W-m)B(s,t,u)\right]$$
$$f_2(s,t,u) = \frac{E-m}{8\pi W}\left[-A(s,t,u) + (W+m)B(s,t,u)\right] \tag{1.10}$$

and

$$f(s,\theta) = f_1(s,t,u) + f_2(s,t,u)\cos\theta$$
$$g(s,\theta) = -f_2(s,t,u)\sin\theta, \tag{1.11}$$

where $W = \sqrt{s}$, $E = \sqrt{m^2+q^2}$, and θ is the angle between the incoming and outgoing nucleons in the centre-of-mass frame (see section 1.2).

Finally we expand f_1 and f_2 in terms of states $\mathrm{L}_{(2I)(2l\pm1)}$ of definite isospin I, orbital angular momentum l and total angular momentum $l \pm \frac{1}{2}$. Here L stands for S ($l=0$), P ($l=1$), D ($l=2$), and so on. We will later truncate the expansion at $l=1$ for purposes of calculation. This gives us six partial waves S_{11}, S_{31}, P_{11}, P_{31}, P_{13} and P_{33}, with corresponding amplitudes $f_{l\pm}^{(I)}(s)$. Then using $x = \cos\theta$, $t = -2q^2(1-\cos\theta)$ we can rewrite f_1, f_2 as functions of s, x to obtain

$$f_{l\pm}(s) = \frac{1}{2}\int_{-1}^{1} dx\,\left[P_l(x)f_1(s,x) + P_{l\pm1}(x)f_2(s,x)\right]. \tag{1.12}$$

The unitarity condition must be satisfied separately by each partial wave

$$\mathrm{Im}\, f_{l\pm}(s) = q|f_{l\pm}(s)|^2, \tag{1.13}$$

which leads to

$$f_{l\pm}(s) = \frac{1}{q}e^{i\delta_{l\pm}(s)}\sin\delta_{l\pm}(s) \tag{1.14}$$

where $\delta_{l\pm}$ is real. the quantities $\delta_{l\pm}$ are known as the phase shifts. Our model will be tested against phase shifts calculated from experimental results.

1.4 Isospin and Crossing Symmetry

In pion-nucleon scattering the initial and final states contain one pion with isospin 1 and one nucleon with isospin $\frac{1}{2}$. Thus, any initial or final state can be expressed as a superposition of states with total isospin $\frac{1}{2}$ and states with total isospin $\frac{3}{2}$. We denote amplitudes of definite total isospin with the superscripts $^{(\frac{1}{2})}$ and $^{(\frac{3}{2})}$.

In our model we implicitly assume invariance under rotations in isospin-space, *i.e.* that the transition matrix $\langle I'', I_3''| S |I', I_3'\rangle$, where I', I'' are the initial and final total isospins and I_3', I_3'' are their components along some axis, is diagonal and that the matrix elements are independent of I_3' and I_3''. The most important effect neglected here is the mass difference between protons and neutrons, and between charged and neutral pions.

It is often convenient to work with the isospin-even (under the exchange of particle labels) and isospin-odd amplitudes, which we will denote with the superscripts $^{(+)}$ and $^{(-)}$. These are defined by

$$T_{ba} = T^{(+)}\tfrac{1}{2}\{\tau_b, \tau_a\} + T^{(-)}\tfrac{1}{2}[\tau_b, \tau_a] = T^{(+)}\delta_{ba} - T^{(-)}i\varepsilon_{abc}\tau_c, \tag{1.15}$$

where T stands for any amplitude, $\boldsymbol{\tau}$ is a vector whose components are the Pauli matrices and the indices a, b refer to incoming and outgoing pions respectively. They can be related to the amplitudes for definite isospin states by

$$\begin{aligned} T^{(+)} &= \tfrac{1}{3}T^{(\frac{1}{2})} + \tfrac{2}{3}T^{(\frac{3}{2})} \\ T^{(-)} &= \tfrac{1}{3}T^{(\frac{1}{2})} - \tfrac{1}{3}T^{(\frac{3}{2})}. \end{aligned} \tag{1.16}$$

Hamilton and Woolcock [10] have pointed out that assuming charge independence is not strictly necessary, since we can take appropriate linear combinations of the amplitudes for the reactions used most commonly in experiments, *i.e.* $\pi^+ + p \to \pi^+ + p$ and $\pi^- + p \to \pi^- + p$, as our definition of $T^{(\pm)}$.

Inspection of figure 1 shows that the contributions of the diagrams in figure 1 (a), (c) and (e) are balanced by the analogous contributions 1 (b), (d) and (f). From this we can show that our model satisfies crossing symmetry. The crossing symmetry condition for pion-nucleon scattering is (see Bransden and Moorhouse [9])

$$\begin{aligned} A^{(\pm)}(s,t,u) &= \pm A^{(\pm)*}(u,t,s) \\ B^{(\pm)}(s,t,u) &= \mp B^{(\pm)*}(u,t,s), \end{aligned} \tag{1.17}$$

but since in our model all the invariant amplitudes are real until the unitarisation procedure is performed, we can ignore the complex conjugate symbols when dealing with invariant amplitudes at the tree level.

A useful feature of crossing symmetry is that the contribution from any one of the crossed diagrams figure 1 (b), (d) or (f) can easily be obtained from its direct equivalent figure 1 (a), (c) or (e) by the substitutions

$$\begin{aligned} A^{(c)}(s,t,u) &= A^{(d)}(u,t,s) \\ B^{(c)}(s,t,u) &= -B^{(d)}(u,t,s). \end{aligned} \tag{1.18}$$

Chapter 2

Description of the Model

To develop our model of pion-nucleon scattering, some of the Feynman diagrams known to contribute to the invariant amplitudes are evaluated. All these are tree diagrams involving known resonances, except for a parameterised contribution needed to describe the strong attraction between pions in a scalar isoscalar state. All these diagrams are shown in figure 1 and discussed in section 2.2. The most difficult question is the proper handling of the spin-$\frac{3}{2}$ propagator, which is discussed in section 2.1.

The amplitudes are then projected into the first six partial waves S_{11}, S_{31}, P_{11}, P_{31}, P_{13} and P_{33} as described in section 1.3. Some of these contributions involve free parameters, such as coupling constants, that cannot be determined from other experiments.

Since all the diagrams evaluated are tree diagrams the resultant partial wave amplitudes are real. The unitarity condition is therefore not satisfied. Instead, unitarity is imposed on the amplitudes by means of one of several ansätze. This procedure is discussed in section 2.4.

In section 2.5 we consider differences between our model and other models of pion-nucleon scattering. In section 2.3 we discuss certain dispersion theory related constraints. We will later impose these constraints for some of our fits.

The resultant phase shifts from the model can be compared with those from analyses in the literature, provided the free parameters in the model are fixed. We use a mechanical optimisation procedure from the Numerical Algorithms Group [11] to minimise a measure of poorness of fit by varying the free parameters. The results of this are discussed in chapter 3.

2.1 Spin-$\frac{3}{2}$ Propagators

When quantum field theory is used to derive the correct propagator for a spin-$\frac{3}{2}$ particle, it becomes necessary to choose a gauge. This introduces an ambiguity, since not all choices of gauge give the same result for the propagator, and the propagators derived do not lead to the same results at tree level.

All the gauges we discuss are special cases of the renormalisable gauge R_ξ, which contains the arbitrary parameter ξ. Each choice of gauge leads to a propagator with a specific disadvantage when used to evaluate tree diagrams. The most important special cases of the renormalisable gauge are $\xi = 0$ (the Landau gauge), 1 (the t'Hooft-Feynman gauge) and ∞ (the unitary gauge).

The unitary propagator, which is usually chosen, is obtained using the unitary gauge. The alternative propagator is derived in a quite different manner, but it has the same advantages (good behaviour at high energy) and disadvantages (a singularity when the spin-$\frac{3}{2}$ particle is on the light-cone) as we would expect from a propagator derived using the Landau gauge.

Both Moussallam and Soni [12] and Nieuwenhuizen [13] choose the unitary gauge (for different applications) without stating their reasons. The principal disadvantage of the unitary gauge is bad behaviour at high energies. The principal disadvantage of non-unitary renormalisable gauges is the pole at $k^2 = \xi M_\Delta^2$, which has the same effect as a spurious resonance of mass $\sqrt{\xi} M_\Delta$ (see Guidry [14]). Effectively, the unitary gauge has its spurious resonance at infinite energy. Since our model is only intended to be accurate at low and intermediate energies in any case, the unitary gauge is the natural one to use.

We do not consider the t'Hooft-Feynman gauge. Its most obvious drawback is that the pole at $k^2 = M_\Delta^2$ is now of order two, so that the phase shift near this energy will not behave like a resonant phase shift. Since this is a region of great interest in pion-nucleon scattering, it is clearly inappropriate to use this gauge.

2.1.1 The Unitary Propagator

By setting $\xi = \infty$ (*i.e.* the unitary gauge) in the most general possible form of the propagator for a massive spin-$\frac{3}{2}$ particle in the renormalisable gauge we obtain what we shall for convenience call the unitary propagator, namely

$$\Pi^{\mu\nu}(k) = i(k^2 - M_\Delta^2 + i\varepsilon)^{-1}(\gamma \cdot k + M_\Delta)$$

$$\times \left(-g^{\mu\nu} + \frac{1}{3}\gamma^\mu\gamma^\nu + \frac{1}{3M_\Delta}(\gamma^\mu k^\nu - k^\mu\gamma^\nu) + \frac{2}{3M_\Delta^2}k^\mu k^\nu \right.$$
$$+\frac{1}{6M_\Delta^2}\left[\frac{2(A^*+1)}{2A^*+1}\gamma^\mu k^\nu + \frac{2(A+1)}{2A+1}k^\mu\gamma^\nu \right.$$
$$\left.\left. -\left|\frac{A+1}{2A+1}\right|^2 \gamma^\mu\gamma\cdot k\gamma^\nu - \frac{(2AA^*+A+A^*)M_\Delta\gamma^\mu\gamma^\nu}{|2A+1|^2}\right]\right) \qquad (2.1)$$

where the parameter A is arbitrary except that $A \neq -\frac{1}{2}$.

This propagator was originally obtained by Fronsdal [15] and by Aurilia and Umezawa [16] using a somewhat different method. They constructed the most general possible lagrangian containing only first derivatives of the spin-$\frac{3}{2}$ field. The number of arbitrary parameters in the propagator and vertices can be reduced to one by the application of very general principles, and it can be shown that physical quantities do not depend on this parameter A.

The conventional choice is $A = -1$, which greatly simplifies the expression. We show the propagator in the symmetric form suggested by Nieuwenhuizen [13],

$$\Pi^S_{\mu\nu}(k) = -i(k^2 - M_\Delta^2 + i\varepsilon)^{-1}$$
$$\times \left[\left(g^{\mu\nu} - \frac{k^\mu k^\nu}{M_\Delta^2}\right)(\gamma\cdot k + M_\Delta)\right.$$
$$\left. +\frac{1}{3}\left(\gamma^\mu + \frac{k^\mu}{M_\Delta}\right)(\gamma\cdot k - M_\Delta)\left(\gamma^\nu + \frac{k^\nu}{M_\Delta}\right)\right]. \qquad (2.2)$$

An alternative form for this propagator is

$$\Pi^S_{\mu\nu}(k) = i(k^2 - M_\Delta^2 + i\varepsilon)^{-1}(\gamma\cdot k + M_\Delta)$$
$$\times \left[-g_{\mu\nu} + \frac{1}{3}\gamma_\mu\gamma_\nu + \frac{1}{3M_\Delta}(\gamma_\mu k_\nu - k_\mu\gamma_\nu) + \frac{2}{3M_\Delta^2}k_\mu k_\nu\right], \qquad (2.3)$$

and this is the form most commonly seen.

2.1.2 The Alternative Propagator

The propagator suggested by Williams [1] was originally derived by Behrends and Fronsdal [17]. We start with the rest frame spin-$\frac{3}{2}$ projection operator

$$\Theta_\mu{}^\nu = g_\mu{}^\nu - \frac{1}{3}\gamma_\mu\gamma^\nu \qquad (2.4)$$

and generalise to an arbitrary frame by using the covariant ansatz

$$g_\mu{}^\nu \to g_\mu^\nu - k_\mu k^\nu/k^2$$
$$\gamma_\mu \to (g_\mu^\sigma - k_\mu k^\sigma/k^2)\gamma_\sigma. \qquad (2.5)$$

From this we obtain the spin-$\frac{3}{2}$ propagator

$$\Pi^W_{\mu\nu}(k) = i(k^2 - M_\Delta^2 + i\varepsilon)^{-1}(\gamma\cdot k + M_\Delta) \times \left(-g_{\mu\nu} + \frac{1}{3}\gamma_\mu\gamma_\nu + \frac{1}{3k^2}(\gamma_\mu\gamma\cdot k k_\nu + k_\mu\gamma\cdot k\gamma_\nu)\right). \quad (2.6)$$

This propagator behaves qualitatively differently from the unitary propagator in a number of ways. Firstly, the propagator is pure spin-$\frac{3}{2}$; all spin-$\frac{1}{2}$ components of the wave function are annihilated by it. As a consequence of this the propagator (as remarked by Benmerrouche *et al* [18]) is not invertible. The propagator also annihilates the z-dependent off mass-shell part of the πNΔ vertex. From a practical point of view this also means that the expressions (*e.g.* for invariant amplitudes) obtained using this propagator are simpler than those obtained using the unitary propagator.

The most serious problem with this propagator is the existence of the $1/k^2$ singularity. This is equivalent to adding a spurious massless spin-$\frac{3}{2}$ state to the πN spectrum. Although $m = 0$ lies well outside the possible range of centre of mass energy of the system, the exchange of the massless particle in the u-channel has a catastrophic practical effect. An *ad hoc* solution to this problem is discussed in subsection 2.2.3.

2.2 Exchanges

The basis of an effective lagrangian model of pion-nucleon scattering is the tree diagrams of figure 1 (a) through (g). We treat the hadrons as though they were fundamental, and assume isospin invariance. This allows us to use the vertex functions and propagators for fundamental particles of those quantum numbers.

The greatest sources of uncertainty in this part of the the model are associated with the correct forms for the propagator for a spin-$\frac{3}{2}$ particle and the coupling at the ρNN vertex, and with the empirical need for the additional scalar isoscalar t-channel exchange shown in figure 1 (h).

2.2.1 Nucleon Exchange

The tree level diagrams for nucleon exchange are shown in Figure 1 (a) and (b) respectively. To evaluate these diagrams we need the spin-$\frac{1}{2}$ propagator

$$P(k) = i(k^2 - m^2 + i\varepsilon)^{-1}(\gamma \cdot k + m), \tag{2.7}$$

where k is the momentum of the internal nucleon line and ε is small and positive. We also require the pseudovector πNN vertex

$$V(PV) = \frac{f_{\pi NN}}{m_\pi}\gamma \cdot q\gamma_5\tau_a, \tag{2.8}$$

for the process $N(p) + \pi^a(q) \rightarrow N(p+q)$, where a is the isospin index.

Intuitively one might expect pseudoscalar coupling

$$V(PS) = g_{\pi NN}\gamma_5\tau_a, \tag{2.9}$$

to be preferred over pseudovector coupling on grounds of simplicity. Also, pseudoscalar coupling has been preferred in the past because it leads to a renormalisable field theory. Because the lagrangian associated with pseudovector coupling, unlike that associated with pseudoscalar coupling, exhibits chiral symmetry, pseudovector coupling is today preferred. Also, the predictions made by $SU(3)$ and Cabibbo theory for pseudovector coupling constants f accord much better with experiment than those that assume pseudoscalar coupling (see Pilkuhn [8]). Finally, pseudovector coupling has been found (see Jaus and Woolcock [19]) to give better results than pseudoscalar coupling when used for the πNN vertex in deuteron photodisintegration. Pseudovector and pseudoscalar coupling are equivalent if the diagrammatic expansion is not truncated, and hence are equally valid in principle (see Cooper *et al* [20]).

The two parameters in these functions (the nucleon mass m and the coupling constant $f_{\pi NN}$) are very well determined from experiments other than those we are attempting to fit, so there is no need to treat them as tunable parameters in our model. We use the physical nucleon mass $m = 939$MeV and $f^2_{\pi NN}/4\pi = 0.079$ from Dumbrajs *et al* [21].

It is then easy to calculate the nucleon tree-level contributions to the invariant amplitudes. The result, as given by Olsson and Osypowski [6], is

$$A_N^{(+)}(s,u) = \frac{f^2_{\pi NN}}{m_\pi^2}4m \tag{2.10}$$

$$A_N^{(-)}(s,u) = 0 \tag{2.11}$$

$$B_N^{(+)}(s,u) = \frac{f_{\pi NN}^2}{m_\pi^2} \frac{4m^2(s-u)}{(u-m^2)(s-m^2)} \tag{2.12}$$

$$B_N^{(-)}(s,u) = \frac{f_{\pi NN}^2}{m_\pi^2} \frac{2(su + m^2 s + m^2 u - 3m^4)}{(u-m^2)(s-m^2)}. \tag{2.13}$$

2.2.2 N(1470) Exchange

Although the energy range of our fit is well below the N(1470) resonance, the contribution to the P_{11} wave due to diagram 1 (e) becomes noticeable around 250 MeV. Since the N(1470) resonance has quantum numbers identical to those for a nucleon, it is trivial to include diagrams 1 (e) and (f) in our calculation and we do so for completeness as much as accuracy. The calculation is a trivial generalisation of subsection 2.2.1 and we obtain

$$\begin{aligned} A_{N^*}^{(d)}(s) &= \frac{f_{\pi NN^*}^2}{m_\pi^2} \frac{(m + M_{N^*})(s-m^2)}{s - M_{N^*}^2} \\ B_{N^*}^{(d)}(s) &= \frac{f_{\pi NN^*}^2}{m_\pi^2} \frac{(s + 2mM_{N^*} + m^2)}{s - M_{N^*}^2}. \end{aligned} \tag{2.14}$$

This leads to two new parameters, M_{N^*} and $f_{\pi NN^*}$. Since the N(1470) resonance corresponds to a laboratory pion energy of approximately 500 MeV, it is obviously impractical to attempt to measure the mass of the N(1470) using experiments up to a maximum laboratory frame pion energy of 250 MeV, which is effectively what we would be doing if we were to permit M_{N^*} to vary freely. We fix its mass at 1450 MeV. Such experiments can, however, provide some information about the value of $f_{\pi NN^*}$ as long as M_{N^*} is fixed, so we shall allow $f_{\pi NN^*}$ to vary as a free parameter. We would expect $f_{\pi NN^*}^2/4\pi \approx 0.015$, the value given by Ericson and Weise [22].

2.2.3 $\Delta(1232)$ Exchange

The tree level diagrams for $\Delta(1232)$ exchange are shown in figure 1 (c) and (d). The most general form for the vertex $N(p) + \pi(q) \to \Delta_\mu(p+q)$, neglecting isospin,

is

$$V_\mu(\pi \mathrm{N}\Delta) = \frac{f_{\pi \mathrm{N}\Delta}}{m_\pi}(q_\mu + z\gamma_\mu \gamma \cdot q), \tag{2.15}$$

where z is an arbitrary constant. The term containing z describes only the off mass-shell behaviour. Unlike the nucleon case we do not feel it is possible to decide which combination of couplings is preferred.

The debate over spin-$\frac{3}{2}$ propagators is described in section 2.1. For the unitary propagator (2.2) or the alternative propagator (2.6) it is possible to obtain the tree-level contributions to the invariant amplitudes. The two propagators are identical on mass-shell, and hence give very similar results near the $\Delta(1232)$ resonance. The invariant amplitudes for the unitary propagator are

$$\begin{aligned}
A_\Delta^{(d)}(s,t) = \frac{1}{6M_\Delta^2}\frac{f_{\pi \mathrm{N}\Delta}^2}{m_\pi^2}\Bigg\{ & \frac{1}{s - M_\Delta^2 + i\varepsilon} \\
& \times \Big[\big(m_\pi^2(m + 2M_\Delta) + (m^2 - M_\Delta^2)(2M_\Delta - m)\big) \\
& \quad \times (m_\pi + m + M_\Delta)\,(m_\pi - m - M_\Delta) \\
& \quad + 3M_\Delta^2(m + M_\Delta)t\Big] \\
& + \Big[-s(2z+1)(4M_\Delta z + m(2z-1)) + 2m_\pi^2(M_\Delta + m) \\
& \quad + M_\Delta^2(2M_\Delta + 3m) + 4M_\Delta m^2 z(2z+1) + 2m^3(2z^2 - 1)\Big]\Bigg\},
\end{aligned} \tag{2.16}$$

$$\begin{aligned}
B_\Delta^{(d)}(s,t) = \frac{1}{6M_\Delta^2}\frac{f_{\pi \mathrm{N}\Delta}^2}{m_\pi^2}\Bigg\{ & \frac{1}{s - M_\Delta^2 + i\varepsilon} \\
& \times \Big[\big(m_\pi^2 - m^2 + 4mM_\Delta - M_\Delta^2\big) \\
& \quad \times (m_\pi + m + M_\Delta)\,(m_\pi - m - M_\Delta) + 3M_\Delta^2 t\Big] \\
& + \Big[s(2z+1)^2 + 2(2z+1)m_\pi^2 \\
& \quad + 2(8z^2 + 4z + 1)mM_\Delta + 2(2z^2 - 2z - 1)m^2 + M_\Delta^2\Big]\Bigg\}
\end{aligned} \tag{2.17}$$

We obtain $T_\Delta^{(c)}$ in the same manner or by the substitutions (1.18). From these we obtain $T_\Delta^{(\pm)}$ for either propagator using (see section 1.4)

$$\begin{aligned}
T_\Delta^{(+)} &= \tfrac{2}{3}\left(+T_\Delta^{(d)} + T_\Delta^{(c)}\right) \\
T_\Delta^{(-)} &= \tfrac{1}{3}\left(-T_\Delta^{(d)} + T_\Delta^{(c)}\right),
\end{aligned} \tag{2.18}$$

where T stands for A or B.

For the alternative propagator we obtain rather simpler expressions:

$$A_\Delta^{(d)}(s,t) = \frac{1}{6}\frac{f_{\pi N\Delta}^2}{m_\pi^2}\frac{1}{s-M_\Delta^2+i\varepsilon}\Big[-3(M_\Delta+m)t-(3m+2M_\Delta)s$$
$$+2(M_\Delta+2m)m^2+4(M_\Delta+m)m_\pi^2$$
$$-\frac{1}{s}(m^2-m_\pi^2)(m^3-2M_\Delta m_\pi^2-mm_\pi^2)\Big] \qquad (2.19)$$

$$B_\Delta^{(d)}(s,t) = \frac{1}{6}\frac{f_{\pi N\Delta}^2}{m_\pi^2}\frac{1}{s-M_\Delta^2+i\varepsilon}\Big[-3t-s+2(m_\pi^2+3m^2+mM_\Delta)$$
$$-\frac{1}{s}(m^2-m_\pi^2)(m^2-m_\pi^2-2mM_\Delta)\Big]. \qquad (2.20)$$

The alternative propagator has the advantage of annihilating the off mass-shell part of the vertex, so that the invariant amplitudes are independent of z. Also, as noted in Jaus and Woolcock [7], its predictions for the threshold P-wave amplitudes are much better than those for the unitary propagator.

A serious practical problem with the alternative propagator is the $1/k^2$ singularity. This leads to a $1/s$ singularity in the direct contribution $T_\Delta^{(d)}$ described by 1 (e) and a $1/u$ singularity in the crossed contribution $T_\Delta^{(c)}$ described by 1 (f). The point $s=0$ lies far from the physical region and so the $1/s$ singularity does not lead to unphysical results. However the $1/u$ singularity leads to a logarithmic singularity in the partial wave amplitudes (before unitarisation) at $T_\pi^{\rm lab} \approx 340$MeV. This is a catastrophic failing, even at the relatively low energies we are considering.

In an attempt to save the good features of the alternative propagator, we can attempt an *ad hoc* modification of the amplitudes it produces. We replace the amplitudes $T_\Delta^{(d)}(s)$ (where $T = A$ or B) by $\tilde{T}_\Delta^{(d)}(s,t)$, and require that:

1. $\tilde{T}_\Delta^{(d)}(s,t)$ is analytic for all $s \neq M_\Delta^2$, removing the singularity at $s=0$,

2. $T_\Delta^{(d)}((m\pm m_\pi)^2,0) = \tilde{T}_\Delta^{(d)}((m\pm m_\pi)^2,0)$, retaining the good results at threshold,

3. $\tilde{T}_\Delta^{(d)}(s,t)$ is bounded for $|s|\to\infty$, making the large s behaviour no less physical than that of $T_\Delta^{(d)}(s,t)$.

4. $\tilde{T}_\Delta^{(d)}(s,t) - T_\Delta^{(d)}(s,t)$ is a function of s only (note that $t=0$ at $s=(m\pm m_\pi)^2$).

These conditions enforce a unique prescription

$$\tilde{T}^{(d)}_{\Delta}(s,t) = T^{(d)}_{\Delta}(s,t) + \frac{M^2_{\Delta}(s-(m+m_\pi)^2)(s-(m-m_\pi)^2)}{(s-M^2_{\Delta})s(m+m_\pi)^2(m-m_\pi)^2} \lim_{s\to 0}(sT^{(d)}_{\Delta}(s,t)) \quad (2.21)$$

which corresponds to making the replacement

$$\frac{1}{s} \to \frac{2m^2+2m^2_\pi - s}{(m+m_\pi)^2(m-m_\pi)^2} \quad (2.22)$$

in the invariant amplitudes. We obtain

$$\begin{aligned}\tilde{A}^{(d)}_{\Delta}(s,t) = \frac{1}{6}\frac{f^2_{\pi N\Delta}}{m^2_\pi}\frac{1}{s-M^2_{\Delta}+i\varepsilon}\Big[&-3(M_\Delta+m)t-(3m+2M_\Delta)s \\ &+2(M_\Delta+2m)m^2+4(M_\Delta+m)m^2_\pi \\ &+\frac{s-2m^2-2m^2_\pi}{(m-m_\pi)^2(m+m_\pi)^2}(m^2-m^2_\pi)(m^3-2M_\Delta m^2_\pi - mm^2_\pi)\Big] \end{aligned} \quad (2.23)$$

$$\begin{aligned}\tilde{B}^{(d)}_{\Delta}(s,t) = \frac{1}{6}\frac{f^2_{\pi N\Delta}}{m^2_\pi}\frac{1}{s-M^2_{\Delta}+i\varepsilon}\Big[&-3t-s+2(m^2_\pi+3m^2+mM_\Delta) \\ &+\frac{s-2m^2-2m^2_\pi}{(m-m_\pi)^2(m+m_\pi)^2}(m^2-m^2_\pi)(m^2-m^2_\pi-2mM_\Delta)\Big], \end{aligned} \quad (2.24)$$

and this modified form of the invariant amplitudes obtained using the alternative propagator is the one we use for comparison with experimental results.

An alternative *ad hoc* modification would be to multiply the invariant amplitudes by the factor

$$(1+q^2/\Lambda^2)^{-1} = \left(s + \frac{(s-(m+m_\pi)^2)(s-(m-m_\pi)^2)}{4\Lambda^2}\right)^{-1} s, \quad (2.25)$$

where q is the magnitude of the three-momentum of the pion or the nucleon in the rest frame. Such a factor could be thought of as a form factor accounting for the finite size of the $\pi N\Delta$ vertex.

This modification has a number of drawbacks relative to the previous one. It introduces a new parameter Λ, whose physical significance is unclear. From a theoretical standpoint the modification produces its own singularities at

$$s = m^2 + m^2_\pi - 2\Lambda^2 \pm 2\sqrt{(\Lambda^2-m^2)(\Lambda^2-m^2_\pi)}, \quad (2.26)$$

although there exist choices of Λ for which these are far enough from the physical region not to be a practical problem. Finally, the fits to experimental data obtained with it are not as good as those obtained with the previous modification.

Regardless of which *ad hoc* modification is used, we obtain the crossed amplitudes by the formula (1.18), thus explicitly retaining crossing symmetry.

2.2.4 Isospin-Odd t-channel Exchanges

As discussed by Ericson and Weise [22], t-channel exchanges in the energy region of interest to us are dominated by the exchange of bosons with $I = J = 1$, and by the poorly understood exchange of two pions in an $I = J = 0$ state. The former contributes to the isospin-odd amplitudes.

There are two established vector-isovector mesons below 2 GeV, known in Particle Data Group [23] as $\rho(770)$ and $\rho(1700)$. We model them with an effective vector-isovector meson ρ, whose mass and coupling constants we allow to vary.

Aside from the propagator for a massive spin-1 particle

$$P^{\mu\nu}(k) = i(k^2 - m_\rho^2 + i\varepsilon)^{-1}(g^{\mu\nu} - k^\mu k^\nu / m_\rho^2) \tag{2.27}$$

we require the vertices

$$V_\mu(\rho^i \pi^b \pi^a) = -g_{\rho\pi\pi}(q'_\mu + q''_\mu) i\varepsilon^{iba}, \tag{2.28}$$

and

$$V_\mu(\rho^i NN) = -ig_{\rho NN}\left(\gamma_\mu + \frac{iK_\rho}{2m}\sigma_{\mu\lambda}k^\lambda\right)\tau^i, \tag{2.29}$$

where k, q', q'' are the 4-momenta of the internal line and the incoming and outgoing pions respectively and a, b are the isospin indices for the incoming and outgoing pions respectively. Since

$$i\varepsilon^{ijk}\tau^i = \frac{1}{2}[\tau^j, \tau^k] \tag{2.30}$$

it is easy to see that there is no vector-isovector contribution to the isospin-even amplitudes. We find that

$$A_\rho^{(-)} = -G_\rho K_\rho \frac{s-u}{4mm_\pi^2}\left(1 - \frac{t}{m_\rho^2}\right)^{-1} \tag{2.31}$$

$$B_\rho^{(-)} = G_\rho(1 + K_\rho)m_\pi^{-2}\left(1 - \frac{t}{m_\rho^2}\right)^{-1} \tag{2.32}$$

where $G_\rho = 2g_{\rho\pi\pi}g_{\rho NN}(m_\pi/m_\rho)^2$. Pion-nucleon scattering is thus able to distinguish only three parameters, G_ρ, K_ρ and m_ρ. We will allow all three to vary freely, which has not always been the case in previous models of this kind.

In practice, G_ρ is effectively determined by the isospin-odd S-wave scattering length. Both Peccei [24] and Olsson and Osypowski [6] use arguments from current algebra to write $G_\rho = (m_\pi/f_\pi)^2$, where $f_\pi \approx 131.6$MeV is the pion decay constant.

K_ρ has been identified (see, for instance, Peccei [24]) with κ_V, the isovector magnetic moment of the nucleon. Olsson and Osypowski [6] go further than this, making the replacements

$$\left(1-\frac{t}{m_\rho^2}\right)^{-1} \to F_1^V(t) \text{ and}$$
$$K_\rho\left(1-\frac{t}{m_\rho^2}\right)^{-1} \to F_2^V(t), \tag{2.33}$$

the isovector electromagnetic form factors of the nucleon. These arguments are based on vector meson dominance, the principle that the nucleon's electromagnetic interactions are mediated almost entirely via vector-isovector meson exchange. Since, however, a simple quark model that makes no reference to the strong interaction at all (see Close [25]) can give quite a reasonable value for κ_V, it is hard to see how this is justified. Also, Bernstein [26] has shown that simple vector meson dominance does not connect κ_V with K_ρ.

The mass m_ρ represents an effective mass for the combined effects of the two mesons being exchanged. Since we have no way of knowing the relative importance of the two mesons we allow the mass to vary freely. If structure at the ρNN vertex gives rise to a form factor (see, for instance, Peccei [24]) this will also be difficult to separate from a change in mass. Hence m_ρ must also be considered to represent any structure at the vertices. One would expect that the exchange of $\rho(770)$ mesons is considerably more important than that of $\rho(1700)$ mesons, so if we assume that structure at the vertices can be neglected then we expect $m_\rho \approx 770$ MeV.

2.2.5 Isospin-Even t-channel Interactions

Although the so-called σ meson is no longer considered to be a true resonance, it is known that a strong attraction exists between low-energy pions in a scalar isoscalar state. This attraction cannot be explained by reference to the established low energy resonances $f_0(975)$ and $f_0(1400)$ (Particle Data Group [23]). It is therefore inappropriate to model the σ as a true meson.

In the absence of a successful model for this interaction, we are forced to make a pure parameterisation, from which we cannot hope to extract any physics. Since the two-pion state has spin and isospin zero, it will contribute to the $A^{(+)}$ invariant amplitude.

Olsson and Osypowski [6] model this interaction as a simple second degree polynomial in t. This seems a poor choice of analytic form, since it must behave very poorly as $t \to \pm\infty$ (although $t \to +\infty$ is of no interest to pion-nucleon scattering). Instead, we use an analytic form inspired by dispersion theory.

$A_\sigma^{(+)}(t)$ can be expected to satisfy the twice-subtracted dispersion relation

$$A_\sigma^{(+)}(t) = a + bt + \frac{t^2}{\pi}\int_{4m_\pi^2}^{\infty} \frac{dt'\,\sigma(t')}{t'^2(t'-t)}, \tag{2.34}$$

where

$$b = \frac{1}{\pi}\int_{4m_\pi^2}^{\infty} \frac{dt\ \sigma(t)}{t^2} \tag{2.35}$$

and the unknown weight function $\sigma(t)$ is adequately smooth. We know that the third term behaves as t^2 for small t and as $-bt$ for large $|t|$, so we choose a parameterisation which has these properties, namely

$$A_\sigma^{(+)}(t) = a + bt + \frac{bct^2}{b - ct}, \tag{2.36}$$

which is in fact bilinear. This leaves three parameters to be determined by comparison with experiment, the same number as in Olsson and Osypowski [6].

2.3 Dispersion Relation Constraints

The unphysical point $\nu = t = 0$, where ν is defined to be $(s-u)/4m$, is of special interest. It is possible, using only very general principles such as analyticity, crossing symmetry and convergence at infinity to extrapolate certain combinations of invariant amplitudes from the physical region to that point.

Gasser *et al* [27] and others have studied the expansion

$$\begin{aligned} D^{(+)}(\nu,t) &\equiv A^{(+)}(\nu,t) + \nu B^{(+)}(\nu,t) \\ &= d_{00}^{(+)} + d_{10}^{(+)}\nu^2 + d_{01}^{(+)}t + \text{higher terms}, \end{aligned} \tag{2.37}$$

and obtained the coefficients $d_{00}^{(+)} = -1.492(24)$, $d_{01}^{(+)} = +1.138(27)$. Note that crossing symmetry requires the function be even in ν.

These quantities are obtained from experimental data on pion-nucleon scattering, using only very general properties of the amplitudes. They are thus almost independent of the model of pion-nucleon scattering we adopt. For this reason, and because they have been so stable, some authors (*e.g.* Olsson and Osypowski [6])

have argued that models of pion-nucleon scattering should be required to satisfy this calculated behaviour at $\nu = t = 0$. There are several arguments against such a course, however. Given that the model will be expected in any case to satisfy the physical data which were used to make the extrapolation, requiring the model to satisfy the extrapolations is less a test of its physical predictions than of its analytic form far from the physical region. Second, there is already good reason to believe that the analytic form is faulty, since the invariant amplitudes of our model certainly do not have the correct high energy behaviour.

We make fits to experiment both with and without imposing the conditions of Gasser *et al* [27]. The imposition of such conditions effectively reduces the number of parameters in the fit by two.

2.4 Unitarity

If we neglect processes whose final product is not a pion and a nucleon, particle number is conserved and hence we expect the partial wave amplitudes to satisfy unitarity. The only such process relevant at our energies is pion production, $\pi + N \rightarrow \pi + \pi + N$, which becomes possible at $T_\pi^{\text{lab}} \approx 170\text{MeV}$. Since pion production is quite small even at 250 MeV, it is reasonable to impose unitarity on our partial wave amplitudes. For instance, the πN channel accounts for more than 99% of $\Delta(1232)$ decays (Particle Data Group [23]).

By summing the contributions discussed in section 2.2, we obtain (real) approximations to the (complex) S- and P- partial wave amplitudes. Each partial wave amplitude can be expressed as $e^{i\delta} \sin\delta$, where δ is known as the phase shift and $\text{Im}\,(\delta) \geq 0$. To satisfy unitarity, δ must be real. Obviously only the trivial case $\delta = n\pi$, n integer, gives a real amplitude. Physically, the imaginary part of the amplitude, along with additional contributions to the real part, derives from higher order diagrams. Our task is to approximate the higher-order (non-tree) diagrams to enforce unitarity, using only our knowledge of the tree diagrams.

There are infinitely many possible unitarisation procedures, none of which is obviously preferred to the others. In our case the unitarisation technique used will make a significant difference only in the case of the P_{33} partial wave. Ericson and Weise [22] use the K-matrix prescription, where $\tan\delta$ is identified with the tree diagram amplitude. In such an ansatz, the resonant phase shift passes through 90°

at $s = M^2$, where M is the mass of the resonance.

Several unitarisation techniques can be considered members of the one parameter family

$$\tan\delta = \frac{\tan\delta_B + \tan\delta_R}{1 + \lambda\tan\delta_B\tan\delta_R}, \tag{2.38}$$

where δ is the total phase shift. δ_B and δ_R are the phase shifts obtained by the K-matrix prescription from the background and resonant parts of the tree diagram amplitude. The parameter λ is $+1$ (Olsson [28]), 0 (K-matrix) or -1 (Noelle [29]). The resonant part of the amplitude is separated from the background part in a somewhat arbitrary way; it is the contribution from the diagram that becomes infinite at resonance. An advantage of the K-matrix prescription here is that there is no need to make such a separation. Some of our fits allow λ to vary as a parameter.

An alternative but computationally expensive approach to unitarisation is the iteration of a scattering equation (*e.g.* Pearce and Jennings [30]). Such a method starts from the Bethe-Salpeter equation, which connects the full scattering amplitude with the half off mass-shell amplitudes arising from the irreducible diagrams. The tree diagrams figure 1 (a) through (g) are a subset of these diagrams and together with figure 1 (h) could be used as an approximation to them. This method thus effectively includes in the calculation all the diagrams that can be reduced to several tree diagrams like those in figure 1, but with the irreducible parts having some or all of their legs off mass-shell. This makes it a generalisation of the methods described above, which consider only tree diagrams with all external lines on mass-shell. To perform the iteration in practice, however, a three-dimensional scattering equation must be obtained by some method from the Bethe-Salpeter four-dimensional scattering equation. As with the infinite number of possible unitarisation procedures, however, there are infinitely many ways in which such a three-dimensional equation can be obtained. Thus the iteration of a scattering equation does not solve the problem of the lack of uniqueness in unitarisation procedures.

2.5 Comparison With Other Models

Here we compare our model with three well-known models of the same general type. Another important model in this field is that of Peccei [24].

2.5.1 Ericson and Weise

A very well known effective lagrangian model of pion-nucleon scattering is that described by Ericson and Weise [22]. Although their model is quite primitive in many ways, they do succeed in obtaining a reasonable fit to the P-wave phase shifts. Ericson and Weise [22] start from the tree diagrams 1 (a) through (f), *i.e.* their model includes the direct and crossed diagrams for the nucleon, N(1470) and $\Delta(1232)$ intermediate states.

The s- and u- channel interactions are handled in a generally non-relativistic manner; only the propagator denominator has its relativistic form, while the spin projection operators and vertex functions are treated non-relativistically. Subtle questions of pseudoscalar versus pseudovector πNN coupling, and the proper form of a spin-$\frac{3}{2}$ propagator, are thus bypassed.

Ericson and Weise do not attempt to fit the S-waves in the same manner as they do the P-waves. Although they do remark that the S-wave scattering lengths are consistent with their being dominated by $\rho(770)$ exchange in the t-channel, there is no attempt to include the s- and u-channel exchanges in the calculation of the S-wave scattering lengths, or to describe the energy dependence of the S-wave phase shifts. Nor are the t-channel contributions to the P-waves considered.

The Ericson and Weise model provides a good qualitative fit to the most salient features of pion-nucleon scattering. If an accurate quantitative fit is to be obtained, however, all of the above problems must be adressed.

2.5.2 Olsson and Osypowski

The model of Olsson and Osypowski is the one which comes closest to ours. They have contributions corresponding to 1 (a), (b), (e), (f), (g) and (h), plus a purely parametric "diffractive" contribution we do not include. Their neglect of the N(1470) is a deliberate attempt by them to avoid any possibility of double-counting, which we do not regard as a concern in this case. Not including the N(1470) would not be very serious if one were only considering the energies our model is intended to address. However, Olsson and Osypowski consider pion laboratory frame energies up to 310 MeV, which corresponds to a centre of mass energy of approximately 1320 MeV, not far below the N(1470) resonance. When fits to phase shifts are performed using the model of Olsson and Osypowski, the neglect of the N(1470)

becomes noticeable in the P_{11} partial wave.

Our handling of the nucleon diagrams is identical to that of Olsson and Osypowski. They use the unitary spin-$\frac{3}{2}$ propagator for the $\Delta(1232)$ diagrams, as do some of our fits. They also allow the off mass-shell parameter z to vary as we do.

Rather than fitting to phase shifts, Olsson and Osypowski have chosen to follow a suggestion of Höhler *et al* [31] in fitting their model to the coefficients in the expansions of $A^{(+)}, A^{(-)}/\nu, B^{(+)}/\nu$ and $B^{(-)}$ about $\nu^2 = t = 0$, where $\nu = (s - u)/4m$. Since the πN phase shift analyses available in the literature are reasonably precise and stable, we prefer to fit to those. By fitting to the shape of the amplitudes far from the physical region Olsson and Osypowski are relying on their model to extrapolate correctly. In our view this cannot be expected unless the model has appropriate high energy behaviour, which neither ours nor that of Olsson and Osypowski does (section 2.3).

Olsson and Osypowski make use of the principles of vector meson dominance to severely constrain the isospin-odd t-channel exchanges. Our reasons for believing their arguments to be unconvincing are stated in subsection 2.2.4.

The most serious defect in the Olsson and Osypowski model is their inclusion of a purely parameterised diffractive contribution to the invariant amplitude $B^{(+)}$. The diffractive contribution is intended to describe the effect of non-resonant inelastic scattering at high energies. Although inelastic scattering is negligible at the energies Olsson and Osypowski consider, they argue that a standard dispersion relation demonstrates that there will nonetheless be a substantial diffractive contribution at lower energies. They give several reasons for believing that there is no significant diffractive contribution to $A^{(+)}$, though this is contradicted by Hamilton and Woolcock [10]. Since both our model and that of Olsson and Osypowski contain (see subsection 2.2.5) a parameterised contribution to $A^{(+)}$ already, we would expect the addition of a diffractive term to be largely absorbed by changes to the σ parameters. Since they have no way to calculate the effect of their diffractive contribution to $B^{(+)}$ they must use two free parameters to describe it. They do attempt to show that the parameters that best fit the data are consistent with the values expected for them from dispersion theory. However, we consider it contrary to the spirit of an effective lagrangian model to isolate a diffractive part of $\mathrm{Im}\, B^{(+)}$ and claim that the dispersion integral over this part gives a contribution $\mathrm{Re}\, B^{(+)}$ at low energies which cannot be accounted for by exchanges involving low-lying

states.

2.5.3 Pearce and Jennings

The most important difference between our model and that of Pearce and Jennings [30] is the method of unitarisation. They consider a variety of scattering equations (see section 2.4), including one which reduces to the K-matrix method ($\lambda = 0$ in (2.38)). They use a bare nucleon mass and πNN coupling constant which are determined by requiring that the known energy and coupling of the nucleon pole be reproduced when the bare potential is fed into the scattering equation.

The model of Pearce and Jennings is intended to address pion laboratory energies up to 400 MeV, substantially higher than the 250 MeV limit we aim to satisfy. They do not include the N(1470) resonance in their calculation, and, almost certainly as a result of this, their model predictions for the P_{11} wave are obviously too low for pion energies above about 270 MeV.

Pearce and Jennings treat K_ρ as a tunable parameter as we do. Like us they obtained values (see section 3.2) lower than those used by the Bonn and Nijmegen potentials, or that obtained by assuming vector meson dominance.

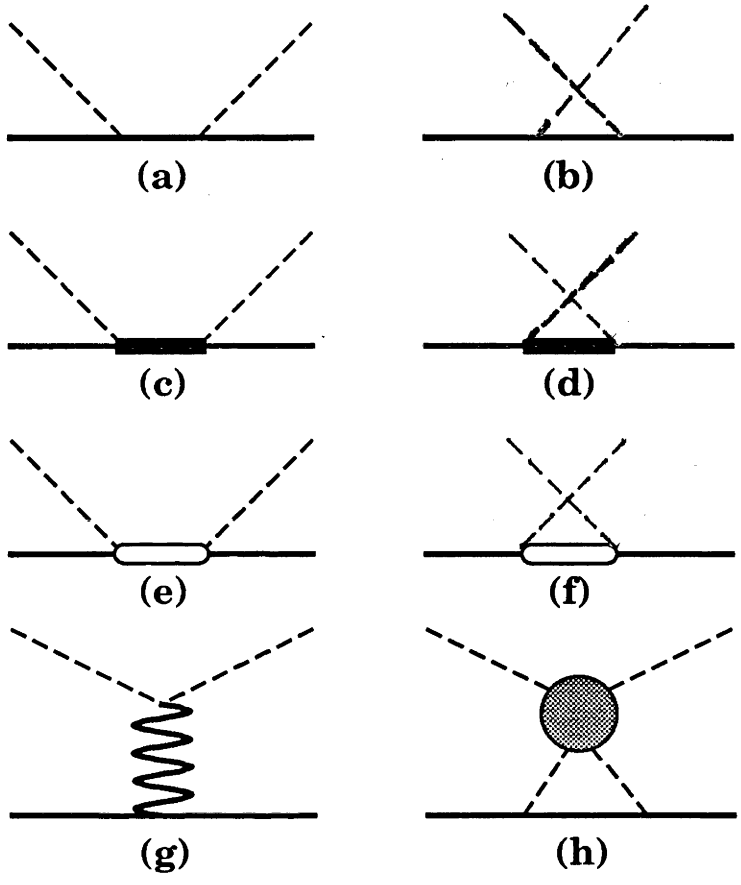

Figure 1: Tree diagrams representing the contributions in the model to pion-nucleon scattering. From left to right and top to bottom they represent direct (s-channel) (a) and crossed (u-channel) (b) nucleon exchange, direct (c) and crossed (d) $\Delta(1232)$ exchange, direct (e) and crossed (f) N(1470) exchange, vector isovector t-channel exchange (g) and (effective) scalar isoscalar t-channel exchange (h).

Chapter 3

Results

The predictions of the model were compared with phase shift analyses from [32]. Although these data are not purely experimental results, the methods by which they are obtained are well established. The fitting procedure is discussed in section 3.1. In section 3.2 we consider fits to the experimental data using slightly different models and free parameter vectors.

3.1 Fitting Procedure

In order to obtain the best possible fit to these data the free parameters are varied to minimise

$$\chi^2 = \sum_i \sum_j \left(\frac{\delta_{ij}^E - \delta_{ij}^M(\boldsymbol{f})}{\delta_{ij}^U} \right)^2 , \tag{3.1}$$

where χ is a measure of poorness of fit, i is an index running over all experimental energies, j is an index running over the partial waves S_{11}, S_{31}, P_{11}, P_{31}, P_{13} and P_{33}, $\delta_{ij}^E \pm \delta_{ij}^U$ is an experimental phase shift with uncertainty, and $\delta_{ij}^T(\boldsymbol{f})$ is the corresponding theoretical prediction when the values of the free parameters form the vector $\boldsymbol{f}$.

Although the χ^2 statistic is the one normally used in such a fit, it does have some drawbacks for this application. The usual measure of poorness of fit is χ^2/N, where N, the number of degrees of freedom, is the number of ordered pairs (i,j) minus the number of elements in $\boldsymbol{f}$. In practice, however, we find it is always possible to reduce χ^2/N by adding another free parameter to the system. Therefore a small χ^2/N cannot on its own be interpreted as a successful model.

This problem is due to the fact that the χ^2/N measure of poorness of fit is intended to decide whether a theory is exactly correct or not. Since all the theories we have considered here are known to be inexact, the χ^2 statistic is in a sense

being misused. The major advantage of the χ^2 is that it permits easy and efficient mechanical optimisation. In any case, the drawbacks of the χ^2 statistic are likely to be common to any algorithmic approach that uses so little information (only the phase shift and its uncertainty) extracted from the experimental results.

An additional problem with the χ^2 statistic is that it implicitly assumes that the error in the phase shift associated with any i, j pair is independent of the error in the phase shift associated with any other such pair. Simple inspection of a phase analysis shows that this is certainly not the case, and these correlations allow the optimisation procedure to find a smaller χ^2/N than would otherwise be possible. Again, the information needed to correct this problem is not available in the analyses we used.

It is worth noting that all these problems would be likely to occur even if a heuristic rather than a mechanical approach were taken to optimisation.

3.2 Fits to Phase Shift Analyses

In table 3.1 we show the optimal parameter sets and corresponding minimum values of χ^2/N for five different fits. Fits (1)–(3) use the standard spin-$\frac{3}{2}$ propagator with different values for the parameter λ in the unitarisation formula (2.38). Fit (1) uses the unitarisation due to Noelle [29], *i.e.* $\lambda = -1$. Fit (2) uses the K-matrix procedure ($\lambda = 0$) and fit (3) the Olsson method of unitarisation ($\lambda = +1$). Fit (4) uses our *ad hoc* modification of the Williams spin-$\frac{3}{2}$ propagator, and Noelle unitarisation. Fit (5) is identical to fit (1), except that we have imposed the additional constraint that certain of the constants in (2.37) should have the values determined by Gasser *et al* [27], specifically $d_{00}^{(+)} = -1.492$ and $d_{01}^{(+)} = +1.138$.

From fits (1) through (3) we see that with a standard spin-$\frac{3}{2}$ propagator and no constraints from Gasser *et al* [27] we obtain substantially inferior fits with the Olsson unitarisation than with either the K-matrix or Noelle unitarisations. Since these three methods of unitarisation can be viewed as a continuum, is is interesting to ask how χ^2/N behaves as λ from (2.38) varies continuously. There is in fact a very shallow minimum at $\lambda = -0.7$.

As λ is varied about this point other parameters of the fit change, but χ^2/N remains nearly constant. The parameters that principally change are $f^2_{\pi N\Delta}/4\pi$, M_Δ and z, *i.e.* those responsible for the behaviour of the P_{33} phase shift near

$s = M_\Delta^2$. Intuitively, the change in λ requires a change in M_Δ in order to have the energy at which the phase shift reaches 90° remain constant. The change in M_Δ then requires changes in the other parameters to keep behaviour far from the resonance constant. These results emphasise that in the absence of an unambiguous unitarisation procedure it is impossible to determine the parameters associated with $\Delta(1232)$ exchange.

The same ambiguity was found by Pearce and Jennings [30], who found z to be -0.124, -0.408 and -0.311 for three different integral equations, which are analogous to our unitarisation procedures. Determination of z is very difficult by any other means, for instance Benmerrouche *et al* [18] used pion photoproduction from nucleons but could only determine $-0.78 < z < 0.30$. The calculation of z is complicated in that case by the existence of two other off mass-shell parameters x and y associated with the $\gamma N\Delta$ vertex, which are also poorly determined. These same parameters are important to deuteron photodisintegration, so the difficulty in determining them is disappointing.

As discussed in section 2.2.2 our fits are not at an energy high enough to permit the accurate determination of $f^2_{\pi NN^*}/4\pi$. The values we obtain vary strongly with λ and are always smaller than those used by Ericson and Weise [22] to describe the behaviour near the resonance (which we do not reach). These results should not be taken too seriously, since there are much better ways of measuring this quantity than the phase shift analyses we considered.

The overall vector-isovector t-channel coupling parameter G_ρ is very well determined by the isospin-odd S-wave scattering length, so it is not surprising that this parameter is very stable in our fits. The mass of our effective vector-isovector meson comes out to be quite close to the mass of the $\rho(770)$, suggesting either that the $I = J = 1$ t-channel exchanges are dominated by that meson, or that the other effects discussed in subsection 2.2.4 are cancelling. The non-minimal coupling parameter K_ρ varies strongly with λ, but always remains much smaller than either $\kappa_V \approx 3.7$ or the values used in the Bonn and Nijmegen potentials (6.1 and 4.3 respectively). We have discussed in subsection 2.2.4 why we do not find this disturbing. Pearce and Jennings [30] also found a large variation in K_ρ, though their values were rather larger than ours: 2.254, 1.437 and 3.156. Since K_ρ has a strong effect on nucleon-nucleon scattering and deuteron photodisintegration it is unfortunate that we cannot determine it better.

The $I = J = 0$ t-channel exchange parameters a, b and c vary considerably with λ. It is difficult to see that any physical interpretation can be placed upon these parameters. The $I = J = 0$ t-channel exchange principally contributes to the isospin-even S-wave amplitude.

From fit (4) we can evaluate the success of our *ad hoc* modification of the amplitudes arising from the alternative spin-$\frac{3}{2}$ propagator. The unitarisation method used, that due to Olsson, gives much a better fit to the data in this case than do the K-matrix and Noelle approaches. This modified fit is in many ways similar to that of Olsson and Osypowski [6], with the new spin-$\frac{3}{2}$ propagator replacing the diffractive contribution to the isospin-even S-wave scattering lengths. The preferred value for K_ρ is much closer to κ_V, which was used for K_ρ by Olsson and Osypowski. This could be considered a fairly successful fit, so it is not possible to dismiss Williams' spin-$\frac{3}{2}$ propagator on the grounds of poor fit to experiment, as long as the *ad hoc* modification is included. There are, of course, many theoretical objections to the Williams propagator, as we discussed in subsection 2.2.3.

In fit (5) we have imposed the values of $d_{00}^{(+)}$ and $d_{01}^{(+)}$ obtained by Gasser *et al* [27] on our fit. This causes a substantial deterioration in the quality of the fit. Given that our model amplitudes are known to have an analytic form incompatible with the behaviour required for such extrapolations, this is not surprising.

Since our values for χ^2/N are only slightly larger than 1, it is tempting to conclude that our model is providing a very good description of pion-nucleon scattering in the energy range we have considered. If this is the case, we should find that each of the partial waves makes an approximately equal contribution to χ^2. In fact we find that three of the partial waves (S_{31}, P_{31} and P_{13}) provide only about 20% of the total. Rather than telling us anything about the model, this tells us that the errors associated with the phase shifts in these partial waves either have been overestimated or (most likely) are strongly correlated with each other. If this is true of these partial waves then we must assume that it may be true of the other partial waves. It is therefore likely that our fit to pion-nucleon scattering is not nearly as good as the value of χ^2/N suggests. As discussed in section 3.1 this is not surprising, and should not be taken to imply the model is a failure.

In figures 2–4 we show our model prediction for each of the six partial waves, along with experimental results from [32]. The version of the model used is fit (1), which gives the best fit. The data from references [], which were actually used

in the fitting, are shown as closed circles with error bars. The data from Helsinki-Karlsruhe [33], which were not, are shown as open circles without error bars.

Inspection of these graphs immediately shows us that the model is successfully fitting the S_{31}, P_{31} and P_{13} partial waves. It is providing an excellent fit to the P_{33} resonant partial wave, but because these phase shifts have been determined so accurately compared with the dramatic manner in which they can change if a parameter is varied there is still a substantial contribution to χ^2/N.

The model is having the greatest difficulty when trying to fit the S_{11} and P_{11} partial waves at high energy. It is interesting to note that the P_{11} partial wave is being significantly affected in this region by the N(1470) resonance, which our model may not handle well since it assumes that the N(1470) decays only to πN, whereas at the resonant energy only 50–70% of the decays are to πN (Particle Data Group [23]).

Our model neglects all resonances above the N(1470). Considering only those resonances with the quantum numbers needed to resonate in one of the partial waves we have attempted to fit, the lowest such resonance is the N(1535). The N(1535) occurs in the S_{11} partial wave, so it is tempting to speculate that it might provide the needed correction. Unlike the P_{11} case, however, there is no evidence of a poorly fitted rise in the phase shift near 250 MeV.

It seems possible for an effective lagrangian model to provide a reasonable description of pion-nucleon scattering up to 250 MeV, although the value of χ^2/N does not really provide the objective measure of the model's success one would like. However the fitting process has had limited success in determining the value of the tunable parameters of the model. In particular, the choice of ansatz used to unitarise the amplitudes has a significant effect on several parameters, and the non-minimal coupling parameters z and K_ρ are very poorly determined. It is thus not possible to use this model to determine the parameters relevant to $\Delta(1232)$ and $\rho(770)$ exchange in other processes, as we had hoped.

	(1)	(2)	(3)	(4)	(5)
M_Δ (MeV)	1247	1230	1217	1217	1247
$f^2_{\pi N\Delta}/4\pi$	0.455	0.376	0.316	0.301	0.443
z	−0.629	−0.550	−0.506		−0.140
$f^2_{\pi NN^*}/4\pi$	0.0047	0.0088	0.0129	0.0005	0.0108
G_ρ	1.160	1.171	1.181	1.187	1.155
K_ρ	−0.474	0.281	0.419	3.139	0.649
m_ρ (MeV)	738	755	763	1077	635
a	0.631	0.691	0.730	0.115	0.858
b	0.313	0.408	0.547	0.436	−0.087
c	0.058	0.116	0.193	0.035	0.002
χ^2/N	1.102	1.155	1.472	1.233	1.504

Table 1: The optimal parameter sets and values of χ^2/N for five different fits to πN S- and P-wave phase shifts up to 250 MeV. (1) Standard $\Delta(1232)$, no constraints, Noelle unitarisation. (2) Standard $\Delta(1232)$, no constraints, K-matrix unitarisation. (3) Standard $\Delta(1232)$, no constraints, Olsson unitarisation. (4) Modified Williams $\Delta(1232)$, no constraints, Olsson unitarisation. (5) Standard $\Delta(1232)$, $d_{00}^{(+)}$ and $d_{01}^{(+)}$ fixed, Noelle unitarisation.

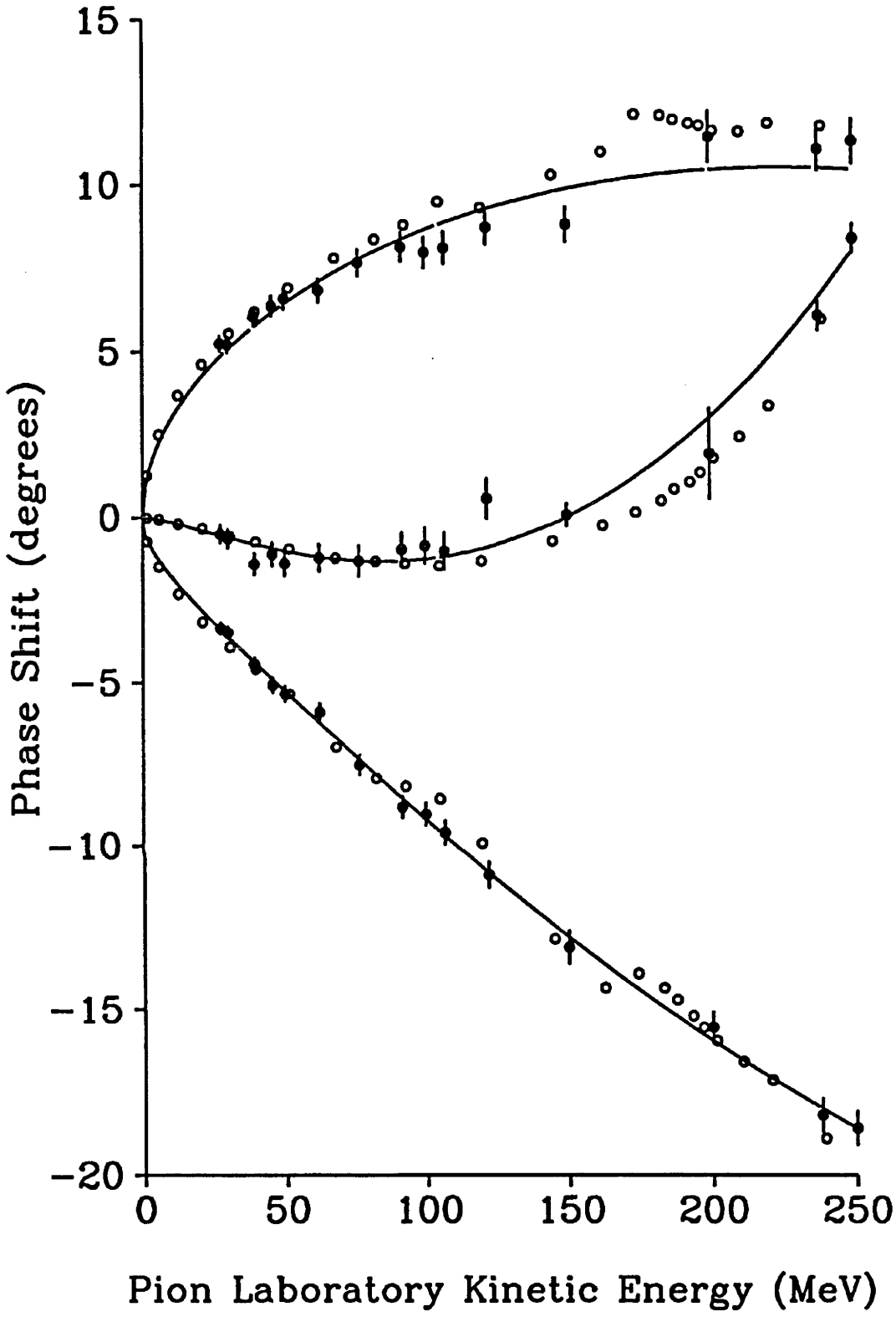

Figure 2: S_{11} (upper curve), P_{11} (middle curve) and S_{31} (lower curve) phase shifts from fit (1) of table 3.1.

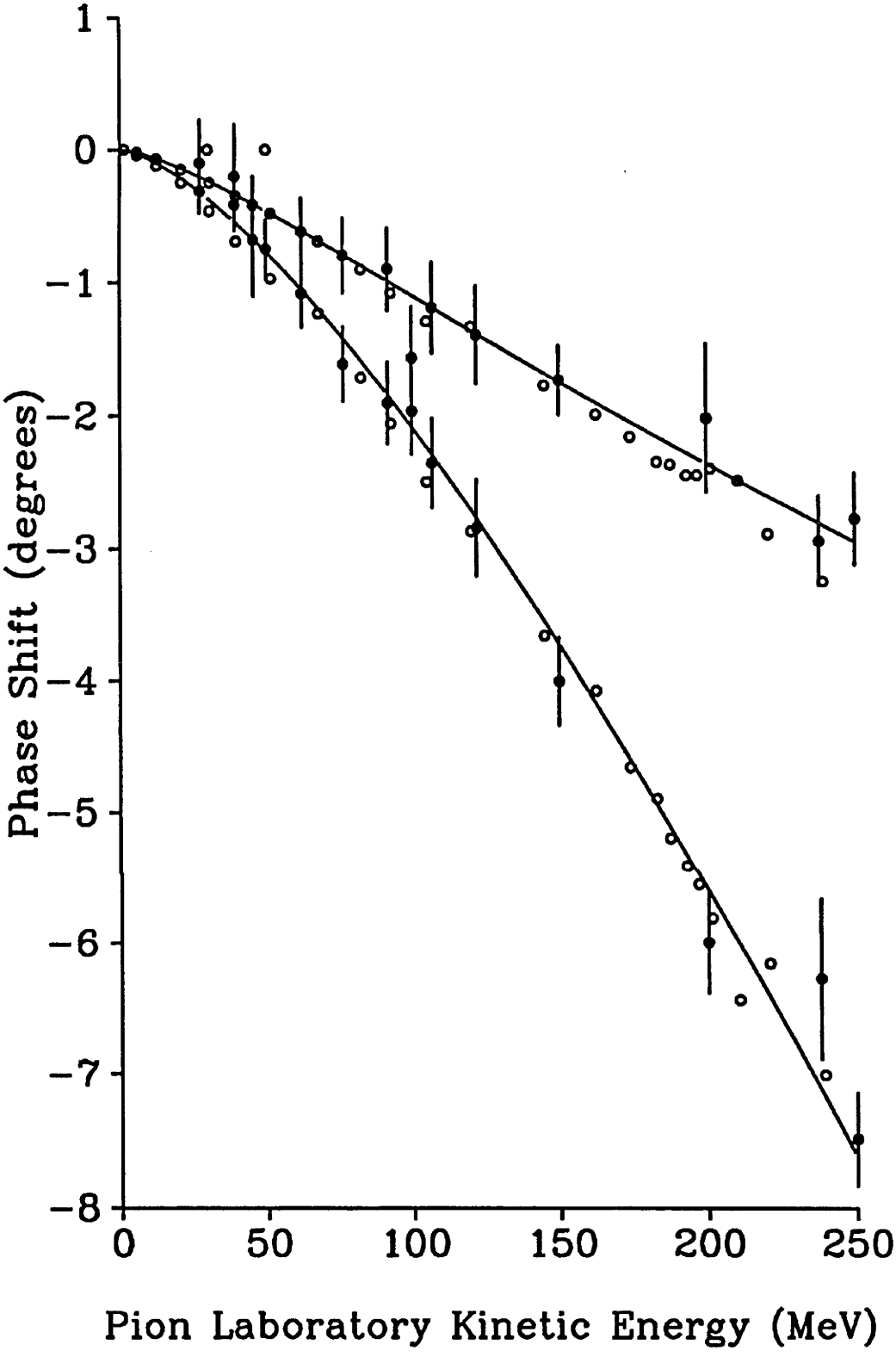

Figure 3: P_{31} (lower curve) and P_{13} (upper curve) phase shifts from the fit (1) of table 3.1.

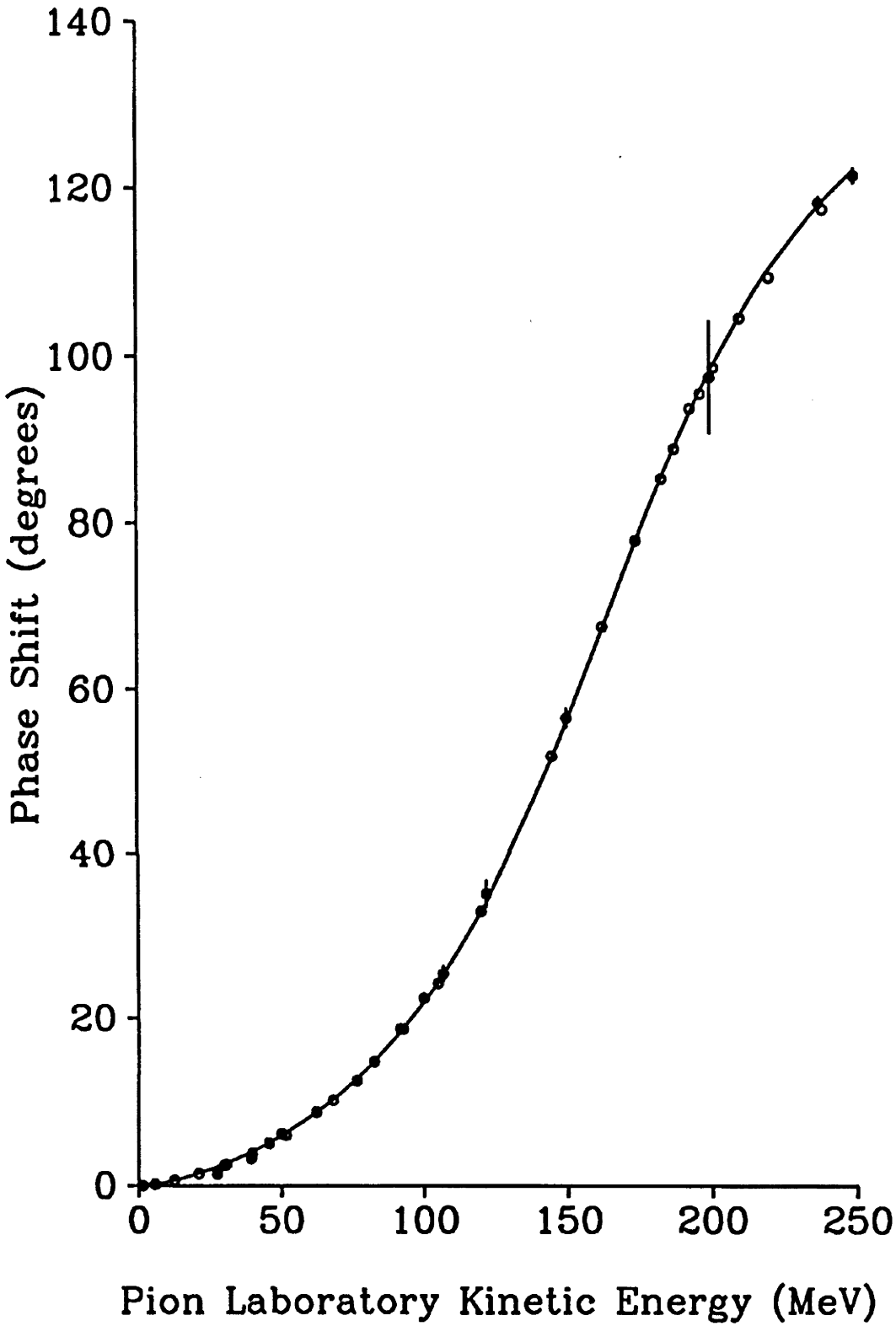

Figure 4: P_{33} (resonant) phase shift from the fit (1) of table 3.1. Some of the closed circles have error bars too small to be visible.

Chapter 4

Introduction

This second part of the thesis concerns the theory and results of a model of deuteron photodisintegration, published in Jaus *et al* [34] and Jaus *et al* [35] respectively. Chapter 5 describes the model, and in particular the ways in which it differs from its immediate linear ancestor, the model of Jaus and Woolcock [7]. In chapter 6 the results obtained from the model are used to confront all the modern data on deuteron photodisintegration observables.

In section 4.1 we place our model in historical perspective and discuss the ways in which it differs from established models of deuteron photodisintegration. A detailed treatment of the formalism of deuteron photodisintegration is included in sections 4.2 and 4.3.

4.1 History

A general survey of deuteron photodisintegration can be found in Arenhövel and Sanzone [36]. Here we will give a brief history of some models of deuteron photodisintegration which are conceptual ancestors of our model.

An early attempt to describe deuteron photodisintegration was made by Partovi [37] (for earlier attempts see references therein). The model gave a reasonable qualitative fit to the deuteron photodisintegration data up to 140 MeV available at the time.

From a theoretical standpoint the model due to Partovi had several approximations. Meson exchange effects were not explicitly included, so the theory describes only an impulse interaction, where one nucleon is a spectator to the absorption of the photon by the other nucleon. Partovi did, however, employ an identity for the conservation of the internal convection current. The effect of this, as discussed in

section 5.1, is to implicitly include meson exchange in the model. For the nucleon-nucleon potential Partovi used the Hamada-Johnson potential [38], which has a very small singlet scattering length. Partovi suggested that better results might have been obtained using a potential that better fitted the singlet scattering length.

Arenhövel and Fabian [39] used several different potentials in calculating theoretical predictions for the forward cross-section. These were compared with experimental results up to 120 MeV, but the agreement was poor. The first effort by Jaus and Woolcock [19] was principally concerned with adding pion exchange to a model of deuteron photodisintegration, in an effort to reduce this discrepancy. They concluded that meson exchange effects were not sufficient to account for it, and suggested that a better understanding of the NN potential was required. One conclusion of this study was that the use of pseudovector πNN coupling gave a better fit to experiment than did the use of pseudoscalar coupling.

Jaus and Woolcock [40] then established a formalism for deuteron photodisintegration. This was a quasipotential formalism that treated in a consistent manner the deuteron bound state and continuum wave functions, and the electromagnetic 4-current. There was also a more careful treatment of the relativistic correction to the impulse approximation, whose importance had been pointed out by Cambi *et al* [41].

Using this formalism, Jaus and Woolcock [42] performed a calculation of the forward cross-section for deuteron photodisintegration up to 120 MeV. A surprising result was the sensitivity of the forward cross-section to charge-dependent effects, particularly the mass difference between charged and uncharged pions. Short range effects were found to be not important.

The calculations of deuteron photodisintegration were greatly extended by Jaus and Woolcock [7], and a comprehensive comparison [43] with experimental data was made. Wave functions for the deuteron and the two-nucleon continuum states were obtained using the Paris potential. The alternative spin-$\frac{3}{2}$ propagator discussed in subsection 2.1.2 was used instead of the conventional unitary one. The model included one meson exchange both with and without the excitation of $\Delta(1232)$ intermediates, and made use of a current conservation law whose justification was flawed. It was found that the fit to experiment was not very good. They suggested that this might be due either to two pion exchange effects, or to defects in the Paris potential.

The application of current conservation used by Jaus and Woolcock [7] was shown by Arenhövel [44] and by Jaus and Woolcock [45] to be impossible to justify. The modified current conservation (MCC) method proposed by Jaus and Woolcock [45] uses instead the identity for the divergence of the internal convection current density used by Partovi [37]. It also became apparent that this MCC method acts to correct for possible defects in the one pion exchange part of the nucleon-nucleon potential. Also, the alternate spin-$\frac{3}{2}$ propagator was abandoned in favour of the original one.

The results of this model were compared [35] with experimental results from the literature. The failure to obtain good agreement with recent very accurate measurements of the forward cross-section while using the Paris potential prompted an attempt to compare various nucleon-nucleon potentials by using them to model deuteron photodisintegration.

4.2 Quasipotential Formalism

For our treatment of deuteron photodisintegration we require a formalism which provides a consistent treatment of the bound and continuum two-nucleon states. We use the quasipotential formalism of Jaus and Woolcock [40].

We start by considering the elastic NN scattering reaction

$$\mathrm{N}_1(\tfrac{1}{2}P + p') + \mathrm{N}_2(\tfrac{1}{2}P - p') \rightarrow \mathrm{N}_1(\tfrac{1}{2}P + p'') + \mathrm{N}_2(\tfrac{1}{2}P - p''). \tag{4.1}$$

As before, singly primed quantities refer to incoming particles and doubly primed quantities to outgoing particles. We have suppressed the helicity indices. Let the amplitude for this reaction be W; then we can use symbolic operator notation to write the Bethe-Salpeter equation

$$W = U + UGW = U + WGU, \tag{4.2}$$

where G is the usual 4-dimensional Green function for the two-nucleon state. The function U is obtained by summing the contributions of all the irreducible NN scattering diagrams, and so has meaning only within some field theoretic description of the NN interaction. The products UGW and WGU imply sums over spinor indices and an integration over an internal relative 4-momentum.

Since 4-dimensional equations such as (4.2) are very difficult to deal with, the quasipotential formalism has been developed. In the quasipotential formalism the

4-dimensional Green's function G is replaced by a 3-dimensional Green's function g by fixing the timelike component of the internal relative momentum. Such a formalism is obviously appropriate to the treatment of states which are described by a single-time wave function, which is the case in nuclear physics scattering experiments. Then (4.2) is replaced by

$$W = V + VgW = V + WgV, \tag{4.3}$$

where V is known as the quasipotential. V and U are related by

$$V - U = V(G - g)U = U(G - g)V. \tag{4.4}$$

Since (4.4) is also a 4-dimensional equation we have not actually reduced the complexity of the problem. However, one could hope to obtain V from U by expanding in a series whose terms correspond to the exchange of bosons between the interacting nucleons.

There are many possible choices for g. We shall use the covariant form of the Blankenbecler and Sugar [46] (BBS) prescription (see also Woloshyn and Jackson [47]). This formulation leads naturally to the Lipmann-Schwinger and Schrödinger equations, and has the property of restricting the sum over spinor indices to positive energy states. The covariant BBS formulation fixes the internal relative momentum $\hat{k} = (\hat{k}_0, \boldsymbol{k})$ by $P \cdot \hat{k} = 0$, which leads to

$$\hat{k}_0 = \frac{\boldsymbol{P} \cdot \boldsymbol{k}}{P_0} = \frac{E(\frac{1}{2}\boldsymbol{P} + \boldsymbol{k})^2 - E(\frac{1}{2}\boldsymbol{P} - \boldsymbol{k})^2}{2P_0}, \tag{4.5}$$

where $E(\boldsymbol{p}) = \sqrt{m^2 + \boldsymbol{p}^2}$. The covariant BBS Green's function is

$$g(P; k) = 2\pi\delta(k_0 - \hat{k}_0)\hat{g}(P; \hat{k})\Lambda_1^+(\tfrac{1}{2}\boldsymbol{Q} + \boldsymbol{k})\Lambda_2^+(\tfrac{1}{2}\boldsymbol{Q} - \boldsymbol{k}), \tag{4.6}$$

where $\Lambda_{1,2}^+$ are the positive energy projection operators,

$$\hat{g}(P; \hat{k}) = \frac{4m^2}{\tilde{E}(P; \hat{k})[P^2 - 4(m^2 - \hat{k}^2)]}, \tag{4.7}$$

Q is an implicit function of P and $\hat{k}$

$$Q(P; \hat{k}) = 2\frac{\sqrt{m^2 - \hat{k}^2}}{\sqrt{P^2}}P, \tag{4.8}$$

and

$$\tilde{E}(P; \hat{k}) = \tfrac{1}{2}Q_0 = \frac{\sqrt{m^2 - \hat{k}^2}}{\sqrt{P^2}}P_0. \tag{4.9}$$

We shall also use the abbreviations $Q' = Q(P; \hat{p}')$ and $Q'' = Q(P; \hat{p}'')$. Note that $Q \cdot \hat{k} = 0$ and hence $(\frac{1}{2}Q \pm \hat{k})^2 = m^2$. Thus the projection operators $\Lambda_{1,2}^+$ remain positive energy projection operators under Lorentz transformations.

Attaching positive energy spinors to V and W we define

$$\hat{V}(P;p'',p') = \overline{u}_1(\tfrac{1}{2}\boldsymbol{P}+\boldsymbol{p}'')\overline{u}_2(\tfrac{1}{2}\boldsymbol{P}-\boldsymbol{p}'')V(P;p'',p')u_1(\tfrac{1}{2}\boldsymbol{P}+\boldsymbol{p}')u_2(\tfrac{1}{2}\boldsymbol{P}-\boldsymbol{p}'), \quad (4.10)$$

and similarly for $\hat{W}$. Using (4.6) we can write (4.3) as

$$\begin{aligned}
&\hat{W}(P;p'',p') \\
&\quad = \hat{V}(P;p'',p') + (2\pi)^{-3}\int d^3k\, \hat{V}(P;p'',\hat{k})\hat{g}(P;\hat{k})\hat{W}(P;\hat{k},p') \\
&\quad = \hat{V}(P;p'',p') + (2\pi)^{-3}\int d^3k\, \hat{W}(P;p'',\hat{k})\hat{g}(P;\hat{k})\hat{V}(P;\hat{k},p'). \qquad (4.11)
\end{aligned}$$

Note that two kinds of spinors are used in (4.11). Where the relative momentum on the appropriate side is an unrestricted 4-momentum we use what we shall call standard spinors, as in (4.10). When the relative momentum on that side is restricted by the BBS condition we use BBS spinors. So for instance

$$\hat{V}(P;p'',\hat{k}) = \overline{u}_1(\tfrac{1}{2}\boldsymbol{P}+\boldsymbol{p}'')\overline{u}_1(\tfrac{1}{2}\boldsymbol{P}-\boldsymbol{p}'')V(P;p'',\hat{k})u_1(\tfrac{1}{2}\boldsymbol{Q}+\boldsymbol{k})u_2(\tfrac{1}{2}\boldsymbol{Q}-\boldsymbol{k}). \quad (4.12)$$

We define the fully restricted potentials $\hat{V}_0, \hat{W}_0$ by

$$\begin{aligned}
\hat{V}_0 &= \hat{V}(P;\hat{p}'',\hat{p}') \\
&= \overline{u}_1(\tfrac{1}{2}\boldsymbol{Q}''+\boldsymbol{p}'')\overline{u}_2(\tfrac{1}{2}\boldsymbol{Q}''-\boldsymbol{p}'')V(P;\hat{p}'',\hat{p}')u_1(\tfrac{1}{2}\boldsymbol{Q}'+\boldsymbol{p}')u_2(\tfrac{1}{2}\boldsymbol{Q}'-\boldsymbol{p}') \quad (4.13)
\end{aligned}$$

and similarly for $\hat{W}_0$. From (4.11), $\hat{W}_0$ satisfies the integral equations

$$\begin{aligned}
&\hat{W}(P;\hat{p}'',\hat{p}') \\
&\quad = \hat{V}(P;\hat{p}'',\hat{p}') + (2\pi)^{-3}\int d^3k\, \hat{V}(P;\hat{p}'',\hat{k})\hat{g}(P;k)\hat{W}(P;\hat{k},\hat{p}') \\
&\quad = \hat{V}(P;\hat{p}'',\hat{p}') + (2\pi)^{-3}\int d^3k\, \hat{W}(P;\hat{p}'',\hat{k})\hat{g}(P;k)\hat{V}(P;\hat{k},\hat{p}'). \qquad (4.14)
\end{aligned}$$

Now if there is a bound state of mass M, there will be a pole in $\hat{W}_0$ at $P^2 = M^2$, and the bound state vertex function must satisfy

$$\begin{aligned}
\hat{\Gamma}(P;\hat{p}'',\hat{p}') &= (2\pi)^{-3}\int d^3k\, \hat{V}(P;\hat{p}'',\hat{k})\hat{g}(P;k)\hat{\Gamma}(P;\hat{k},\hat{p}') \\
\overline{\hat{\Gamma}(P;\hat{p}'',\hat{p}')} &= (2\pi)^{-3}\int d^3k\, \hat{V}(P;\hat{p}'',\hat{k})\hat{g}(P;k)\overline{\hat{\Gamma}(P;\hat{k},\hat{p}')}, \qquad (4.15)
\end{aligned}$$

where $P_0 = \sqrt{M^2+\boldsymbol{P}^2}$. The normalisation condition for $\hat{\Gamma}$ is

$$\begin{aligned}
1 = -4m\Bigg[&(2\pi)^{-3}\int d^3p\, \overline{\hat{\Gamma}(P;\hat{p})}\, \frac{\partial \hat{g}(P;\hat{p})}{\partial(P^2)}\bigg|_{P^2=M^2}\hat{\Gamma}(P;\hat{p}) \\
&+(2\pi)^{-6}\int d^3(p'',p')\, \overline{\hat{\Gamma}(P;\hat{p}'')}\hat{g}(P;\hat{p}'') \\
&\times \frac{\partial \hat{V}(P;\hat{p}'',\hat{p}')}{\partial(P^2)}\bigg|_{P^2=M^2}\hat{g}(P;\hat{p}')\hat{\Gamma}(P;\hat{p}')\Bigg]. \qquad (4.16)
\end{aligned}$$

From this one can show that $\hat{\Gamma}(P;\hat{p})$ is a Lorentz invariant.

Since there exists only one two-nucleon bound state, we can set M equal to the deuteron mass. We define a deuteron wavefunction

$$\phi(\boldsymbol{P};\boldsymbol{p}) = \sqrt{\frac{\tilde{E}(P;\hat{p})}{m}}\hat{g}(P;\hat{p})\hat{\Gamma}(P;\hat{p}) \tag{4.17}$$

and a modified quasipotential $\tilde{V}$ by

$$\tilde{V}(P;\boldsymbol{p}'',\boldsymbol{p}') = \sqrt{\frac{m}{\tilde{E}(P;\hat{p}'')}}\hat{V}(P;\hat{p}'',\hat{p}')\sqrt{\frac{m}{\tilde{E}(P;\hat{p}')}}, \tag{4.18}$$

where $P_0 = \sqrt{M^2 + \boldsymbol{P}^2}$ as before. It is convenient at this time to define $\tilde{W}$ from $\hat{W}_0$ in the same way, that is

$$\tilde{W}(P;\boldsymbol{p}'',\boldsymbol{p}') = \sqrt{\frac{m}{\tilde{E}(P;\hat{p}'')}}\hat{W}(P;\hat{p}'',\hat{p}')\sqrt{\frac{m}{\tilde{E}(P;\hat{p}')}}. \tag{4.19}$$

We now rewrite (4.15) as

$$\phi(\boldsymbol{P};\boldsymbol{p}) = \hat{g}(P;\hat{p})\frac{\tilde{E}(P;\hat{p})}{m}(2\pi)^{-3}\int d^3k\,\tilde{V}(P;\boldsymbol{p},\boldsymbol{k})\phi(\boldsymbol{P};\boldsymbol{k}), \tag{4.20}$$

and using the definition of $\hat{g}$ this is

$$\frac{M^2 - 4m^2 + 4\hat{p}^2}{4m}\phi(\boldsymbol{P};\boldsymbol{p}) = (2\pi)^{-3}\int d^3k\,\tilde{V}(P;\boldsymbol{p},\boldsymbol{k})\phi(\boldsymbol{P};\boldsymbol{k}). \tag{4.21}$$

Using (4.16), the normalisation condition for ϕ is

$$\begin{aligned} 1 = {} & (2\pi)^{-3}\int d^3p\,|\phi(\boldsymbol{P};\boldsymbol{p})|^2 \\ & -\frac{2m}{\sqrt{M^2+P^2}}\int d^3(p'',p')\,\overline{\phi(\boldsymbol{P};\boldsymbol{p}'')}\,\frac{\partial\tilde{V}(P;\boldsymbol{p}'',\boldsymbol{p}')}{\partial P_0}\bigg|_{P^2=M^2}\phi(\boldsymbol{P};\boldsymbol{p}'). \end{aligned} \tag{4.22}$$

We now transform the deuteron wave function to the rest state. The rotationless Lorentz transform which maps the 4-vector $P = (P_0, \boldsymbol{P})$ to $\overset{\circ}{P} = (\sqrt{P^2}, \boldsymbol{0})$ also maps $\hat{p} = (\hat{p}_0, \boldsymbol{p})$ to $\overset{\circ}{p} = (0, \overset{\circ}{\boldsymbol{p}})$, where

$$\begin{aligned} \overset{\circ}{\boldsymbol{p}} &= \boldsymbol{p} - \frac{\boldsymbol{p}\cdot\boldsymbol{P}\boldsymbol{P}}{P_0\left(P_0 + \sqrt{P^2}\right)} \\ &\approx \boldsymbol{p} - \frac{\boldsymbol{p}\cdot\boldsymbol{P}\boldsymbol{P}}{8m^2}. \end{aligned} \tag{4.23}$$

From the definition (4.17), the normalisation condition (4.22) and the invariance properties of $\tilde{E}$, $\hat{g}$ and $\hat{\Gamma}$, the quantity

$$\sqrt{\frac{P_0}{\sqrt{P^2}}}\phi(\boldsymbol{P};\boldsymbol{p}) \tag{4.24}$$

is a Lorentz invariant, and so ϕ will transform as

$$\phi(\mathbf{0};\mathring{\boldsymbol{p}}) = \sqrt{\frac{P_0}{\sqrt{P^2}}}\phi(\boldsymbol{P};\boldsymbol{p}). \tag{4.25}$$

Then (4.21) becomes

$$\frac{M^2 - 4m^2 - 4\,\mathring{\boldsymbol{p}}^2}{4m}\phi(\mathbf{0};\mathring{\boldsymbol{p}}) = (2\pi)^{-3}\int d^3\mathring{k}\,\tilde{V}(\mathring{P};\mathring{\boldsymbol{p}},\mathring{\boldsymbol{k}})\phi(\mathbf{0};\mathring{\boldsymbol{k}}). \tag{4.26}$$

This is simply the non-relativistic Schrödinger equation in momentum space. The eigenvalue $(M^2 - 4m^2)/4m$ reduces to the non-relativistic eigenvalue $M - 2m$ in the weak binding limit, which is a good approximation in the case of the deuteron. The above equations provide a covariant description of the deuteron in an arbitrary frame.

Suppose that we have a two-nucleon continuum state with 3-momentum $\boldsymbol{P}$ and relative 3-momentum $\boldsymbol{p}_0$, so that

$$P_0 = E(\tfrac{1}{2}\boldsymbol{P} + \boldsymbol{p}_0) + E(\tfrac{1}{2}\boldsymbol{P} - \boldsymbol{p}_0) = 2\overline{E}(\boldsymbol{P};\boldsymbol{p}_0), \tag{4.27}$$

where (4.27) serves to define $\overline{E}(\boldsymbol{P};\boldsymbol{k})$. Inspection of (4.7) shows that for $P_0 = 2\overline{E}(\boldsymbol{P};\boldsymbol{p}_0)$, $\hat{g}(P;\boldsymbol{k})$ is singular when $\boldsymbol{k}$ belongs to a two-dimensional manifold. To specify the behaviour of $\hat{g}$ in the neighbourhood of this singularity we define

$$\hat{g}^{(\pm)}(P;\hat{k}) = \frac{4m^2}{\tilde{E}(P;\hat{k})\left[4\overline{E}(\boldsymbol{P};\boldsymbol{p}_0)^2 - \boldsymbol{P}^2 - 4(m^2 - \hat{k}^2) \pm i\varepsilon\right]}, \tag{4.28}$$

where ε is small and positive. The amplitude $\tilde{W}$ defined in (4.19) has a cut along the real axis of the P_0-plane for

$$P_0 \geq 2\overline{E}(\boldsymbol{P};\mathbf{0}) = 2\sqrt{m^2 + \tfrac{1}{4}\boldsymbol{P}^2}. \tag{4.29}$$

We denote the two branches of $\tilde{W}$ as $P_0 \to 2\overline{E}(\boldsymbol{P};\mathbf{0})$ from above and below by the superscripts $^{(+)}$ and $^{(-)}$ respectively. Then from (4.14) $\tilde{W}^{(\pm)}$ satisfies the singular integral equations

$$\tilde{W}^{(\pm)}(P;\boldsymbol{p}'',\boldsymbol{p}')$$
$$= \tilde{V}(P;\boldsymbol{p}'',\boldsymbol{p}')$$
$$+(2\pi)^{-3}\int d^3k\,\tilde{V}(P;\boldsymbol{p}'',\boldsymbol{k})\frac{\tilde{E}(P;\hat{k})}{m}\hat{g}^{(\pm)}(P;\hat{k})\tilde{W}^{(\pm)}(P;\boldsymbol{k},\boldsymbol{p}')$$
$$= \tilde{V}(P;\boldsymbol{p}'',\boldsymbol{p}')$$
$$+(2\pi)^{-3}\int d^3k\,\tilde{W}^{(\pm)}(P;\boldsymbol{p}'',\boldsymbol{k})\frac{\tilde{E}(P;\hat{k})}{m}\hat{g}^{(\pm)}(P;\hat{k})\tilde{V}(P;\boldsymbol{k},\boldsymbol{p}'). \quad (4.30)$$

Also,

$$\overline{\tilde{W}^{(\pm)}(P;\boldsymbol{p}'',\boldsymbol{p}')} = \tilde{W}^{(\mp)}(P;\boldsymbol{p}',\boldsymbol{p}'')$$
$$\overline{\tilde{V}(P;\boldsymbol{p}'',\boldsymbol{p}')} = \tilde{V}(P;\boldsymbol{p}',\boldsymbol{p}''). \quad (4.31)$$

Defining the scattering wave functions

$$\Phi^{(\pm)}(\boldsymbol{P},\boldsymbol{p}_0;\boldsymbol{p}) = \sqrt{\frac{\tilde{E}(P;\hat{p}_0)}{m}}$$
$$\times\left[(2\pi)^3\delta^{(3)}(\boldsymbol{p}-\boldsymbol{p}_0)+\frac{\tilde{E}(P;\hat{p}_0)}{m}\hat{g}^{(\pm)}(P;\hat{p})\tilde{W}^{(\pm)}(P;\boldsymbol{p},\boldsymbol{p}_0)\right], \quad (4.32)$$

where $\tilde{W}^{(\pm)}$ is half on mass-shell, it follows from scattering theory that $\Phi^{(\pm)}$ satisfy the inhomogeneous equations

$$\Phi^{(\pm)}(\boldsymbol{P},\boldsymbol{p}_0;\boldsymbol{p}) = \sqrt{\frac{\tilde{E}(P;\hat{p}_0)}{m}}(2\pi)^3\delta^{(3)}(\boldsymbol{p}-\boldsymbol{p}_0)$$
$$+\frac{\tilde{E}(P;\hat{p})}{m}\hat{g}^{(\pm)}(P;\hat{p})(2\pi)^{-3}\int d^3k\,\tilde{V}(P;\boldsymbol{p},\boldsymbol{k})\Phi^{(\pm)}(\boldsymbol{P},\boldsymbol{p}_0;\boldsymbol{k}). \quad (4.33)$$

On transformation to the rest frame (4.33) becomes

$$\Phi^{(\pm)}(0,\mathring{\boldsymbol{p}}_0;\mathring{\boldsymbol{p}}) = \sqrt{\frac{E(\mathring{\boldsymbol{p}}_0)}{m}}(2\pi)^3\delta^{(3)}(\mathring{\boldsymbol{p}}-\mathring{\boldsymbol{p}}_0)$$
$$+\frac{m}{\mathring{\boldsymbol{p}}_0^{\,2}-\mathring{\boldsymbol{p}}^{\,2}\pm i\varepsilon}(2\pi)^{-3}\int d^3k\,\tilde{V}(\mathring{P};\mathring{\boldsymbol{p}},\mathring{\boldsymbol{k}})\Phi^{(\pm)}(0,\mathring{\boldsymbol{p}}_0;\mathring{\boldsymbol{k}}), \quad (4.34)$$

where

$$\Phi^{(\pm)}(0,\mathring{\boldsymbol{p}}_0;\mathring{\boldsymbol{p}}) = \sqrt{\frac{P_0}{\sqrt{P^2}}}\Phi^{(\pm)}(\boldsymbol{P},\boldsymbol{p}_0;\boldsymbol{p}), \quad (4.35)$$

as in (4.25), with the definition of $\mathring{\boldsymbol{p}}_0$ analogous to (4.23). The corresponding

Schrödinger equation in momentum space is

$$\frac{\overset{\circ}{p}_0^{\,2} - \overset{\circ}{\boldsymbol{p}}^{\,2}}{m}\Phi^{(\pm)}(0,\overset{\circ}{p}_0;\overset{\circ}{\boldsymbol{p}}) = (2\pi)^{-3}\int d^3\overset{\circ}{k}\,\tilde{V}(\overset{\circ}{P};\overset{\circ}{\boldsymbol{p}},\overset{\circ}{\boldsymbol{k}})\Phi^{(\pm)}(0,\overset{\circ}{p}_0;\overset{\circ}{\boldsymbol{k}}). \tag{4.36}$$

We can now turn to the process

$$\gamma(q) + \mathrm{N}_1(\tfrac{1}{2}P' + p') + \mathrm{N}_2(\tfrac{1}{2}P' - p') \to \mathrm{N}_1(\tfrac{1}{2}P'' + p'') + \mathrm{N}_2(\tfrac{1}{2}P'' - p''). \tag{4.37}$$

The S-matrix for this process is related to the electromagnetic current operator $J^\mu(0)$ by

$$\begin{aligned}&\langle P'';p''|\,S\,|P';p';q,\varepsilon\rangle\\ &= -i(2\pi)^{-\frac{3}{2}}(2\pi)^4\delta^{(4)}(P''-P'-q)\varepsilon_\mu\,\langle P'';p''|\,J^\mu(0)\,|P';p'\rangle\,,\end{aligned} \tag{4.38}$$

where ε is the polarisation 4-vector of the photon, and the single particle plane wave states are normalised by

$$\langle \boldsymbol{k}''|\boldsymbol{k}'\rangle = 2E(\boldsymbol{k}')\delta^{(3)}(\boldsymbol{k}''-\boldsymbol{k}'). \tag{4.39}$$

Now define $\hat{M}^\mu$ by

$$\langle P'';p''|\,J^\mu(0)\,|P';p'\rangle = 4m^2(2\pi)^{-6}\hat{M}^\mu(P'',P';p'',p'), \tag{4.40}$$

noting that $\hat{M}$ has standard spinors on both sides.

In order to address deuteron photodisintegration we need to be able to evaluate the matrix element of the electromagnetic current between two-nucleon bound and continuum states. The deuteron is the only bound state, and we shall denote it by $|d;\boldsymbol{P}\rangle$, where

$$P = \left(\sqrt{M^2+\boldsymbol{P}^2},\boldsymbol{P}\right) \tag{4.41}$$

is the 4-momentum of the deuteron. Considering first the matrix element between two two-nucleon bound states, we find

$$\begin{aligned}\langle d;\boldsymbol{P}''|\,J^\mu(0)\,|d;\boldsymbol{P}'\rangle \;&= 4m(2\pi)^{-9}\int d^3(p'',p')\,\overline{\hat{\Gamma}(P'';\hat{p}'')}\hat{g}(P'';\hat{p}'')\\ &\quad\times\hat{\Lambda}^\mu(P'',P';\hat{p}'',\hat{p}')\hat{g}(P';\hat{p}')\hat{\Gamma}(P';\hat{p}'),\end{aligned} \tag{4.42}$$

where

$$\begin{aligned}&\hat{\Lambda}(P'',P';\hat{p}'',\hat{p}')\\ &\quad= (2\pi)^{-6}\int d^3(k'',k')\,\left[(2\pi)^3\delta^{(3)}(\boldsymbol{p}''-\boldsymbol{k}'') - \hat{V}(P'';\hat{p}'',\hat{k}'')\hat{g}(P'';\hat{k}'')\right]\\ &\qquad\times\hat{M}(P'',P';\hat{k}'',\hat{k}')\left[(2\pi)^3\delta^{(3)}(\boldsymbol{p}'-\boldsymbol{k}') - \hat{g}(P';\hat{k}')\hat{V}(P';\hat{p}',\hat{k}')\right]\end{aligned} \tag{4.43}$$

is the two-nucleon 4-current density.

We can rewrite this in terms of the modified quasipotential and the deuteron wave function defined in (4.17) as

$$\begin{aligned}\langle d;\boldsymbol{P}''|\,J^{\mu}(0)\,|d;\boldsymbol{P}'\rangle &= 4m(2\pi)^{-9}\\ &\times\int d^3(p'',p')\,\overline{\phi(\boldsymbol{P}'';\boldsymbol{p}'')}\tilde{\Lambda}(P'',P';\boldsymbol{p}'',\boldsymbol{p}')\phi(\boldsymbol{P}';\boldsymbol{p}'),\end{aligned}\tag{4.44}$$

where

$$\tilde{\Lambda}(P'',P';\boldsymbol{p}'',\boldsymbol{p}') = \sqrt{\frac{m}{\tilde{E}(P'';\hat{p}'')}}\hat{\Lambda}(P'',P';\hat{p}'',\hat{p}')\sqrt{\frac{m}{\tilde{E}(P';\hat{p}')}}\tag{4.45}$$

is a modified two-nucleon current density. $\tilde{\Lambda}$ is thus the correct two nucleon current to use when calculating matrix elements from non-relativistic wave functions.

Next we must consider the matrix element of $J^{\mu}(0)$ between a continuum and a bound two-nucleon state, which is the matrix element relevant to deuteron photodisintegration. We use the two-nucleon continuum normalisation

$$\langle 2N;\boldsymbol{P}'',\boldsymbol{p}''|2N;\boldsymbol{P}',\boldsymbol{p}'\rangle = 4E(\boldsymbol{p}_1')E(\boldsymbol{p}_2')\delta^{(3)}(\boldsymbol{p}_1''-\boldsymbol{p}_1')\delta^{(3)}(\boldsymbol{p}_2''-\boldsymbol{p}_2'),\tag{4.46}$$

where $\boldsymbol{p}_1' = \frac{1}{2}\boldsymbol{P}'+\boldsymbol{p}'$, $\boldsymbol{p}_1'' = \frac{1}{2}\boldsymbol{P}''+\boldsymbol{p}''$, $\boldsymbol{p}_2' = \frac{1}{2}\boldsymbol{P}'-\boldsymbol{p}'$ and $\boldsymbol{p}_2'' = \frac{1}{2}\boldsymbol{P}''-\boldsymbol{p}''$. With this normalisation, the equation analogous to (4.17) is

$$\begin{aligned}&\langle 2N;\boldsymbol{P}'',\boldsymbol{p}_0|\,J^{\mu}(0)\,|d;\boldsymbol{P}'\rangle\\ &= 4m^{\frac{3}{2}}(2\pi)^{-\frac{21}{2}}\int d^3(k',p')\,\hat{M}^{\mu}(P'',P';\hat{p}_0,\hat{k}')\\ &\quad\times\left[(2\pi)^3\delta^{(3)}(\boldsymbol{k}'-\boldsymbol{p}')-\hat{g}(P';\hat{k}')\hat{V}(P';\hat{k}',\hat{p}')\right]\hat{g}(P';\hat{p}')\hat{\Gamma}(P';\hat{p}')\\ &= 4m^{\frac{3}{2}}(2\pi)^{-\frac{21}{2}}\int d^3(p'',p')\,\overline{\Phi^{(-)}(\boldsymbol{P}'',\boldsymbol{p}_0,\boldsymbol{p}'')}\\ &\quad\times\tilde{\Lambda}^{\mu}(P'',P';\boldsymbol{p}'',\boldsymbol{p}')\phi(\boldsymbol{P}';\boldsymbol{p}').\end{aligned}\tag{4.47}$$

The quantity $\hat{M}^{\mu}$ is in principle obtained from the complete set of diagrams describing the process (4.37). We can decompose $\hat{M}^{\mu}$ in the same fashion as we decomposed the NN scattering amplitude W in (4.2). Defining M^{μ} by removing the spinors from $\hat{M}^{\mu}$, and reverting to the symbolic notation of (4.2), we have

$$M^{\mu} = K^{\mu}+WGK^{\mu}+K^{\mu}GW+WGK^{\mu}GW,\tag{4.48}$$

where K^{μ} is obtained by summing all irreducible diagrams that contribute to (4.37). In practice the expansion in irreducible diagrams must be truncated at some level

of approximation. Figure 1 in Jaus and Woolcock [40] shows the impulse approximation, one pion exchange and two pion exchange diagrams for deuteron photodisintegration that contribute to K^μ.

Now consider the matrix element of $J^\mu(0)$ between two bound states, obtained by substituting (4.48) into (4.42) and (4.43). Equation (4.15) shows that $\hat{\Gamma}$ on the right or left of (4.42) is annihilated by the factors in square brackets in (4.43). Thus only the last term contributes to the matrix element of M^μ and we can write

$$M^\mu \doteq WGK^\mu GW, \tag{4.49}$$

where the symbol $\doteq$ denotes equality when a matrix element is taken.

The Green function G can be split into four parts, using the identity

$$\begin{aligned} E(\boldsymbol{q})(\gamma\cdot q+m) = {} & m(q_0+E(\boldsymbol{q}))\sum_r u^{(r)}(\boldsymbol{q})\bar{u}^{(r)}(\boldsymbol{q}) \\ & + m(q_0-E(\boldsymbol{q}))\sum_r v^{(r)}(-\boldsymbol{q})\bar{v}^{(r)}(-\boldsymbol{q}). \end{aligned} \tag{4.50}$$

Just one of these parts, which we shall call G_{++}, contains two internal positive energy states, so that, attaching positive energy spinors to (4.49), we have sixteen terms in $\hat{M}^\mu$, which we write

$$\begin{aligned} \hat{M}_0 &= \hat{M}^\mu(P'',P';\hat{p}'',\hat{p}') \\ &= (2\pi)^{-8}\int d^3(k'',k')\,\hat{W}(P';\hat{p}'',k'')G_{++}(P'';k'') \\ &\quad \times\hat{K}^\mu(P'',P';k'',k')G_{++}(P';k')\hat{W}(P';\hat{p}',k')+\cdots, \end{aligned} \tag{4.51}$$

where all the remaining terms contain at least one negative energy state, and

$$G_{++}(P;p) = -i\frac{m^2}{E(\frac{1}{2}\boldsymbol{P}+\boldsymbol{p})E(\frac{1}{2}\boldsymbol{P}-\boldsymbol{p})}\frac{1}{(p_0-x_1(P;\boldsymbol{p})+i\varepsilon)(p_0+x_2(P;\boldsymbol{p})-i\varepsilon)}, \tag{4.52}$$

where

$$\begin{aligned} x_1(P;\boldsymbol{p}) &= E(\tfrac{1}{2}\boldsymbol{P}+\boldsymbol{p})-\tfrac{1}{2}P_0 \\ x_2(P;\boldsymbol{p}) &= E(\tfrac{1}{2}\boldsymbol{P}-\boldsymbol{p})-\tfrac{1}{2}P_0. \end{aligned} \tag{4.53}$$

In the case of the two impulse approximation diagrams there are only eight terms, since one of the nucleons is a spectator and its propagator appears only once.

We now consider the terms which contain at least one negative energy state. The only terms which contribute at the 1πE level are those in which K^μ is given by

the impulse approximation diagrams and there is exactly one negative energy state adjacent to the vertex where the photon is absorbed. This is simply the pair current (PC) contribution, which is suppressed if pseudovector coupling is used, in which case the seagull contribution has a similar effect. All the other terms involving at least one negative energy state are at least at the 2πE level. If pseudovector coupling is used then these terms are very small; however in that case a seagull interaction is necessary to preserve gauge invariance. If pseudoscalar coupling is used then these terms can be quite large, but are to a large extent cancelled by a class of 2πE contributions. These are generated by a $\pi\pi$NN contact interaction and arise quite naturally in a chiral invariant theory. They are usually simulated by a σNN interaction. In our calculations we use pseudovector πNN coupling and include the $\gamma\pi$NN seagull interaction to preserve gauge invariance.

We therefore consider only the first term of (4.51), and write

$$\hat{\Lambda}^{\mu}(P'',P';\hat{p}'',\hat{p}') \doteq (2\pi)^{-8}\int d^4(k'',k')\,\hat{V}(P'';\hat{p}'',k'')G_{++}(P'';k'') \times\hat{K}^{\mu}(P'',P';k'',k')G_{++}(P'';k'')\hat{V}(P';k',\hat{p}'). \tag{4.54}$$

Defining $\hat{\Lambda}_0$ by analogy with $\hat{W}_0$ we can use symbolic notation to write (4.54) as

$$\hat{\Lambda}_0^{\mu} \doteq \hat{V}G_{++}\hat{K}^{\mu}G_{++}\hat{V}. \tag{4.55}$$

Note that the right hand side of (4.54) is free of zeros and poles.

The situation is slightly more complex when we take the matrix element between a bound state and a continuum state. The equation analogous to (4.49) is

$$M^{\mu} \doteq K^{\mu}GW + WGK^{\mu}GW, \tag{4.56}$$

and retaining only positive energy states we have

$$\hat{M}_0^{\mu} \doteq \hat{K}^{\mu}G_{++}\hat{W} + \hat{W}^{(+)}G_{++}\hat{K}^{\mu}G_{++}\hat{W}. \tag{4.57}$$

The appearance of $\hat{W}^{(+)}$ implies that $\Phi^{(-)}$ must be used in (4.47). Using (4.43), we obtain in symbolic notation the equation analogous to (4.54),

$$\hat{\Lambda}_0^{\mu} \doteq \left(\mathbb{1} - \hat{V}_0\hat{g}^{(+)}\right)\hat{K}^{\mu}G_{++}\hat{V} + \hat{V}G_{++}\hat{K}^{\mu}G_{++}\hat{V}. \tag{4.58}$$

Note that the cut in $\hat{M}_0$ for $P_0'' \geq \sqrt{4m^2 + \boldsymbol{P}''^2}$, which appeared along with $W^{(+)}$, is absent from $\hat{\Lambda}_0$.

Using techniques developed in section III of Jaus and Woolcock [40] it can be shown that the results gained by calculating matrix elements between two bound states using (4.54) and between a bound state and a continuum state using (4.58) are formally identical. For convenience, therefore, we can use (4.54) as the basis of all calculations. For each irreducible diagram this allows us to calculate $\hat{\Lambda}^0$ and hence $\tilde{\Lambda}$. The results for the individual contributions are given in section 5.2.

4.3 The Differential Cross-Section and the Multipole Expansion

In order to connect the differential cross-section for deuteron photodisintegration in the centre-of-mass frame to the matrix elements of the electromagnetic current operator we need to define a set of axes. Writing the reaction in the centre-of-mass frame as

$$\gamma(q_0, \boldsymbol{q}) + d(\sqrt{M^2 + q_0^2}, -\boldsymbol{q}) \rightarrow p(\sqrt{m^2 + p_0^2}, \boldsymbol{p}_0) + n(\sqrt{m^2 + p_0^2}, -\boldsymbol{p}_0), \qquad (4.59)$$

where M is the mass of the deuteron and m is the mass of either nucleon, we choose axes so that Oz is along $\boldsymbol{p}_0$ and Oy is along $\boldsymbol{q} \times \boldsymbol{p}_0$. The scattering angle θ is the angle (in the centre of mass frame) between the incoming photon and the outgoing proton. The component along Oz of the spin of the deuteron is m_d, and the final state has total spin s and a component of spin along Oz of m_s. To fix the photon within this scheme we must also define a second set of axes with Oz' along $\boldsymbol{q}$ and Oy' arbitrary. Let ϕ be the angle of the right-handed rotation about Oz that takes the axis Oy' into Oy. We then choose the transverse gauge, so that the polarisation 4-vector $\varepsilon^{(\mu)}$ of an incoming photon with helicity μ is defined by

$$\varepsilon^{(\pm 1)} = (0, \boldsymbol{\varepsilon}^{(\pm 1)}), \qquad (4.60)$$

where

$$\boldsymbol{\varepsilon}^{(\pm 1)} = \frac{1}{\sqrt{2}} (\mp \boldsymbol{e}_{x'} - i \boldsymbol{e}_{y'}) . \qquad (4.61)$$

The centre of mass photon energy q_0 and the magnitude of the centre of mass momentum of either outgoing nucleon p_0 are related to each other through the centre of mass total energy W by

$$q_0 + \sqrt{M^2 + q_0^2} = W = 2\sqrt{m^2 + q_0^2}. \qquad (4.62)$$

If q_0^{lab} is the laboratory frame photon energy, we have

$$q_0 = \frac{q_0^{\rm lab}}{\sqrt{1+\dfrac{2q_0^{\rm lab}}{M}}},$$
$$p_0 = \sqrt{\tfrac{1}{2}Mq_0^{\rm lab} - (m^2 - \tfrac{1}{4}M^2)}. \tag{4.63}$$

Instead of using the modified two nucleon current density $\tilde{\Lambda}$ defined in (4.45) it is convenient to follow Jaus and Woolcock [42] by using the electromagnetic current density j defined by

$$\tilde{\Lambda}(P'', P'; \boldsymbol{p}'', \boldsymbol{p}') = \frac{\sqrt{\sqrt{P''^2}\sqrt{P'^2}}}{2m} ej(P'', P'; \boldsymbol{p}'', \boldsymbol{p}'). \tag{4.64}$$

The centre of mass differential cross-section can then be obtained from the current density j by

$$\frac{d\sigma}{d\Omega}(q_0, \theta; sm_s, \mu m_d) = \left|T(q_0, \theta\phi; sm_s, \mu m_d)\right|^2, \tag{4.65}$$

where

$$T(q_0, \theta\phi; sm_s, \mu m_d) = -\sqrt{\frac{p_0}{q_0}\frac{\alpha M}{8\pi}}(2\pi)^{-6}$$
$$\times \int d^3(p'', p')\, \Phi^{(-)}_{sm_s}(\boldsymbol{p}_0; \boldsymbol{p}'')^* \varepsilon^{(\mu)} \cdot j(q_0, \boldsymbol{q}; \boldsymbol{p}'', \boldsymbol{p}') \phi_{m_d}(-\boldsymbol{q}; \boldsymbol{p}'), \tag{4.66}$$

where α is the fine structure constant, $\varepsilon^{(\mu)}$ is the polarisation 4-vector of the photon, $\Phi^{(-)}_{sm_s}$ is the outgoing wave function for the two-nucleon continuum state and ϕ_{m_d} is the wave function of the deuteron. By writing j in (4.66) as a function of q_0 and $\boldsymbol{q}$ rather than P'' and P' we indicate that we are dealing with the current density in the centre of mass frame, where the external momenta are

$$P'' = (W, \boldsymbol{0}), \quad P' = (\sqrt{M^2 + q_0^2}, -\boldsymbol{q}). \tag{4.67}$$

The connection with the notation of Partovi [37] can be established from equation (2.30) of Jaus and Woolcock [40]; the incoming scattering wave function $\Psi^{(-)}$ used by Partovi is the coordinate space equivalent of the function $\Phi^{(-)}$ introduced in (4.66), and is exactly our function $\Psi^{(-)}$ if one makes the replacement $\Omega_{\rm N} \to 1$ which is in turn related to the scattering wave function $\Phi^{(-)}(\boldsymbol{P}, \boldsymbol{p}_0; \boldsymbol{p})$ defined in (4.32) by

$$\Phi^{(-)}_{sm_s}(\boldsymbol{p}_0; \boldsymbol{p}'') = \sqrt{\frac{2m}{W}} \Phi^{(-)}(\boldsymbol{0}, \boldsymbol{p}_0; \boldsymbol{p}''). \tag{4.68}$$

We need to transform the deuteron wave function to the rest frame, which was performed in the last part of section III of Jaus and Woolcock [40]. The effect is to

introduce an effective 4-current density operator $\tilde{j}$ which is used when the deuteron wave function is calculated in the rest frame. After these steps (4.66) becomes

$$T(q_0,\theta\phi;sm_s,\mu m_d) = -\sqrt{\frac{p_0}{q_0}\frac{\alpha M}{8\pi}}(2\pi)^{-6}$$
$$\times\int d^3(p'',p')\,\Phi^{(-)}_{sm_s}(\boldsymbol{p}_0;\boldsymbol{p}'')^*\varepsilon^{(\mu)}\cdot\tilde{\boldsymbol{j}}(q_0,\boldsymbol{q};\boldsymbol{p}'',\boldsymbol{p}')\phi_{m_d}(\boldsymbol{0};\boldsymbol{p}'). \tag{4.69}$$

We now Fourier transform $\tilde{\boldsymbol{j}}(q_0,\boldsymbol{q};\boldsymbol{p}'',\boldsymbol{p}')$ twice, first by transforming the photon 3-momentum $\boldsymbol{q}$ into $\boldsymbol{\xi}$:

$$\tilde{\boldsymbol{j}}(q_0,\boldsymbol{\xi};\boldsymbol{p}'',\boldsymbol{p}') = (2\pi)^{-3}\int d^3q\,\exp(-i\boldsymbol{q}\cdot\boldsymbol{\xi})\tilde{\boldsymbol{j}}(q_0,\boldsymbol{q};\boldsymbol{p}'',\boldsymbol{p}'). \tag{4.70}$$

Note that when we transform $\boldsymbol{q}\leftrightarrow\boldsymbol{\xi}$ q_0 remains constant, so we are using the off mass-shell properties of the quantities on the right hand side. These continuations are available if the quantities are calculated from Feynman diagrams.

We then transform the difference of the internal relative momentum variables $\boldsymbol{p}''-\boldsymbol{p}'$ into an internal relative space coordinate $\boldsymbol{x}$. The other degree of freedom in $\boldsymbol{p}'',\boldsymbol{p}'$ is included as $\boldsymbol{p}'$ and becomes the gradient operator acting to the right, that is, on the deuteron wave function. We write this operator $\vec{\boldsymbol{\nabla}}_x$. Thus the electromagnetic current has a quasilocal form in coordinate space. Then we can use the form of $\varepsilon^{(\mu)}$ in (4.60) and (4.61) to write (4.66) as

$$T(q_0,\theta\phi;sm_s,\mu m_d) = \sqrt{\frac{p_0}{q_0}\frac{\alpha M}{8\pi}}$$
$$\times\int d^3\xi\,\exp i\boldsymbol{q}\cdot\boldsymbol{\xi}\int d^3x\,\Psi^{(-)}_{sm_s}(p_0;\boldsymbol{x})^*\varepsilon^{(\mu)}\cdot\tilde{\boldsymbol{j}}(q_0,\boldsymbol{\xi};\boldsymbol{x},\vec{\boldsymbol{\nabla}}_x)\psi_{m_d}(\boldsymbol{x}). \tag{4.71}$$

The deuteron wave function in coordinate space is written

$$\psi_{m_d}(\boldsymbol{x}) = \frac{1}{\sqrt{4\pi}}\frac{1}{x}\left(u(x)+S_{12}\tilde{w}(x)\right)\chi_{1m}, \tag{4.72}$$

where

$$S_{12} = 3(\boldsymbol{\sigma}_1\cdot\hat{\boldsymbol{x}})(\boldsymbol{\sigma}_2\cdot\hat{\boldsymbol{x}})-\boldsymbol{\sigma}_1\cdot\boldsymbol{\sigma}_2, \tag{4.73}$$

is the usual quadrupole operator,

$$\tilde{w}(x) = \sqrt{\frac{1}{8}}w(x) \tag{4.74}$$

and χ_{1m} is the spin wave function. Note that we have made here an implicit spinor reduction that replaces the 4-spinors introduced in (4.10) with 2-spinors, not only in the wave functions but also in the potential.

Making the standard expansion into electric and magnetic multipoles, equation (4.71) becomes

$$T(q_0, \theta\phi; sm_s, \mu m_d) = e^{i\mu\phi} t(q_0, \theta; sm_s, \mu m_d) \tag{4.75}$$

where

$$\begin{aligned} & t(q_0, \theta; sm_s, \mu m_d) \\ & = \sum_{\mathrm{L}} d^{(\mathrm{L})}_{\mu, m_s - m_d}(\theta) \left[\langle sm_s | \, E^{(\mathrm{L})} \, | m_d \rangle + \mu \, \langle sm_s | \, M^{(\mathrm{L})} \, | m_d \rangle \right], \end{aligned} \tag{4.76}$$

where

$$\begin{aligned} \langle sm_s | \, E^{(\mathrm{L})} \, | m_d \rangle &= \langle sm_s | \, E_1^{(\mathrm{L})} \, | m_d \rangle + \langle sm_s | \, E_2^{(\mathrm{L})} \, | m_d \rangle \, , \\ \langle sm_s | \, E_1^{(\mathrm{L})} \, | m_d \rangle &= \sqrt{\frac{p_0}{q_0} \frac{\alpha M}{8\pi}} \sqrt{\frac{2\pi(2L+1)}{L(L+1)}} i^{L+1} \int d^3x \, \Psi^{(-)}_{sm_s}(p_0; \boldsymbol{x})^* \\ & \times \int d^3\xi \, \left[\left(\frac{1}{q_0} \nabla_\xi \left(1 + \xi \frac{\partial}{\partial \xi} \right) \right) \left(j_{\mathrm{L}}(q_0 \xi) Y^{(\mathrm{L})}_{m_s - m_d}(\hat{\boldsymbol{\xi}}) \right) \right] \\ & \cdot \tilde{\jmath}(q_0, \boldsymbol{\xi}; \boldsymbol{x}, \nabla_x) \psi_{m_d}(\boldsymbol{x}), \\ \langle sm_s | \, E_2^{(\mathrm{L})} \, | m_d \rangle &= \sqrt{\frac{p_0}{q_0} \frac{\alpha M}{8\pi}} \sqrt{\frac{2\pi(2L+1)}{L(L+1)}} i^{L+1} \int d^3x \, \Psi^{(-)}_{sm_s}(p_0; \boldsymbol{x})^* \\ & \times \int d^3\xi \, q_0 j_{\mathrm{L}}(q_0 \xi) Y^{(\mathrm{L})}_{m_s - m_d}(\hat{\boldsymbol{\xi}}) \boldsymbol{\xi} \cdot \tilde{\boldsymbol{\jmath}}(q_0, \boldsymbol{\xi}; \boldsymbol{x}, \nabla_x) \psi_{m_d}(\boldsymbol{x}), \end{aligned} \tag{4.77}$$

$$\begin{aligned} \langle sm_s | \, M^{(\mathrm{L})} \, | m_d \rangle &= \sqrt{\frac{p_0}{q_0} \frac{\alpha M}{8\pi}} \sqrt{\frac{2\pi(2L+1)}{L(L+1)}} i^{L} \int d^3x \, \Psi^{(-)}_{sm_s}(p_0; \boldsymbol{x})^* \\ & \times \int d^3\xi \, j_{\mathrm{L}}(q_0 \xi) \boldsymbol{L}_\xi Y^{(\mathrm{L})}_{m_s - m_d}(\hat{\boldsymbol{\xi}}) \cdot \tilde{\boldsymbol{\jmath}}(q_0, \boldsymbol{\xi}; \boldsymbol{x}, \vec{\nabla}_x) \psi_{m_d}(\boldsymbol{x}). \end{aligned} \tag{4.78}$$

Here $\boldsymbol{x}$ is the vector separation of the nucleons, and $j_{\mathrm{L}}(q_0\xi)$ is a spherical Bessel function. The operator $\vec{\nabla}_x$ acts on the deuteron wave function as discussed above. The bound state and continuum two nucleon wave functions $\psi_{m_d}(\boldsymbol{x})$ and $\Phi^{(-)}_{sm_s}(\boldsymbol{p}_0; \boldsymbol{p}'')$ must be calculated using a nucleon-nucleon potential from the literature. We have performed calculations using the Bonn [2], Paris [3] and Moscow [4] potentials.

Making use of the Wigner-Eckart theorem and parity restrictions on the multipole amplitudes, we can obtain any multipole amplitude provided we have the $j = L-1, L, L+1$ components of the expressions for $\langle 11 | \, E^{(\mathrm{L})}, M^{(\mathrm{L})} \, | 0 \rangle$, $\langle 10 | \, E^{(\mathrm{L})}, M^{(\mathrm{L})} \, | -1 \rangle$ and $\langle 00 | \, E^{(\mathrm{L})}, M^{(\mathrm{L})} \, | -1 \rangle$.

Following Jaus and Woolcock [43], we now write expressions for some observables in terms of the multipole amplitudes. The differential cross-section is defined in

terms of the multipole amplitudes in equations (4.65), (4.66) and (4.75) through (4.78). For photons with a degree of linear polarisation Σ_l along Ox',

$$\frac{d\sigma}{d\Omega}(\theta\phi) = I_0(\theta)(1 + \Sigma_l \Sigma(\theta)\cos 2\phi), \tag{4.79}$$

where

$$I_0(\theta) = \tfrac{1}{3} \sum_{sm_s m_d} |t(\theta; sm_s, +1m_d)|^2 \tag{4.80}$$

is the unpolarised differential cross-section and

$$I_0(\theta)\Sigma(\theta) = -\tfrac{1}{3} \sum_{sm_s m_d} t(\theta; sm_s, +1m_d)\overline{t(\theta; sm_s, -1m_d)}. \tag{4.81}$$

The quantity $\Sigma(\theta)$ is the γ-asymmetry. The total cross-section in terms of the multipole amplitudes is

$$\begin{aligned}\sigma_t = {} & \frac{8\pi}{3} \sum_{\mathrm{L}} \frac{1}{2L+1} \\ & \times \left[\tfrac{1}{2}|\langle 10|E^{(\mathrm{L})}|0\rangle|^2 + \tfrac{1}{2}|\langle 10|M^{(\mathrm{L})}|0\rangle|^2 + |\langle 11|E^{(\mathrm{L})}|1\rangle|^2 + |\langle 11|M^{(\mathrm{L})}|1\rangle|^2 \right. \\ & + |\langle 11|E^{(\mathrm{L})}|0\rangle|^2 + |\langle 11|M^{(\mathrm{L})}|0\rangle|^2 + |\langle 11|E^{(\mathrm{L})}|-1\rangle|^2 + |\langle 11|M^{(\mathrm{L})}|-1\rangle|^2 \\ & + |\langle 10|E^{(\mathrm{L})}|-1\rangle|^2 + |\langle 10|M^{(\mathrm{L})}|-1\rangle|^2 \\ & \left. + |\langle 00|E^{(\mathrm{L})}|-1\rangle|^2 + |\langle 00|M^{(\mathrm{L})}|-1\rangle|^2\right].\end{aligned} \tag{4.82}$$

The other quantity which has been measured experimentally is the polarisation of the outgoing neutron. This is the same as measuring the analysing power for the radiative capture reaction $np \to d\gamma$ when polarised neutrons are incident on an unpolarised proton target. The polarisation of the outgoing neutron for $\gamma d \to pn$ and unpolarised photons and deuterons is

$$\begin{aligned}I_0(\theta)A_y^{(n)}(\theta) &= \frac{1}{6} \sum_{s'm_s' s''m_s'' \mu m_d} \langle s''m_s''|\sigma_y^{(n)}|s'm_s'\rangle\, t(\theta; s'm_s', \mu m_d)\overline{t(\theta; s''m_s'', \mu m_d)} \\ &= \frac{\sqrt{2}}{3} \sum_{m_d} \mathrm{Im}\left[t(\theta; 10, 1m_d)\{\overline{t(\theta; 11, 1m_d)} - \overline{t(\theta; 1-1, 1m_d)}\}\right. \\ &\qquad \left. t(\theta; 00, 1m_d)\{\overline{t(\theta; 11, 1m_d)} + \overline{t(\theta; 1-1, 1m_d)}\}\right].\end{aligned} \tag{4.83}$$

Chapter 5

Description of the Model

In this chapter we develop a theoretical model for deuteron photodisintegration. Section 5.1 concerns the modified current conservation (MCC) method. In section 5.2 the various diagrams which contribute to the electromagnetic current density are individually considered and calculated. This leads to expressions for the contributions to the electric and magnetic multipole amplitudes, which are displayed in section 5.3.

5.1 Current Conservation

In this section we consider the way in which the current conservation law for the electromagnetic 4-current density can be used in the calculation of that part of the electric multipole amplitude denoted by $E_1^{(\mathrm{L})}$ in (4.77). The amplitudes $E_2^{(\mathrm{L})}$ and $M^{(\mathrm{L})}$ are calculated directly from the effective 3-current density $\tilde{\boldsymbol{j}}$.

The current conservation law can be stated in momentum space using the two-nucleon electromagnetic current defined in (4.64) as

$$(P'' - P') \cdot \langle f(P'')| j(P'', P') |i(P')\rangle = 0, \tag{5.1}$$

where P', P'' are on mass-shell, and the photon momentum $q = P'' - P'$ is in general off mass-shell. This law is true on very general grounds, and must apply to the electromagnetic current obtained by evaluating the irreducible Feynman diagrams. However Arenhövel [44] and Jaus and Woolcock [45] have shown that there is no straightforward way in which this result can be applied to the calculation of the electric multipole amplitudes.

In order to see why this is so, we turn first to the expression in terms of the electromagnetic current density for the contribution to the electric multipoles known

as $E_1^{(\mathrm{L})}$, and defined in (4.77). This is the part of $E^{(\mathrm{L})}$ which we wish to calculate using current conservation. Integrating by parts we obtain

$$\begin{aligned}\langle sm_s|\, E_1^{(\mathrm{L})}\,|m_d\rangle &= -\sqrt{\frac{\alpha p_0 M}{2q_0}}\sqrt{\frac{2L+1}{2L(L+1)}}i^{L+1}\\ &\times\int d^3x\,\Psi^{(-)}_{sm_s}(p_0;\boldsymbol{x})^*\\ &\times\int d^3\xi\,\left(1+\xi\frac{d}{d\xi}\right)j_{\mathrm{L}}(q_0\xi)Y^{(\mathrm{L})}_{m_s-m_d}(\hat{\boldsymbol{\xi}})q_0\boldsymbol{\nabla}_\xi\cdot\tilde{\boldsymbol{j}}(q_0,\boldsymbol{\xi};\boldsymbol{x},\boldsymbol{\nabla}_x)\psi_{m_d}(\boldsymbol{x}).\end{aligned}\tag{5.2}$$

Using (4.62) the magnitude p_0 of the momentum of either outgoing nucleon satisfies

$$4\left(m^2+p_0^2\right)=\left(q_0+\sqrt{M^2+q_0^2}\right)^2.\tag{5.3}$$

Equation (5.1) remains true when we replace j by $\tilde{j}=(\tilde{\rho},\tilde{\boldsymbol{j}})$. Transforming to coordinate space, (5.1) becomes

$$\int d^3x\,\Psi^{(-)}_{sm_s}(\tilde{p}_0;\boldsymbol{x})\left(\boldsymbol{q}\cdot\tilde{\boldsymbol{j}}(q_0,\boldsymbol{q};\boldsymbol{x})-q_0\tilde{\rho}(q_0,\boldsymbol{q};\boldsymbol{x})\right)\psi_{m_d}(\boldsymbol{x})=0,\tag{5.4}$$

where the effective momentum $\tilde{p}_0$ is no longer p_0 but is given by

$$4\left(m^2+\tilde{p}_0^2\right)=\left(q_0+\sqrt{M^2+\boldsymbol{q}^2}\right)^2.\tag{5.5}$$

Fourier transforming (5.4) from $\boldsymbol{q}$ into $\boldsymbol{\xi}$ we obtain

$$\int d^3x\,\Psi^{(-)}_{sm_s}(\tilde{p}_0;\boldsymbol{x})\int d^3\xi\,\left(i\boldsymbol{\nabla}_\xi\cdot\tilde{\boldsymbol{j}}(q_0,\boldsymbol{\xi};\boldsymbol{x})-q_0\tilde{\rho}(q_0,\boldsymbol{\xi};\boldsymbol{x})\right)\exp(i\boldsymbol{q}\cdot\boldsymbol{\xi})\psi_{m_d}(\boldsymbol{x})=0,\tag{5.6}$$

In their work, Jaus and Woolcock [42, 7] assumed the equality

$$i\boldsymbol{\nabla}_\xi\cdot\tilde{\boldsymbol{j}}(q_0,\boldsymbol{\xi};\boldsymbol{x})\doteq q_0\tilde{\rho}(q_0,\boldsymbol{\xi};\boldsymbol{x}),\tag{5.7}$$

in order to rewrite (5.2) in terms of the charge density $\tilde{\rho}$. However, this equality cannot be deduced from (5.6), because of the dependence of $\tilde{p}_0$ on $\boldsymbol{q}$. This dependence could be removed by forcing the photon to be real, *i.e.* setting $q_0=|\boldsymbol{q}|$, but then (5.6) is not sufficiently general to deduce (5.7).

We will now describe the modified current conservation (MCC) method used in this calculation, as derived by Jaus and Woolcock [45]. We start by considering the convection current density. We wish to evaluate the divergence of the internal convection current

$$\int d^3x\,\Psi^{(-)}_{sm_s}(p_0;\boldsymbol{x})^*\boldsymbol{q}\cdot\boldsymbol{j}(\text{int.conv.};\boldsymbol{q},\boldsymbol{x})\psi_{m_d}(\boldsymbol{x}),\tag{5.8}$$

where

$$\boldsymbol{j}(\text{int.conv.};\boldsymbol{q},\boldsymbol{x}) = \frac{1}{2m}\left[\left(\hat{e}_1 \exp\left(\tfrac{1}{2}i\boldsymbol{q}\cdot\boldsymbol{x}\right) - \hat{e}_2 \exp\left(-\tfrac{1}{2}i\boldsymbol{q}\cdot\boldsymbol{x}\right)\right)\left(-i\,\overrightarrow{\boldsymbol{\nabla}}_x\right)\right.$$
$$\left. + \left(+i\,\overleftarrow{\boldsymbol{\nabla}}_x\right)\left(\hat{e}_1 \exp\left(\tfrac{1}{2}i\boldsymbol{q}\cdot\boldsymbol{x}\right) - \hat{e}_2 \exp\left(-\tfrac{1}{2}i\boldsymbol{q}\cdot\boldsymbol{x}\right)\right)\right] \tag{5.9}$$

and

$$\hat{e}_i = \tfrac{1}{2}(\mathbb{1} + \tau_{iz}). \tag{5.10}$$

Transforming to coordinate space the equations of motion (4.21) and (4.33) for the initial and final states we have

$$\left(-\frac{1}{m}\boldsymbol{\nabla}^2 + V(\boldsymbol{x})\right)\psi_{m_d}(\boldsymbol{x}) = \frac{1}{4m}(M^2 - 4m^2)\psi_{m_d}(\boldsymbol{x})$$
$$\left(-\frac{1}{m}\boldsymbol{\nabla}^2 + V(\boldsymbol{x})\right)\Psi^{(-)}_{sm_s}(p_0;\boldsymbol{x}) = \frac{p_0^2}{m}\Psi^{(-)}_{sm_s}(p_0;\boldsymbol{x}). \tag{5.11}$$

Note that the potential V and current density j are operators depending not only on $\boldsymbol{x}$ but also on $\boldsymbol{\nabla}_x$, though we have not written this explicitly.

We can then rewrite the divergence (5.8) in terms of the non-relativistic impulse approximation charge density

$$\rho^{(0)}(\boldsymbol{q};\boldsymbol{x}) = \hat{e}_1 \exp\left(\tfrac{1}{2}i\boldsymbol{q}\cdot\boldsymbol{x}\right) + \hat{e}_2 \exp\left(-\tfrac{1}{2}i\boldsymbol{q}\cdot\boldsymbol{x}\right) \tag{5.12}$$

as

$$\int d^3x\, \Psi^{(-)}_{sm_s}(p_0;\boldsymbol{x})^*\boldsymbol{q}\cdot\boldsymbol{j}(\text{int.conv.};\boldsymbol{q},\boldsymbol{x})\psi_{m_d}(\boldsymbol{x})$$
$$= q_0F(q_0)\int d^3x\, \Psi^{(-)}_{sm_s}(p_0;\boldsymbol{x})^*\rho^{(0)}(\boldsymbol{q};\boldsymbol{x})\psi_{m_d}(\boldsymbol{x})$$
$$-\int d^3x\, \left(V(\boldsymbol{x})\Psi^{(-)}_{sm_s}(p_0;\boldsymbol{x})^*\rho^{(0)}(\boldsymbol{q};\boldsymbol{x})\psi_{m_d}(\boldsymbol{x})\right.$$
$$\left. -\Psi^{(-)}_{sm_s}(p_0;\boldsymbol{x})^*\rho^{(0)}(\boldsymbol{q};\boldsymbol{x})V(\boldsymbol{x})\psi_{m_d}(\boldsymbol{x})\right), \tag{5.13}$$

where

$$q_0F(q_0) = \frac{p_0^2}{m} - \frac{M^2 - 4m^2}{4m} = \frac{q_0}{2m}\left(q_0 + \sqrt{M^2 + q_0^2}\right). \tag{5.14}$$

In a shorthand notation where $\doteq$ again denotes equality when a matrix element is taken,

$$\boldsymbol{q}\cdot\boldsymbol{j}(\text{int.conv.}) \doteq q_0F(q_0)\rho^{(0)} - \left[V,\rho^{(0)}\right]. \tag{5.15}$$

It follows from (5.2) and (5.13) that

$$\langle sm_s|\, E_1^{(L)}(\text{int.conv.})\,|m_d\rangle = -\sqrt{\frac{\alpha p_0 M}{2q_0}}\sqrt{\frac{2L+1}{2L(L+1)}}\,i^L$$
$$\times\left[F(q_0)\int d^3x\, \Psi^{(-)}_{sm_s}(p_0;\boldsymbol{x})^*F^{(L)}_{m_s-m_d}(q_0;\boldsymbol{x})\psi_{m_d}(\boldsymbol{x})\right.$$

$$-\frac{1}{q_0}\int d^3x\ \Big(V(\boldsymbol{x})\Psi^{(-)}_{sm_s}(p_0;\boldsymbol{x})^* F^{(\mathrm{L})}_{m_s-m_d}(q_0;\boldsymbol{x})\psi_{m_d}(\boldsymbol{x})$$
$$-\Psi^{(-)}_{sm_s}(p_0;\boldsymbol{x})^* F^{(\mathrm{L})}_{m_s-m_d}(q_0;\boldsymbol{x})V(\boldsymbol{x})\psi_{m_d}(\boldsymbol{x})\Big)\Big], \tag{5.16}$$

where

$$F^{(\mathrm{L})}_{m_s-m_d}(q_0;\boldsymbol{x}) = (\hat{e}_1 + (-1)^L\hat{e}_2)\left(1 + x\frac{d}{dx}\right) j_{\mathrm{L}}(\tfrac{1}{2}q_0x)Y^{(\mathrm{L})}_{m_s-m_d}(\hat{\boldsymbol{x}}). \tag{5.17}$$

By using the explicit form of the matrix element between the initial and final physical states of the divergence of the internal convection current density, we have obtained (5.13) and (5.16). These equations allow us to circumvent the difficulties associated with (5.6) described above, at least for the internal convection part of the current. The other pieces of the current density are dealt with below.

Both Partovi [37] and Arenhövel [44] make the unnecessary approximation

$$F(q_0) = 1 + \frac{q_0}{4m}, \tag{5.18}$$

(using $A = 2$ and $c_{\mathrm{RF}} = -1$ in the case of Arenhövel). In fact a good approximation is

$$F(q_0) = 1 + \frac{q_0 - B}{2m}, \tag{5.19}$$

where $B = 2m - M$ is the deuteron binding energy. To use (5.18) consistently it would be necessary to modify the commutator term on the right hand side of (5.13) (see Jaus and Woolcock [45]) but it is quite straightforward to use the exact relation (5.14).

We develop the modified current conservation (MCC) scheme by decomposing the effective electromagnetic current density into impulse approximation and meson exchange parts

$$\tilde{\boldsymbol{j}} = \tilde{\boldsymbol{j}}(\mathrm{IA}) + \boldsymbol{j}(\mathrm{ME}). \tag{5.20}$$

Note that the effective meson exchange current density is not significantly different from the actual meson exchange current density. We decompose the meson exchange part into one pion exchange, medium range and short range parts,

$$\tilde{\boldsymbol{j}} = \tilde{\boldsymbol{j}}(\mathrm{IA}) + \boldsymbol{j}(1\pi\mathrm{E}) + \boldsymbol{j}(\mathrm{MR}) + \boldsymbol{j}(\mathrm{SR}). \tag{5.21}$$

The last three terms on the right hand side of (5.21) are by analogy with nucleon-nucleon potentials, which usually have a recognisable one pion exchange part. The division of the remainder of the potential into short and medium range parts is

essentially arbitrary, but medium range effects are taken to include both two- and three-pion exchange interactions, including ρ and ω exchange and the σ interaction. We further decompose the impulse approximation part into a non-relativistic impulse approximation part and a relativistic correction part,

$$\tilde{\boldsymbol{j}}(\mathrm{IA}) = \boldsymbol{j}(\mathrm{NRIA}) + \tilde{\boldsymbol{j}}(\mathrm{RC}), \tag{5.22}$$

and then decompose the non-relativistic impulse approximation part into centre of mass, internal convection and spin parts,

$$\boldsymbol{j}(\mathrm{NRIA}) = \boldsymbol{j}(\mathrm{c.m.conv.}) + \boldsymbol{j}(\mathrm{int.conv.}) + \boldsymbol{j}(\mathrm{spin}). \tag{5.23}$$

It can easily be shown that for several of these parts the divergence of the electromagnetic current density will have no effect on the scattering amplitude. In particular, the divergence of the spin part of the current density is zero. The centre of mass convection part of the current density is proportional to $\boldsymbol{q}$, and since $\boldsymbol{\epsilon} \cdot \boldsymbol{q} = 0$ in the transverse gauge we have adopted it cannot contribute to the reaction amplitude.

We do not employ current conservation in dealing with certain other parts of current density. The electric and magnetic multipole amplitudes due to $\Delta(1232)$ exchange are calculated directly from diagrams in which a π or $\rho(770)$ meson is exchanged, and this part of the current density is exactly conserved. The amplitudes due to the relativistic correction to the impulse approximation are calculated directly from $\tilde{\boldsymbol{j}}(\mathrm{RC})$.

We use (5.15) to write

$$\begin{aligned}
&\boldsymbol{q} \cdot \boldsymbol{j}(\mathrm{int.conv.}) + \boldsymbol{q} \cdot \boldsymbol{j}(1\pi\mathrm{E}) + \boldsymbol{q} \cdot \boldsymbol{j}(\mathrm{MR}) + \boldsymbol{q} \cdot \boldsymbol{j}(\mathrm{SR}) \\
&\quad \doteq q_0 F(q_0)\rho^{(0)} + \left(\boldsymbol{q} \cdot \boldsymbol{j}(1\pi\mathrm{E}) - \left[V(1\pi E), \rho^{(0)}\right]\right) \\
&\quad + \left(\boldsymbol{q} \cdot \boldsymbol{j}(\mathrm{MR}) - \left[V(\mathrm{MR}), \rho^{(0)}\right]\right) + \left(\boldsymbol{q} \cdot \boldsymbol{j}(\mathrm{SR}) - \left[V(\mathrm{SR}), \rho^{(0)}\right]\right).
\end{aligned} \tag{5.24}$$

Partovi [37] neglects all but the first term on the right hand side, and replaces $F(q_0)$ with $1 + q_0/4m$. Since this approximation leads to quite reasonable results, the last three terms on the right hand side of (5.24) must involve significant cancellation. This suggests that even though the multipole amplitudes are being calculated using only $\rho^{(0)}$, meson exchange effects are being included implicitly via the wave functions.

The next order of approximation is to include also the second term on the right hand side of (5.24), which we shall call the 1πE mismatch correction. This is the approximation we use for calculations. From the standard expression for $V(1\pi\mathrm{E})$ to leading order, and the explicit expressions for $\boldsymbol{j}(1\pi\mathrm{E})$ to leading order contained in Jaus and Woolcock [42] as (2.12) and (2.13), it can easily be shown that (quoting equation (17) of Jaus and Woolcock [45])

$$\boldsymbol{q}\cdot\boldsymbol{j}(1\pi\mathrm{E}) = q_0\rho(1\pi\mathrm{E}) + [V(1\pi\mathrm{E}),\rho^{(0)}], \tag{5.25}$$

where $\rho(1\pi\mathrm{E})$ is defined in equation (18) of that paper. This result continues to hold if a monopole form factor is introduced at the πNN vertex when calculating $\boldsymbol{j}(1\pi\mathrm{E})$, $\rho(1\pi\mathrm{E})$ and $V(1\pi\mathrm{E})$.

The calculations of Jaus and Woolcock [42] show that the first term on the right hand side of (5.25) has only a small effect on the electric multipole amplitudes. From this we can see that the second term on the right hand side of (5.24) involves a strong cancellation. We assume there is a similar cancellation within the third and fourth terms on the right hand side of (5.24). We therefore expect that the sum of these last two terms is small compared with the terms within the parentheses, that is

$$\langle f|\,\boldsymbol{q}\cdot\boldsymbol{j}(\mathrm{MR}+\mathrm{SR})\,|i\rangle \approx \langle f|\,[V(\mathrm{MR}+\mathrm{SR}),\rho^{(0)}]\,|i\rangle\,. \tag{5.26}$$

Medium and short range effects on the electric multipole amplitudes are estimated in this fashion in nearly all calculations of deuteron photodisintegration. Since the medium range contributions are incompletely understood and the short-range contributions are unknown, we cannot use any more accurate method.

We now turn to a close examination of the second term on the right hand side of (5.24), which lies at the heart of the modified current conservation method. The internal convection part of the current obeys (5.15), which we now write

$$\langle f|\,\boldsymbol{q}\cdot\boldsymbol{j}(\mathrm{int.conv.})\,|i\rangle = q_0F(q_0)\,\langle f|\,\rho^{(0)}\,|i\rangle - \langle f|\,[V,\rho^{(0)}]\,|i\rangle\,, \tag{5.27}$$

where the initial and final states are calculated using the true potential V. Adding together (5.27), (5.26) and the equation obtained by taking matrix elements of both sides of (5.25), we have the practical form of the current conservation law

$$\begin{aligned}&\langle f|\,\boldsymbol{q}\cdot\boldsymbol{j}(\mathrm{int.conv.}+1\pi\mathrm{E}+\mathrm{MR}+\mathrm{SR})\,|i\rangle\\ &\quad\approx q_0F(q_0)\,\langle f|\,\rho^{(0)}\,|i\rangle + q_0\,\langle f|\,\rho(1\pi\mathrm{E})\,|i\rangle\,.\end{aligned} \tag{5.28}$$

We would like to calculate the right hand side of (5.28), but to do so we require initial and final wave functions obtained from the true potential V. However the nucleon-nucleon potential V_0 actually used for calculating wave functions may differ from the true nucleon-nucleon potential $V = V_0 + V_1$ by a small amount V_1 which is unknown. This might be due to charge dependent effects, since Jaus and Woolcock [42] have shown that the use of the correct charged and neutral pion masses and coupling constants has a surprisingly significant effect on the forward cross-section. Medium and short range effects are poorly understood and are parameterised in different ways in different potentials. Also the coupling constants and cutoff parameters used in NN potentials are underdetermined by the data on which they are based. For instance Haidenbauer *et al* [48] give several different variants of the Bonn potential; each of these is claimed to give acceptable fits to nucleon-nucleon data, but their values for $f_{\pi NN}$ and Λ_N are significantly different.

Only the initial and final states obtained from V_0 are available for the calculation of matrix elements. The counterpart of (5.27) is

$$\langle f_0 |\, \boldsymbol{q} \cdot \boldsymbol{j}(\text{int.conv.}) \,| i_0 \rangle = q_0 F(q_0) \langle f_0 |\, \rho^{(0)} \,| i_0 \rangle - \langle f_0 |\, [V_0, \rho^{(0)}] \,| i_0 \rangle \,, \tag{5.29}$$

where the initial and final states are calculated using V_0. Since the left hand sides of (5.27) and (5.29) are small ($O(m^{-1})$) and approximately equal, their difference will be negligible. Hence

$$q_0 F(q_0) \langle f |\, \rho^{(0)} \,| i \rangle \approx q_0 F(q_0) \langle f_0 |\, \rho^{(0)} \,| i_0 \rangle + \langle f |\, [V, \rho^{(0)}] \,| i \rangle - \langle f_0 |\, [V_0, \rho^{(0)}] \,| i_0 \rangle \,. \tag{5.30}$$

Combining this with (5.28) leads to

$$\begin{aligned} \langle f |\, \boldsymbol{q} \cdot \boldsymbol{j}(\text{int.conv.} + 1\pi\text{E} + \text{MR} + \text{SR}) \,| i \rangle &\approx q_0 F(q_0) \langle f_0 |\, \rho^{(0)} \,| i_0 \rangle \\ + q_0 \langle f |\, \rho(1\pi\text{E}) \,| i \rangle + \langle f |\, [V, \rho^{(0)}] \,| i \rangle &- \langle f_0 |\, [V_0, \rho^{(0)}] \,| i_0 \rangle \,. \end{aligned} \tag{5.31}$$

The small difference between the third and fourth terms of (5.31) derives from the correction V_1 to the potential and the consequent difference between the wave functions obtained from V and V_0. We wish somehow to take account of this difference. Jaus and Woolcock [42, 43] have shown that deuteron photodisintegration observables are insensitive to short range (≤ 0.8 fm) effects, so the main contribution to this difference can be expected to come from 1πE. We therefore write (5.31) as

$$\langle f|\, \boldsymbol{q}\cdot\boldsymbol{j}(\text{int.conv.}+1\pi\text{E}+\text{MR}+\text{SR})\,|i\rangle \approx q_0 F(q_0)\,\langle f_0|\,\rho^{(0)}\,|i_0\rangle$$
$$+\langle f|\,\boldsymbol{q}\cdot\boldsymbol{j}(1\pi\text{E})\,|i\rangle - \langle f_0|\,[V_0(1\pi\text{E}),\rho^{(0)}]\,|i_0\rangle\,, \tag{5.32}$$

where $V_0(1\pi\text{E})$ is the one pion exchange part of V_0, *i.e.* the one pion exchange part of the nucleon-nucleon potential used for calculating wave functions. In order to parameterise the unknown matrix element $\langle f|\,\boldsymbol{q}\cdot\boldsymbol{j}(1\pi\text{E})\,|i\rangle$ we need to introduce an effective current density $\boldsymbol{j}_{\text{eff}}(1\pi\text{E})$ which satisfies

$$\langle f|\,\boldsymbol{q}\cdot\boldsymbol{j}(1\pi\text{E})\,|i\rangle \approx \langle f_0|\,\boldsymbol{q}\cdot\boldsymbol{j}_{\text{eff}}(1\pi\text{E})\,|i_0\rangle\,. \tag{5.33}$$

The right hand side of (5.32) is then expressed entirely in terms of wave functions calculated from the assumed potential V_0. The effective current density $\boldsymbol{j}_{\text{eff}}(1\pi\text{E})$ is characterised by the parameters $f_{\pi\text{NN}}$ and Λ_{N} which can only be obtained by fitting to deuteron photodisintegration data, and only by such a fit can one judge whether the approximation (5.33) is reasonable. Examination of the mismatch between the parameters needed to fit deuteron photodisintegration observables and those used in the NN potential provides a measure of how realistic the NN potential is.

5.2 Contributions to the Electromagnetic Current Density

The electromagnetic current defined in (4.64) is in principle calculated by summing all the irreducible Feynman diagrams for the process (4.37). In practice we limit ourselves to those diagrams in figure 5.

5.2.1 Impulse Approximation

The impulse approximation is represented by figure 5 (a), in which one nucleon is a spectator to the photon's absorption by the other nucleon. Figure 5 represents the contribution we shall call $\tilde{\boldsymbol{j}}_1(\text{IA})$; there is an analogous diagram where the other nucleon absorbs the photon, which leads to the contribution we call $\tilde{\boldsymbol{j}}_2(\text{IA})$.

The first two terms on the right hand side of (5.23) have been considered in section 5.1. The internal convection current $\tilde{\boldsymbol{j}}(\text{int.conv.})$ is given in coordinate space in (5.9); in momentum space it is

$$\tilde{\boldsymbol{j}}_1(\text{int.conv.};q_0,\boldsymbol{q};\boldsymbol{p}'',\boldsymbol{p}') \doteq \frac{1}{m}(2\pi)^3\delta^{(3)}(\boldsymbol{p}''-\boldsymbol{p}'-\tfrac{1}{2}\boldsymbol{q})\hat{e}_1\boldsymbol{p}', \tag{5.34}$$

where $\doteq$ as usual denotes equality when a matrix element is taken, and $\hat{e}_i$ is defined

in (5.10). The spin part of the current in momentum space is

$$\boldsymbol{j}_1(\text{spin}; q_0, \boldsymbol{q}; \boldsymbol{p}'', \boldsymbol{p}') \doteq \frac{1}{2m}(2\pi)^3\delta^{(3)}(\boldsymbol{p}'' - \boldsymbol{p}' - \tfrac{1}{2}\boldsymbol{q})(\hat{e}_1 + \hat{\kappa}_1)i\boldsymbol{\sigma}_1 \times \boldsymbol{q}, \tag{5.35}$$

where

$$\hat{\kappa}_i = \tfrac{1}{2}(\kappa_S \mathbb{1} + \kappa_V \tau_{iz}). \tag{5.36}$$

We require the impulse approximation $\tilde{\boldsymbol{j}}(\text{IA})$ to the effective current density, whose matrix element is to be taken between rest frame wave functions. This calculation is performed in section 3 of Jaus and Woolcock [40], and using equation (3.25) from that work we can obtain $\tilde{\boldsymbol{j}}$. In practice the only part of $\tilde{\boldsymbol{j}}$ which differs significantly from $\boldsymbol{j}$ is $\tilde{\boldsymbol{j}}(\text{IA})$. $\tilde{\boldsymbol{j}}(\text{IA})$ has been evaluated up to $O(m^{-3})$ in the centre of mass frame by Jaus and Woolcock [42], for convenience we quote the relativistic correction part of it here:

$$\begin{aligned}
\tilde{\boldsymbol{j}}_1(\text{RC}; q_0, \boldsymbol{q}; \boldsymbol{p}'', \boldsymbol{p}') \doteq & -\frac{1}{2m}(2\pi)^3\delta^{(3)}(\boldsymbol{p}'' - \boldsymbol{p}' - \tfrac{1}{2}\boldsymbol{q}) \\
& \times \Bigg[(\hat{e}_1 + \hat{\kappa}_1)i\boldsymbol{\sigma}_1 \times \boldsymbol{q}\frac{q_0\hat{\kappa}_1}{2m}(\boldsymbol{q} + 2i\boldsymbol{\sigma}_1 \times \boldsymbol{p}') \\
& \frac{\hat{e}_1}{2m^2}(2\boldsymbol{p}'^2\boldsymbol{p}' + \boldsymbol{q}\cdot\boldsymbol{p}'i\boldsymbol{\sigma}_1 \times \boldsymbol{p}' + \boldsymbol{p}'^2 i\boldsymbol{\sigma}_1 \times \boldsymbol{q}) \\
& -\frac{\hat{\kappa}_1}{2m^2}i\boldsymbol{q} \times \boldsymbol{p}'\boldsymbol{\sigma}_1 \times \boldsymbol{p}' - \frac{\hat{e}_1}{4m^2}\boldsymbol{p}'i\boldsymbol{q}\cdot((\boldsymbol{\sigma}_1 - \boldsymbol{\sigma}_2) \times \boldsymbol{p}')\Bigg]
\end{aligned} \tag{5.37}$$

We can extract three pieces of $\tilde{\boldsymbol{j}}(\text{RC})$: one of $O(m^{-2})$

$$\begin{aligned}
&\tilde{\boldsymbol{j}}_1(\text{RC}, O(m^{-2}); q_0, \boldsymbol{q}; \boldsymbol{p}'', \boldsymbol{p}') \\
&\quad = -\frac{1}{4m^2}q_0\hat{\kappa}_1(2\pi)^3\delta^{(3)}(\boldsymbol{p}'' - \boldsymbol{p}' - \tfrac{1}{2}\boldsymbol{q})(\boldsymbol{q} + 2i\boldsymbol{\sigma}_1 \times \boldsymbol{p}'),
\end{aligned} \tag{5.38}$$

one due to magnetic moment coupling, of $O(m^{-3})$,

$$\begin{aligned}
&\tilde{\boldsymbol{j}}_1(\text{RC}, O(m^{-3}), \text{m.m.}; q_0, \boldsymbol{q}; \boldsymbol{p}'', \boldsymbol{p}') \\
&\quad = -\frac{1}{4m^3}\hat{\kappa}_1(2\pi)^3\delta^{(3)}(\boldsymbol{p}'' - \boldsymbol{p}' - \tfrac{1}{2}\boldsymbol{q})i\boldsymbol{q} \times \boldsymbol{p}'\boldsymbol{\sigma}_1 \cdot \boldsymbol{p}',
\end{aligned} \tag{5.39}$$

and one due to charge coupling, of $O(m^{-3})$,

$$\begin{aligned}
\tilde{\boldsymbol{j}}_1(\text{RC}, O(m^{-3}), \text{ch.}; q_0, \boldsymbol{q}; \boldsymbol{p}'', \boldsymbol{p}') = & -\frac{1}{4m^3}\hat{e}_1(2\pi)^3\delta^{(3)}(\boldsymbol{p}'' - \boldsymbol{p}' - \tfrac{1}{2}\boldsymbol{q}) \\
& \times \left\{-2\boldsymbol{p}'^2\boldsymbol{p}' - \boldsymbol{p}'^2 i\boldsymbol{\sigma}_1 \times \boldsymbol{q} - \boldsymbol{p}'\cdot\boldsymbol{q}i\boldsymbol{\sigma}_1 \times \boldsymbol{p}' + \tfrac{1}{2}\boldsymbol{p}'\right\}.
\end{aligned} \tag{5.40}$$

The charge coupling term has a negligible contribution to the multipole amplitudes. The magnetic moment coupling terms are proportional to either κ_V or κ_S. Since $\kappa_S \approx -0.012$ is much smaller in magnitude than $\kappa_V \approx 3.706$ we can neglect terms $O(m^{-3}\kappa_S)$. This means that the only amplitudes proportional to κ_S which need to be taken into account are those of $O(m^{-2})$ with a singlet final state which contribute to $E^{(1)}$. Of the amplitudes proportional to κ_V we consider at $O(m^{-2})$ those contributing to the multipoles $E^{(1)}$, $M^{(2)}$ and $E^{(3)}$ with triplet final states and $M^{(1)}$ and $E^{(2)}$ with singlet final states, and at $O(m^{-3})$ those contributing to $E^{(1)}$ with triplet final states and $M^{(1)}$ with singlet final states. These amplitudes are given in section 5.3.

5.2.2 One Pion Exchange Without a $\Delta(1232)$ Intermediate

The pion exchange contribution to the electromagnetic current is represented by figures 5 (b) (the pion current contribution, which we shall denote πC) and (c) (the seagull contribution, which we shall denote SG). Sections IV through VI of Jaus and Woolcock [40] contain an extensive treatment of pion exchange effects. As discussed in that work, the deuteron photodisintegration data favour pseudovector coupling rather than pseudoscalar, although they are identical to leading order.

It is important to note that the exchange of a neutral pion makes no contribution at leading order to either of these diagrams. This is obvious in the case of the pion current, since $V(\gamma\pi^0\pi^0) = 0$. In the case of the seagull diagram we have $V(\gamma\pi^0 pp) = V(\gamma\pi^0 nn) = 0$. Thus any contribution to the reaction amplitude is due entirely (at leading order) to the exchange of charged pions. At higher orders the small difference in mass and coupling constant between charged and neutral pions has a negligible effect. Accordingly we use the charged pion mass $m_{\pi^\pm}$ and coupling constant $f_{\pi^- pn} = f_{\pi^+ np}$ throughout when calculating $\boldsymbol{j}(1\pi\mathrm{E})$. This has a surprisingly significant effect, since the mismatch between the pion mass used in $\boldsymbol{j}(1\pi\mathrm{E})$ and that used in $V_0(1\pi\mathrm{E})$ affects the variation with energy of the forward cross-section.

All the 1πE operators contain denominators of the form $m_\pi^2 + (\boldsymbol{p} \pm \frac{1}{2}\boldsymbol{q})^2 - \frac{1}{4}q_0^2$ from the pion propagator. If an expansion is made in powers of $\boldsymbol{q}$ the terms will

contain factors $\tilde{\omega}^{-2n}$, where n is a positive integer,

$$\tilde{\omega}^2 = \tilde{m}_\pi^2 + \boldsymbol{p}^2 \tag{5.41}$$

and $\tilde{m}_\pi$ is an effective "energy dependent pion mass", defined by

$$\tilde{m}_\pi^2 = m_\pi^2 - \tfrac{1}{4}q_0^2, \tag{5.42}$$

which we have used throughout this calculation.

In order to evaluate the electric and magnetic multipoles we must integrate expressions derived from the current density over x. However, some of these integrals are logarithmically divergent when point vertices are used. The physical reason for this is that the structure of the strong vertices is being neglected. To correct for this a monopole form factor $(\Lambda_{\rm N}^2 - m_\pi^2)/(\Lambda_{\rm N}^2 - k^2)$ is included at the πNN and $\gamma\pi$NN vertices. The 1πE operators then depend on an effective monopole cutoff

$$\tilde{\Lambda}_{\rm N}^2 = \Lambda_{\rm N}^2 - \tfrac{1}{4}q_0^2. \tag{5.43}$$

In addition, the inclusion of a cutoff destroys the current conservation law, unless new terms are added to the πC contribution to the current density. This leads to the replacements (see pp. 686–7 of Jaus and Woolcock [42])

$$\omega^{-2n}(\boldsymbol{p}) \to \left(1 - (\Lambda_{\rm N}^2 - m_\pi^2)\frac{\partial}{\partial \Lambda_{\rm N}^2}\right)(\omega^{-2n}(\boldsymbol{p}) - \Omega^{-2n}(\boldsymbol{p})), \tag{5.44}$$

where $\omega(\boldsymbol{p})$ is defined in (5.41) and

$$\Omega^2(\boldsymbol{p}) = \Lambda_{\rm N}^2 + \boldsymbol{p}^2. \tag{5.45}$$

The introduction of a form factor also leads to a change in the 1πE nucleon-nucleon potential: the leading part of the 1πE NN potential becomes

$$\tilde{V}_\pi(\boldsymbol{p}) = -\frac{f_{\pi{\rm NN}}^2}{m_\pi^2}\boldsymbol{\tau}_1 \cdot \boldsymbol{\tau}_2 \frac{\boldsymbol{\sigma}_1 \cdot \boldsymbol{p}\boldsymbol{\sigma}_2 \cdot \boldsymbol{p}}{\omega^2(\boldsymbol{p})}\frac{(\Lambda_{\rm N}^2 - m_\pi^2)^2}{\Omega^4(\boldsymbol{p})}, \tag{5.46}$$

and the various forms of the Bonn potential [2] are modified in just this way. The Paris potential [3], on the other hand, uses a different type of cutoff procedure. In our MCC scheme of calculation we modify $\boldsymbol{j}_{\rm eff}(1\pi{\rm E})$ by means of a monopole form factor with parameter $\Lambda_{\rm N}$. However $V_0(1\pi{\rm E})$, the assumed potential defined in (5.32), is exactly the 1πE part of the potential being used.

For the current density due to the seagull and pion current diagrams to leading order we have

$$
\begin{aligned}
\boldsymbol{j}(\mathrm{SG};P'',P';\boldsymbol{p}'',\boldsymbol{p}') &\doteq \frac{f^2_{\pi\mathrm{NN}}}{m_\pi^2} i(\boldsymbol{\tau}_1\times\boldsymbol{\tau}_2)_z \\
&\times\left[\frac{\boldsymbol{\sigma}_1\boldsymbol{\sigma}_2\cdot(\boldsymbol{p}-\frac{1}{2}\boldsymbol{q})}{\omega^2(\boldsymbol{p}-\frac{1}{2}\boldsymbol{q})-\frac{1}{4}q_0^2}+\frac{\boldsymbol{\sigma}_2\boldsymbol{\sigma}_1\cdot(\boldsymbol{p}+\frac{1}{2}\boldsymbol{q})}{\omega^2(\boldsymbol{p}+\frac{1}{2}\boldsymbol{q})-\frac{1}{4}q_0^2}\right], \\
\boldsymbol{j}(\pi\mathrm{C};P'',P';\boldsymbol{p}'',\boldsymbol{p}') &\doteq -2\frac{f^2_{\pi\mathrm{NN}}}{m_\pi^2} i(\boldsymbol{\tau}_1\times\boldsymbol{\tau}_2)_z\boldsymbol{p} \\
&\times\frac{\boldsymbol{\sigma}_1\cdot(\boldsymbol{p}+\frac{1}{2}\boldsymbol{q})\boldsymbol{\sigma}_2\cdot(\boldsymbol{p}-\frac{1}{2}\boldsymbol{q})}{[\omega^2(\boldsymbol{p}+\frac{1}{2}\boldsymbol{q})-\frac{1}{4}q_0^2][\omega^2(\boldsymbol{p}-\frac{1}{2}\boldsymbol{q})-\frac{1}{4}q_0^2]},
\end{aligned}
\tag{5.47}
$$

where $\omega(\boldsymbol{k})$ is defined in (5.41) and $\boldsymbol{p}=\boldsymbol{p}''-\boldsymbol{p}'$. The symbol $\doteq$ denotes approximate equality when a matrix element is taken of each side, by analogy with the symbol $\doteq$ defined after (4.49). Except for the appearance of the term $-\frac{1}{4}q_0^2$ they are well known. After expanding to second order in $\boldsymbol{q}$ the expressions in coordinate space contain the functions $F_n(m_\pi x)=(m_\pi x)^n Y_0(m_\pi x)$, where Y_0 is defined in (5.113). Inclusion of the form factor leads to the replacement

$$
F_n(m_\pi x)\to F_n(m_\pi x)-F_n(\Lambda_{\mathrm{N}}x)+\frac{\Lambda_{\mathrm{N}}^2-m_\pi^2}{2\Lambda_{\mathrm{N}}}\frac{\partial F_n(\Lambda_{\mathrm{N}}x)}{\Lambda_{\mathrm{N}}},
\tag{5.48}
$$

after which we make the replacements $m_\pi\to\tilde{m}_\pi$ and $\Lambda_{\mathrm{N}}\to\tilde{\Lambda}_{\mathrm{N}}$.

We now wish to apply the modified current conservation scheme to the calculation of the $1\pi\mathrm{E}$ mismatch correction defined in section 5.1. To leading order

$$
\begin{aligned}
\boldsymbol{q}\cdot\boldsymbol{j}(1\pi\mathrm{E}) &= \tfrac{1}{4}q_0 i(\boldsymbol{\tau}_1\times\boldsymbol{\tau}_2)_z\left(\exp(\tfrac{1}{2}i\boldsymbol{q}\cdot\boldsymbol{x})-\exp(\tfrac{1}{2}-i\boldsymbol{q}\cdot\boldsymbol{x})\right) \\
&\times\left(F_{\mathrm{II}}(1\pi\mathrm{E})\boldsymbol{\sigma}_1\cdot\boldsymbol{\sigma}_2+F_{\mathrm{IV}}(1\pi\mathrm{E})S_{12}\right),
\end{aligned}
\tag{5.49}
$$

where S_{12} is defined in (4.73). After applying the form factor modification described above we have

$$
\begin{aligned}
F_{\mathrm{II}}(1\pi\mathrm{E}) &= \frac{4}{3q_0}\frac{f^2_{\pi\mathrm{NN}}}{4\pi}m_\pi^{-2} \\
&\times\left\{\tilde{m}_\pi^3 Y_0(\tilde{m}_\pi x)-\tilde{\Lambda}_{\mathrm{N}}^3 Y_0(\tilde{\Lambda}_{\mathrm{N}}x)+\tfrac{1}{2}(\Lambda_{\mathrm{N}}^2-m_\pi^2)\tilde{\Lambda}_{\mathrm{N}}(2-\tilde{\Lambda}_{\mathrm{N}}x)Y_0(\tilde{\Lambda}_{\mathrm{N}}x)\right\} \\
F_{\mathrm{IV}}(1\pi\mathrm{E}) &= \frac{4}{3q_0}\frac{f^2_{\pi\mathrm{NN}}}{4\pi}m_\pi^{-2} \\
&\times\left\{\tilde{m}_\pi^3 Y_2(\tilde{m}_\pi x)-\tilde{\Lambda}_{\mathrm{N}}^3 Y_2(\tilde{\Lambda}_{\mathrm{N}}x)-\tfrac{1}{2}(\Lambda_{\mathrm{N}}^2-m_\pi^2)\tilde{\Lambda}_{\mathrm{N}}^2 x Y_1(\tilde{\Lambda}_{\mathrm{N}}x)\right\},
\end{aligned}
\tag{5.50}
$$

where the functions Y_i are defined in (5.113).

We now write to leading order the $1\pi\mathrm{E}$ part of the potentials we use. For the Paris potential [3] this contribution is easily identified as

$$\tfrac{1}{4}(3+\boldsymbol{\tau}_1\cdot\boldsymbol{\tau}_2)f(x)g_1^a\left\{Y_0(m_{\pi^0}x)\boldsymbol{\sigma}_1\cdot\boldsymbol{\sigma}_2+Y_2(m_{\pi^0}x)S_{12}\right\}$$
$$+\tfrac{1}{4}(1-\boldsymbol{\tau}_1\cdot\boldsymbol{\tau}_2)f(x)g_0^a\left\{Y_0(m_{\bar{\pi}}x)\boldsymbol{\sigma}_1\cdot\boldsymbol{\sigma}_2+Y_2(m_{\bar{\pi}}x)S_{12}\right\}, \tag{5.51}$$

which is the usual 1πE potential with a cutoff function

$$f(x)=(1+(px)^{-\beta})^{-1},\quad p=1.25\,\mathrm{fm}^{-1},\ \beta=10. \tag{5.52}$$

The other constants are given in [3]. Note that the Paris potential uses two pion masses. It follows that

$$\left[V(\text{Paris; local } 1\pi\text{E}),\rho^{(0)}\right]=\tfrac{1}{4}q_0 i(\boldsymbol{\tau}_1\times\boldsymbol{\tau}_2)_z(\exp(\tfrac{1}{2}i\boldsymbol{q}\cdot\boldsymbol{x})-\exp(-\tfrac{1}{2}i\boldsymbol{q}\cdot\boldsymbol{x}))$$
$$\times\left(F_{\mathrm{II}}(\text{Paris})\boldsymbol{\sigma}_1\cdot\boldsymbol{\sigma}_2+F_{\mathrm{IV}}(\text{Paris})S_{12}\right), \tag{5.53}$$

where

$$F_{\mathrm{II}}(\text{Paris})=q_0^{-1}f(x)\left(g_1^aY_0(m_{\pi^0}x)-g_0^aY_0(m_{\bar{\pi}}x)\right)$$
$$F_{\mathrm{IV}}(\text{Paris})=q_0^{-1}f(x)\left(g_1^aY_2(m_{\pi^0}x)-g_0^aY_2(m_{\bar{\pi}}x)\right). \tag{5.54}$$

There are several slightly different forms of the Bonn potential; we have used the potential described as potential B in Table A.3, appendix A.3 of reference [2]. This is an energy independent quasilocal coordinate space potential. When this potential is used instead of the Paris potential, equation (5.54) is replaced by

$$F_{\mathrm{II}}(\text{Bonn})=\tfrac{1}{3}q_0^{-1}\frac{g^2}{4\pi}\left(\frac{m_{\bar{\pi}}}{m}\right)^2 m_{\bar{\pi}}$$
$$\times\left\{Y_0(m_{\bar{\pi}}x)-\frac{\Lambda_{\mathrm{N}}^{\mathrm{B}}}{m_{\bar{\pi}}}Y_0(\Lambda_{\mathrm{N}}^{\mathrm{B}}x)-\frac{1}{2}\left(\frac{\Lambda_{\mathrm{N}}^{\mathrm{B}\,2}}{m_{\bar{\pi}}^2}-1\right)\frac{\Lambda_{\mathrm{N}}^{\mathrm{B}}}{m_{\bar{\pi}}}\Lambda_{\mathrm{N}}^{\mathrm{B}}xY_0(\Lambda_{\mathrm{N}}^{\mathrm{B}}x)\right\}$$
$$F_{\mathrm{IV}}(\text{Bonn})=\tfrac{1}{3}q_0^{-1}\frac{g^2}{4\pi}\left(\frac{m_{\bar{\pi}}}{m}\right)^2 m_{\bar{\pi}}$$
$$\times\left\{Y_2(m_{\bar{\pi}}x)-\left(\frac{\Lambda_{\mathrm{N}}^{\mathrm{B}}}{m_{\bar{\pi}}}\right)^3Y_2(\Lambda_{\mathrm{N}}^{\mathrm{B}}x)-\frac{1}{2}\left(\frac{\Lambda_{\mathrm{N}}^{\mathrm{B}\,2}}{m_{\bar{\pi}}^2}-1\right)\frac{\Lambda_{\mathrm{N}}^{\mathrm{B}}}{m_{\bar{\pi}}}\Lambda_{\mathrm{N}}^{\mathrm{B}}xY_1(\Lambda_{\mathrm{N}}^{\mathrm{B}}x)\right\}, \tag{5.55}$$

where $m_{\bar{\pi}}=138.03$ MeV, $\Lambda_{\mathrm{N}}^{\mathrm{B}}=2000$ MeV and

$$\frac{1}{3}\frac{g^2}{4\pi}\left(\frac{m_{\bar{\pi}}}{m}\right)^2 m_{\bar{\pi}}=14.81572\,\mathrm{MeV}. \tag{5.56}$$

Defining the functions F_{II} and F_{IV} as

$$F_{\mathrm{II,IV}}=F_{\mathrm{II,IV}}(1\pi\mathrm{E})-F_{\mathrm{II,IV}}(\text{potential}), \tag{5.57}$$

where the potential is Paris or Bonn, we have

$$(F_{\mathrm{II}}\boldsymbol{\sigma}_1\cdot\boldsymbol{\sigma}_2+F_{\mathrm{IV}}S_{12})(u\mathbb{1}+\tilde{w}S_{12})\chi_{m_d}^{(1)}=(U\mathbb{1}+\tilde{W}S_{12})\chi_{m_d}^{(1)}, \tag{5.58}$$

where

$$U = F_{\rm II} u + 8 F_{\rm IV} \tilde{w}$$
$$\tilde{W} = F_{\rm II} \tilde{w} + F_{\rm IV}(u - 2\tilde{w}), \tag{5.59}$$

and $\tilde{w}(x)$ is defined in (4.74). From this we determine the contribution to the amplitudes $E_1^{(L)}$ for $L = 1, 3, 5$ arising from the 1πE mismatch correction.

We also calculate to leading order the amplitudes $M^{(1)}$ from the terms of $\boldsymbol{j}(1\pi\mathrm{E})$ linear in $\boldsymbol{q}$ and the amplitudes $M^{(2)}$ and $E_2^{(1)}$ from the terms in $\boldsymbol{j}(1\pi\mathrm{E})$ which are quadratic in $\boldsymbol{q}$. At $O(m^{-1})$ we use the parts of $\boldsymbol{j}(1\pi\mathrm{E})$ which are independent of or proportional to $\boldsymbol{q}$. The part of $\boldsymbol{j}(1\pi\mathrm{E})$ which is independent of $\boldsymbol{q}$ is used to calculate the amplitudes $E_1^{(1)}$ from the electric dipole operator

$$\boldsymbol{D}(q_0; \boldsymbol{x}, \boldsymbol{\nabla}_x) = -i \frac{1}{q_0} \boldsymbol{j}(q_0, 0; \boldsymbol{x}, \boldsymbol{\nabla}_x). \tag{5.60}$$

A convenient way to express $\boldsymbol{D}$ is in terms of the operators $\boldsymbol{D}_i$ defined in (4.2) of Jaus and Woolcock [42]. $\boldsymbol{D}$ is then written in terms of functions G_i. As mentioned above equation (5.117), the terms in $G_{\rm II}$ and $G_{\rm IV}$ proportional to q_0 (which are of leading order) are omitted under the modified current conservation scheme.

The part of $\boldsymbol{j}(1\pi\mathrm{E})$ of $O(m^{-1})$ which is linear in $\boldsymbol{q}$ leads to the 1πE contribution to the magnetic dipole moment operator

$$\boldsymbol{M}(q_0; \boldsymbol{x}, \boldsymbol{\nabla}_x) = -\tfrac{1}{2} i \boldsymbol{\nabla}_q \times \boldsymbol{j}(q_0, \boldsymbol{q}; \boldsymbol{x})\Big|_{\mathbf{q}=\mathbf{0}}. \tag{5.61}$$

The expression for $\boldsymbol{M}$ at $O(m^{-1})$ is given in equation (4.15) of Jaus *et al* [34]. Note that the expression given in equation (4.1) of Jaus and Woolcock [7] contains misprints.

5.2.3 One Pion Exchange With a $\Delta(1232)$ Intermediate

Figure 5 (d) is the only diagram which contributes to deuteron photodisintegration. The analogous diagram in which the pion is exchanged first gives no contribution when the initial state has isospin zero, as does a deuteron. Figure 5 (d) actually represents two diagrams, corresponding to the absorption of the photon on one nucleon or the other.

Compared with one pion exchange without $\Delta(1232)$ intermediates our understanding of one pion exchange with $\Delta(1232)$ intermediates is rather poor. This is partly a consequence of the uncertainty concerning the value of the off mass-shell parameters x, y and z which we shall introduce shortly. As a result, it makes little

difference which of the possible values for m_π we choose to use, and for convenience in programming we shall use $m_\pi = m_{\pi^\pm}$ as for ordinary one pion exchange.

The vertex $V(\pi\mathrm{N}\Delta)$ for the reaction $\Delta_\mu(p_\Delta) + \pi(k) \to \mathrm{N}(p_\Delta + k)$ is given in (2.15), while that for $\gamma(\varepsilon_\lambda, q) + \mathrm{N}(p) \to \Delta_\nu(q + p)$ is

$$V(\gamma\mathrm{N}\Delta) = -ie\frac{f_{\gamma\mathrm{N}\Delta}}{m_\pi}\left\{(q_\nu\gamma_\lambda - g_{\nu\lambda}\gamma\cdot q) + y\gamma_\nu(\gamma\cdot q\gamma_\lambda - \gamma_\lambda\gamma\cdot q)\right.$$
$$\left.+\frac{\alpha}{m}\left[(g_{\nu\lambda}p\cdot q - q_\nu p_\lambda) + x\gamma_\nu(\gamma_\lambda p\cdot q - \gamma\cdot q p_\lambda)\right]\right\}\gamma_5. \quad (5.62)$$

The relationship between our notation and that of Benmerrouche *et al* [18] is

$$x = -X - \tfrac{1}{2}, \quad y = -Y - \tfrac{1}{2}, \quad z = -Z - \tfrac{1}{2}, \quad (5.63)$$

$$f_{\gamma\mathrm{N}\Delta} = \frac{g_1}{m}, \quad \alpha = \frac{g_2}{2g_1}. \quad (5.64)$$

Note that from the form of the $\gamma\mathrm{N}\Delta$ vertex we know the current density must be exactly conserved.

The undetermined constants x, y and z of (5.62) describe off mass-shell behaviour. In a previous calculation Jaus and Woolcock [7] made use of the alternative spin-$\frac{3}{2}$ propagator described in subsection 2.1.2. This has the convenient feature of annihilating all the off mass-shell terms. Criticisms of this propagator pointed out by Benmerrouche *et al* [18] and in section 2.1 have led us to employ the unitary spin-$\frac{3}{2}$ propagator in this calculation.

In practice we find that x, y and z can all be varied considerably about $x = y = z = 0$ without substantially affecting the fit. It is obviously inappropriate, therefore, to attempt to fix these parameters by deuteron photodisintegration experimental results, and so we have chosen to set $x = y = z = 0$. Davidson *et al* [49] have made fits to pion photoproduction which suggest that $\alpha \approx 0.7$, although the uncertainty is quite large.

In the same manner as in subsection 5.2.2 the expansion in powers of $\boldsymbol{q}$ of the expressions containing the pion propagator leads to the quantity $\tilde{m}_\pi$. The introduction of a monopole form factor $(\Lambda_\Delta^2 - m_\pi^2)/(\Lambda_\Delta^2 - k^2)$ with cutoff parameter Λ_Δ at the $\pi\mathrm{N}\Delta$ vertex leads similarly to a quantity

$$\tilde{\Lambda}_\Delta^2 = \Lambda_\Delta^2 - \tfrac{1}{4}q_0^2, \quad (5.65)$$

by analogy with (5.43), and the substitution

$$\omega^{-n}(\boldsymbol{p}) \to \omega^{-n}(\boldsymbol{p}) - \frac{\Lambda_\Delta^2 - m_\pi^2}{\Lambda_\Delta^2 - \Lambda_\mathrm{N}^2}(\Lambda_\mathrm{N}^2 + \boldsymbol{p}^2)^{-\frac{1}{2}n} + \frac{\Lambda_\mathrm{N}^2 - m_\pi^2}{\Lambda_\Delta^2 - \Lambda_\mathrm{N}^2}(\Lambda_\Delta^2 + \boldsymbol{p}^2)^{-\frac{1}{2}n}, \quad (5.66)$$

where $\omega(\boldsymbol{p})$ is defined in (5.41) and $n = 2, 4$. There is definite evidence (see Dillig

and Brack [50] and Mathiot *et al* [51]) that Λ_Δ is smaller than Λ_N.

Since in the centre of mass frame the 4-momentum of the intermediate $\Delta(1232)$ in the diagram of figure 5 (d) is

$$p_\Delta \approx \left(m + q_0 - \frac{\boldsymbol{p}' \cdot \boldsymbol{q}}{2m} + \frac{\boldsymbol{q}^2}{8m}, \boldsymbol{p}' + \tfrac{1}{2}\boldsymbol{q} \right), \tag{5.67}$$

we have

$$p_\Delta^2 - M_\Delta^2 \approx -M_\Delta^2 + m^2 + 2mq_0 - \boldsymbol{p}'^2 - 2\boldsymbol{p}' \cdot \boldsymbol{q} + q_0^2. \tag{5.68}$$

Rather than writing here $q_0^2 = \boldsymbol{q}^2$, as did Jaus and Woolcock [7], we retain the q_0^2 term in the present calculation. Then after an expansion in powers of $\boldsymbol{q}$ an effective mass $\tilde{m}$ appears given by

$$\tilde{m}^2 = M_\Delta^2 - (m + q_0)^2. \tag{5.69}$$

By making the replacement $q_0^2 \to \boldsymbol{q}^2$, Jaus and Woolcock [7] effectively neglected the effect on the multipole amplitudes of the q_0^2 term in (5.67), since they truncated the expansion in powers of $\boldsymbol{q}$ below the order at which the effects of a term $\boldsymbol{q}^2$ in the $\Delta(1232)$ propagator denominator appear. At the higher energies we consider it has a significant effect, and we therefore take it into account directly, although by doing so we do not actually increase the order of the calculation.

The use of the form (5.68) to approximate the $\Delta(1232)$ propagator denominator has two major effects on the Δ contribution to the current density. First, the contribution is multiplied by the enhancement factor

$$\left(1 - \frac{q_0(2m + q_0)}{M_\Delta^2 - m^2} \right)^{-1}. \tag{5.70}$$

Second, the deuteron wave function is multiplied by the factor

$$\left(1 + \frac{\boldsymbol{p}'^2}{\tilde{m}^2} \right)^{-1} \tag{5.71}$$

when calculating matrix elements for the Δ contribution. This has the effect of folding of the deuteron wave functions, leading to the replacements

$$\begin{aligned} u(x) &\to U(x) \\ &= \tilde{m} \left[e^{-\tilde{m}x} \int_0^x dy\, u(y) \sinh(\tilde{m}y) + \sinh(\tilde{m}x) \int_x^\infty dy\, u(y) e^{-\tilde{m}y} \right], \\ w(x) &\to W(x) \\ &= \tilde{m} \left[Z_1(x) \int_0^x dy\, w(y) Z_2(y) + Z_2(x) \int_x^\infty dy\, w(y) Z_1(y) \right], \end{aligned} \tag{5.72}$$

where the deuteron wave functions u and w are defined in (4.72), and

$$Z_1(x) = e^{-\tilde{m}x}\left(1 + \frac{3}{\tilde{m}x} + \frac{3}{\tilde{m}^2x^2}\right)$$
$$Z_2(x) = \left(1 + \frac{3}{\tilde{m}^2x^2}\right)\sinh(\tilde{m}x) - \frac{3}{\tilde{m}x}\cosh(\tilde{m}x). \tag{5.73}$$

Because we have truncated our diagrammatic expansion we need to consider putting the effect of the finite width of the $\Delta(1232)$ resonance into our calculation. Correcting the error of Jaus and Woolcock [7] pointed out by Glasgow-Mainz [52], below the pion production threshold (approximately $q_0 = m_\pi$) the width is zero, although there is a small energy-dependent contribution to the $\Delta(1232)$ mass which we neglect. Above the threshold we have $\Gamma(q_0) \propto p^3$ (because the $\Delta(1232)$ is a P-wave resonance), where

$$p^2 = \frac{(s-(m+m_\pi)^2)(s-(m-m_\pi)^2)}{4s}, \tag{5.74}$$

and $s \approx (m+q_0)^2$. It can easily be shown that for laboratory energies up to 200 MeV the effect of the $\Delta(1232)$ width is negligible, and we omit it from this calculation.

The $\Delta(1232)$ contribution to $\boldsymbol{j}_1$ can be expressed in terms of the overall coupling $g_\Delta = f_{\pi NN}f_{\pi N\Delta}f_{\gamma N\Delta}$ and the cutoff parameter Λ_Δ. $f_{\pi NN}$ is very accurately known, but there is some uncertainty in the product $f_{\pi N\Delta}f_{\gamma N\Delta}$. The fit to low energy photoproduction from nucleons data by Olsson and Osypowski [53] gives $f_{\pi N\Delta}f_{\gamma N\Delta} = 0.552 \pm 0.018$. From the constituent quark model (see Jaus and Woolcock [43]) we can obtain $f_{\pi N\Delta}f_{\gamma N\Delta} = 0.497 f_{\pi NN}$. The sum rule of Chemtob and Rho [54], which does not include corrections of $O(m^{-1})$, leads to the result $f_{\pi N\Delta}f_{\gamma N\Delta} = 0.434$. In a previous calculation Jaus and Woolcock [43] adopted $f_{\pi N\Delta}f_{\gamma N\Delta} = 0.48$, but noted that the value was rather uncertain. We have chosen to allow g_Δ to vary to fit experimental data.

Jaus and Woolcock [42] in their equation (2.21) give $\boldsymbol{j}_1(\Delta)$ to leading order in the centre of mass frame without the form factor as

$$\begin{aligned}
&\boldsymbol{j}_1(\Delta;\text{c.m.};\boldsymbol{p}'',\boldsymbol{p}') \\
&\quad\dot{\approx}\,(4\pi)m_\pi^{-4}F_\Delta(\boldsymbol{\tau}_1-\boldsymbol{\tau}_2)_z\frac{1}{\omega^2(\boldsymbol{p}-\frac{1}{2}\boldsymbol{q})-\frac{1}{4}q_0^2} \\
&\qquad\times\left[ai\boldsymbol{q}\times\boldsymbol{p}+b(\boldsymbol{\sigma}_1\cdot\boldsymbol{q}\boldsymbol{p}-\boldsymbol{p}\cdot\boldsymbol{q}\boldsymbol{\sigma}_1)+\tfrac{1}{2}b(\boldsymbol{q}^2\boldsymbol{\sigma}_1-\boldsymbol{\sigma}_1\cdot\boldsymbol{q}\boldsymbol{q})-\tfrac{1}{2}(b+c)q_0^2\boldsymbol{\sigma}_1\right] \\
&\qquad\times\boldsymbol{\sigma}_2\cdot(\boldsymbol{p}-\tfrac{1}{2}\boldsymbol{q}),
\end{aligned} \tag{5.75}$$

where (specialising equation (2.22) of Jaus and Woolcock [42] to the case $x = y = z = 0$)

$$
\begin{aligned}
a &= \tfrac{2}{3}(1 - m/M_\Delta)^{-1}, \\
b &= -\tfrac{1}{3}(1 - m/M_\Delta)^{-1}, \\
c &= (m/3M_\Delta)(2m/M_\Delta - 1)(1 - m/M_\Delta)^{-1} + \tfrac{1}{3}\alpha, \\
F_\Delta &= \frac{f_{\pi NN} f_{\pi N\Delta} f_{\gamma N\Delta}}{4\pi} \frac{2m_\pi}{3M_\Delta} \left(1 - \frac{2q_0(m+q_0)}{M_\Delta^2 - m^2}\right)^{-1}
\end{aligned}
\tag{5.76}
$$

and $\boldsymbol{p} = \boldsymbol{p}'' - \boldsymbol{p}'$. Jaus and Woolcock [42] then expand up to terms quadratic in $\boldsymbol{q}$ and q_0 to obtain their equation (2.23) for $\boldsymbol{j}_1(\Delta) + \boldsymbol{j}_2(\Delta)$. To leading order, the part of $\boldsymbol{j}(\Delta)$ which is independent of $\boldsymbol{q}$ leads to contributions to the amplitudes $E_1^{(1)}$ via the electric dipole operator. This is governed by the single function

$$
G_{\rm III} = -\frac{q_0}{2m_\pi} F_\Delta (b + c) \frac{Y_1(m_\pi x)}{m_\pi x}. \tag{5.77}
$$

The amplitudes $M^{(1)}$ are calculated from the terms in $\boldsymbol{j}(\Delta)$ which are linear in $\boldsymbol{q}$, and the amplitudes $E_2^{(1)}$ and $M^{(2)}$ from the terms quadratic in $\boldsymbol{q}$.

At $O(m^{-1})$ we consider only the part of $\boldsymbol{j}(\Delta)$ which is independent of $\boldsymbol{q}$. It leads to an electric dipole operator $\boldsymbol{D}(\Delta, O(m^{-1}))$ given by equations (4.2) and (4.4) of Jaus and Woolcock [42], with the leading order term (proportional to q_0) deleted from the definition of $G_{\rm III}$.

Some insight into why the $\Delta(1232)$ contribution is so insensitive to the off mass-shell parameters may be obtained by noting that the principal effect of the contribution is on the magnetic dipole amplitudes with a singlet final state. These amplitudes are independent of c, thus their only dependence on x, y and z is via the single number $(y + z + 2yz(1 + m/M_\Delta))$ (see Jaus and Woolcock [42] for details). This latter quantity tends to be constrained by pion photoproduction fits to be near zero. It would need to become quite large (of the order of 2) to have a significant effect, and even then it could to some extent be absorbed into a change in g_Δ.

We consider this to be a reasonably good theoretical description of the aspects of one pion exchange with a $\Delta(1232)$ intermediate which are important to deuteron photodisintegration. However no accurate determinations of the parameters g_Δ and Λ_Δ are available, so they are varied in the fitting of the experimental data.

5.2.4 Vector Meson Exchange

Apart from their contributions to the multipole amplitudes $E_1^{(L)}$ via the potential, medium- and short-range interactions make a significant contribution only via

the magnetic dipole amplitudes involving a singlet final state. These contributions are usually expressed in terms of the functions $H_{\rm I}$ and $H_{\rm II}$ defined by Chemtob and Rho [54] via the magnetic moment operator in coordinate space. In the special case where the initial state has $T = 0$,

$$\begin{aligned}\boldsymbol{M}(\boldsymbol{x}) = &\frac{1}{4m}(\boldsymbol{\tau}_1 - \boldsymbol{\tau}_2)_z \\ &\times \left[H_{\rm I}(x)(\boldsymbol{\sigma}_1 - \boldsymbol{\sigma}_2) + H_{\rm II}(x)((\boldsymbol{\sigma}_1 - \boldsymbol{\sigma}_2)\cdot\hat{\boldsymbol{x}}\hat{\boldsymbol{x}} - \tfrac{1}{3}(\boldsymbol{\sigma}_1 - \boldsymbol{\sigma}_2))\right]. \quad (5.78)\end{aligned}$$

Using the vertices

$$V(\gamma\omega\pi) = -ie\frac{g_{\gamma\omega\pi}}{m_\omega}\varepsilon_{\lambda\mu\alpha\beta}q^\alpha k^\beta \delta_{n3} \quad (5.79)$$

for $\gamma(\varepsilon_\lambda, q) + \omega_\mu(k) \to \pi_n(q+k)$ and

$$V(\omega{\rm NN}) = -ig_{\omega{\rm NN}}\left(\gamma_\mu + \frac{iK_\omega}{2m}\sigma_{\mu\nu}k^\nu\right) \quad (5.80)$$

for $\omega_\mu(k) + {\rm N}(p) \to {\rm N}(k+p)$, the contribution to the functions $H_{\rm I}$ and $H_{\rm II}$ from the mixed $\gamma\omega\pi$ current shown in figure 5 (e) can be evaluated to leading order (see Jaus and Woolcock [7] or Chemtob and Rho [54]) as

$$\begin{aligned}H_{\rm I} &= -\tfrac{1}{3}F_{\gamma\omega\pi}\left[Y_0(m_\pi x) - \left(\frac{m_\omega}{m_\pi}\right)^3 Y_0(m_\omega x)\right], \\ H_{\rm II} &= -F_{\gamma\omega\pi}\left[Y_2(m_\pi x) - \left(\frac{m_\omega}{m_\pi}\right)^3 Y_2(m_\omega x)\right], \end{aligned} \quad (5.81)$$

where (correcting a misprint in equation (6.7) of Jaus and Woolcock [7])

$$F_{\gamma\omega\pi} = \frac{f_{\pi{\rm NN}}g_{\gamma\omega\pi}g_{\omega{\rm NN}}}{4\pi}\left(1 - \frac{m_\pi^2}{m_\omega^2}\right)^{-1}\frac{2mm_\pi^2}{m_\omega^3}. \quad (5.82)$$

The next order would be important if the magnitude of K_ω were large, but all the evidence suggests this is not the case.

We must also consider the current density arising from the exchange of a $\rho(770)$ meson, either with or without a $\Delta(1232)$ intermediate state. For diagrams that do not involve a $\Delta(1232)$ state we have the usual $\rho{\rm NN}$ vertex (2.29) and the $\gamma\rho{\rm NN}$ seagull vertex

$$V(\gamma\rho{\rm NN}) = -\frac{ieg_{\rho{\rm NN}}K_\rho}{2m}\sigma_{\mu\lambda}\varepsilon_{3ab}\tau_b, \quad (5.83)$$

where ε_λ is the polarisation of the incoming photon and the $\rho(770)$ has spin index

μ and isospin index a. For the $\gamma\rho\rho$ vertex corresponding to

$$\gamma(\varepsilon_\lambda, q) + \rho_{\mu,a}(p - \tfrac{1}{2}q) \to \rho_{\nu,b}(p + \tfrac{1}{2}q) \tag{5.84}$$

we use the form in Lee and Yang [55],

$$V(\gamma\rho\rho) = e\varepsilon_{3ab}[2p_\lambda g_{\mu\nu} - p_\mu g_{\nu\lambda} - p_\nu g_{\mu\lambda} + (\kappa_\rho + \tfrac{1}{2})(q_\mu g_{\nu\lambda} - q_\nu g_{\mu\lambda})], \tag{5.85}$$

where κ_ρ, the anomalous magnetic moment of the $\rho(770)$, is probably about 1.

Expanding in powers of m^{-1}, we need to go to $O(m^{-2})$ to obtain the lowest order non-zero magnetic dipole operator. The important contributions at $O(m^{-2})$ come from the $\rho(770)$ current and seagull diagrams shown in Figure 5 (f) and (g) respectively, and the $\rho(770)$ pair current. Since K_ρ is so large, we need only consider the part proportional to $(1 + K_\rho)^2$. The contributions to $H_{\rm I}$ and $H_{\rm II}$ are

$$\begin{aligned} H_{\rm I} &= F_\rho[(m_\rho x - 1)Y_0(m_\rho x) + \kappa_\rho(\tfrac{1}{3}m_\rho x Y_1(m_\rho x) - Y_0(m_\rho x))], \\ H_{\rm II} &= F_\rho \kappa_\rho m_\rho x Y_1(m_\rho x), \end{aligned} \tag{5.86}$$

where

$$F_\rho = \frac{g^2_{\rho\rm NN}}{4\pi}\frac{m_\rho}{2m}(1 + K_\rho)^2, \tag{5.87}$$

which agrees with Riska [56] if we set $\kappa_\rho = 0$. Note that the individual values of $g^2_{\rho\rm NN}/4\pi$ and K_ρ have no effect on deuteron photodisintegration other than through their combination F_ρ.

Vector meson exchange with a $\Delta(1232)$ intermediate is represented by figure 5 (h). As in simple one pion exchange (subsection 5.2.2) the analogous diagram where the photon is absorbed second makes no contribution when the initial state has $T = 0$. The form of the $\rho{\rm N}\Delta$ vertex is simply that for the $\gamma{\rm N}\Delta$ vertex (5.62), with the substitution $f_{\gamma{\rm N}\Delta} \to f_{\rho{\rm N}\Delta}$. The contribution calculated to leading order by Jaus and Woolcock [7]

$$\begin{aligned} H_{\rm I} &= 0 \\ H_{\rm II} &= 3F_{\rho\Delta}Y_2(m_\rho x), \end{aligned} \tag{5.88}$$

where

$$F_{\rho\Delta} = \frac{4}{9}\frac{f_{\gamma{\rm N}\Delta}f_{\rho{\rm N}\Delta}g_\rho}{4\pi}\frac{m_\rho^3(1 + K_\rho)}{m_\pi^2(M_\Delta - m)}\left(1 - \frac{q_0(2m + q_0)}{M_\Delta^2 - m^2}\right)^{-1}, \tag{5.89}$$

is correct for the special case $x = y = z = 0$, despite the change of spin-$\frac{3}{2}$ propagators between the calculations.

We must also consider the effect of structure at the ρNN, ρNΔ and ωNN vertices. We have represented this with a monopole form factor $\Lambda_{\rm V}^2/(\Lambda_{\rm V}^2 - k^2)$. This is the form suggested for low momentum transfer in the extended vector meson dominance model of Gari and Krümpelmann [57]. It is the form considered appropriate for use in conjunction with a large K_ρ, such as the value of around 6 obtained by Pietarinen (reported in section 9 of Dumbrajs *et al* [21]). In practice the results of calculations by Jaus and Woolcock [7] were found to be almost independent of $\Lambda_{\rm V}$, which is why it is sufficient for our purposes to use a single value of $\Lambda_{\rm V}$ for all three vertices.

For the $\gamma\omega\pi$ current this leads to the replacement

$$\begin{aligned}
&m_\pi^3 Y_i(m_\pi x) - m_\omega^3 Y_i(m_\omega x) \\
&\quad\to \frac{\Lambda_{\rm V}^2}{\Lambda_{\rm V}^2 - m_\pi^2} m_\pi^3 Y_i(m_\pi x) \\
&\qquad - \frac{\Lambda_{\rm V}^2(\Lambda_{\rm N}^2 - m_\pi^2)}{(\Lambda_{\rm N}^2 - m_\omega^2)(\Lambda_{\rm V}^2 - m_\omega^2)} m_\omega^3 Y_i(m_\omega x) \\
&\qquad + \frac{\Lambda_{\rm V}^2(m_\omega^2 - m_\pi^2)}{(\Lambda_{\rm V}^2 - \Lambda_{\rm N}^2)(\Lambda_{\rm N}^2 - m_\omega^2)} \Lambda_{\rm N}^3 Y_i(\Lambda_{\rm N} x) \\
&\qquad - \frac{\Lambda_{\rm V}^2(\Lambda_{\rm N}^2 - m_\pi^2)(m_\omega^2 - m_\pi^2)}{(\Lambda_{\rm V}^2 - m_\pi^2)(\Lambda_{\rm V}^2 - \Lambda_{\rm N}^2)(\Lambda_{\rm V}^2 - m_\omega^2)} \Lambda_{\rm V}^3 Y_i(\Lambda_{\rm V} x),
\end{aligned} \tag{5.90}$$

where $i = 0$ or 2. The modification for ρ exchange is entirely analogous to (5.48), with the replacements $(\Lambda_{\rm N}^2 - m_\pi^2) \to \Lambda_{\rm V}^2$ and $\Lambda_{\rm N} \to \Lambda_{\rm V}$.

5.3 Selected Expressions for Multipole Amplitudes

In this section we give expressions for the most important terms in the electric and magnetic multipole amplitudes $\langle sm_s|\, E^{(\rm L)}\,|m_d\rangle$ and $\langle sm_s|\, M^{(\rm L)}\,|m_d\rangle$.

5.3.1 Internal Convection

The internal convection contribution to the electric multipole amplitudes is obtained by adding together the terms known as $E_1^{(\rm L)}$, which we obtain from (5.16), and $E_2^{(\rm L)}$, which is obtained from (5.9). We first make the definitions

$$\tilde{F}(q_0) = \frac{\sqrt{M^2 + q_0^2} + \frac{1}{2}q_0}{2m}, \tag{5.91}$$

$$g_{\rm L}(\tfrac{1}{2}q_0x) = \left(1 + x\frac{d}{dx}\right) j_{\rm L}(\tfrac{1}{2}q_0x)$$
$$= j_{\rm L}(\tfrac{1}{2}q_0x) + \frac{L}{2L+1}(\tfrac{1}{2}q_0x) j_{\rm L-1}(\tfrac{1}{2}q_0x)$$
$$-\frac{L+1}{2L+1}(\tfrac{1}{2}q_0x) j_{\rm L+1}(\tfrac{1}{2}q_0x), \tag{5.92}$$

and $x_\pi = m_\pi x$.

Then

$$\langle 00|\, E^{(\rm L)}(\text{int.conv.})\, |-1\rangle = 0,$$
$$\langle 1, (m_d+1)|\, E^{(\rm L)}(\text{int.conv.})\, |m_d\rangle = \frac{\beta}{2q_0}\int_0^\infty dx\, I^{(\rm L)}_{m_d}(x), \tag{5.93}$$

where

$$I^{(\rm L)}_{-1}(x) = U^{(\rm L)}(x)\left\{F^{(\rm L\text{-}1)}_{\rm l10}(x) - F^{(\rm L+1)}_{\rm L10}(x)\right\}$$
$$+ \tilde{W}^{(\rm L)}\left\{\frac{6(L-1)}{2L-1}F^{(\rm L\text{-}1)}_{\rm (L\text{-}2)10}(x) - \frac{2(L+1)}{2L-1}F^{(\rm L\text{-}1)}_{\rm L10}(x)\right.$$
$$\left. + \frac{2L}{2L+3}F^{(\rm L+1)}_{\rm L10}(x) - \frac{6(L+2)}{2L+3}F^{(\rm L+1)}_{\rm (L+2)10}(x)\right\},$$
$$I^{(\rm L)}_0(x) = U^{(\rm L)}(x)\left\{\frac{L}{L-1}F^{(\rm L\text{-}1)}_{\rm L11}(x) + \frac{2L+1}{L(L+1)}F^{(\rm L)}_{\rm L11}(x) - \frac{L+2}{L+1}F^{(\rm L+1)}_{\rm L11}(x)\right\}$$
$$+ \tilde{W}^{(\rm L)}(x)\left\{-\frac{6(L-1)}{2L-1}F^{(\rm L\text{-}1)}_{\rm (L\text{-}2)11}(x) - \frac{2(L-1)(L+1)}{L(2L-1)}F^{(\rm L\text{-}1)}_{\rm L11}(x)\right.$$
$$-\frac{2(2L+1)}{L(L+1)}F^{(\rm L)}_{\rm L11}(x) - \frac{2L(L+2)}{(L+1)(2L+3)}F^{(\rm L+1)}_{\rm L11}(x)$$
$$\left. + \frac{6(L+2)}{2L+3}F^{(\rm L+1)}_{\rm (L+2)11}(x)\right\}, \tag{5.94}$$

where

$$U^{(\rm L)}(x) = \tilde{F}(q_0) g_{\rm L}(\tfrac{1}{2}q_0x) u(x) - \frac{q_0}{2m} j_{\rm L}(\tfrac{1}{2}q_0x) x u'(x),$$
$$\tilde{W}^{(\rm L)}(x) = \tilde{F}(q_0) g_{\rm L}(\tfrac{1}{2}q_0x) \tilde{w}(x) - \frac{q_0}{2m} j_{\rm L}(\tfrac{1}{2}q_0x) x \tilde{w}'(x), \tag{5.95}$$

and

$$\beta = \sqrt{\frac{\alpha q_0 M}{2p_0}}. \tag{5.96}$$

The deuteron wave function is defined in terms of u and $\tilde{w}$ in (4.72). The definition of the continuum wave functions and of the radial functions $F^{(j)}_{lsm_s}$ in terms of the quantities in Partovi [37] is given in appendix B of Jaus and Woolcock [42].

5.3.2 Relativistic Correction

For the relativistic correction it is not difficult to give expressions for general L to leading order ($O(m^{-2})$). We define the symbols

$$\kappa_a^{(\mathrm{L})} = \begin{cases} \kappa_{\mathrm{S}}, \text{ L odd} \\ \kappa_{\mathrm{V}}, \text{L even} \end{cases}$$
$$\kappa_b^{(\mathrm{L})} = \begin{cases} \kappa_{\mathrm{V}}, \text{L odd} \\ \kappa_{\mathrm{S}}, \text{ L even} \end{cases} . \tag{5.97}$$

In the remainder of this section we shall not show explicitly the radial dependence of the various functions. Then the electric multipole amplitudes for the relativistic correction to the impulse approximation are

$$\begin{aligned} &\langle 00|\, E^{(\mathrm{L})}(\mathrm{RC}; O(m^{-2}))\, |-1\rangle \\ &\quad = \frac{\beta\kappa_a^{(\mathrm{L})}(2L+1)}{2q_0m^2}\int_0^\infty dx\, x^{-2}(xu' - u + 2x\tilde{w}' + 4\tilde{w})g_{\mathrm{L}}F_{\mathrm{L}00}^{(\mathrm{L})} \end{aligned} \tag{5.98}$$

and

$$\langle 1, (m_d+1)|\, E^{(\mathrm{L})}(\mathrm{RC}; O(m^{-2}))\, |m_d\rangle = \frac{\beta\kappa_b^{(\mathrm{L})}}{2q_0m^2}\int_0^\infty dx\, x^{-2} I_{m_d}^{(\mathrm{L})}, \tag{5.99}$$

where the functions $I^{(\mathrm{L})}$ are defined by

$$\begin{aligned} I_{-1}^{(\mathrm{L})} &= -H_1^{(\mathrm{L})}F_{(\mathrm{L}\text{-}2)10}^{(\mathrm{L}\text{-}1)} + H_2^{(\mathrm{L})}F_{(\mathrm{L})10}^{(\mathrm{L}\text{-}1)} + H_3^{(\mathrm{L})}F_{(\mathrm{L})10}^{(\mathrm{L}+1)} - H_4^{(\mathrm{L})}F_{(\mathrm{L}+2)10}^{(\mathrm{L}+1)}, \\ I_0^{(\mathrm{L})} &= H_1^{(\mathrm{L})}F_{(\mathrm{L}\text{-}2)11}^{(\mathrm{L}\text{-}1)} + \frac{L-1}{L}H_2^{(\mathrm{L})}F_{(\mathrm{L})11}^{(\mathrm{L}\text{-}1)} + \frac{L+2}{L+1}H_3^{(\mathrm{L})}F_{(\mathrm{L})11}^{(\mathrm{L}+1)} \\ &\quad + H_4^{(\mathrm{L})}F_{(\mathrm{L}+2)11}^{(\mathrm{L}+1)} + H_5^{(\mathrm{L})}F_{(\mathrm{L})11}^{(\mathrm{L})} \end{aligned} \tag{5.100}$$

using

$$\begin{aligned} H_1^{(\mathrm{L})} &= \frac{6(L-1)(L+1)}{2L-1}(x\tilde{w}'g_{\mathrm{L}} + 3L\tilde{w}j_{\mathrm{L}}), \\ H_2^{(\mathrm{L})} &= (L+1)\left\{(xu'-u)g_{\mathrm{L}} - \frac{2(L-2)}{2L-1}x\tilde{w}'g_{\mathrm{L}} - 2\tilde{w}g_{\mathrm{L}} + \frac{6L(L+1)}{2L-1}\tilde{w}j_{\mathrm{L}}\right\}, \\ H_3^{(\mathrm{L})} &= L\left\{(xu'-u)g_{\mathrm{L}} - \frac{2(L+3)}{2L+3}x\tilde{w}'g_{\mathrm{L}} - 2\tilde{w}g_{\mathrm{L}} + \frac{6L(L+1)}{2L+3}\tilde{w}j_{\mathrm{L}}\right\}, \\ H_4^{(\mathrm{L})} &= \frac{6L(L+2)}{2L+3}(x\tilde{w}'g_{\mathrm{L}} - 3(L+1)\tilde{w}j_{\mathrm{L}}), \\ H_5^{(\mathrm{L})} &= \frac{2L+1}{L(L+1)}\left\{(xu' - u - 4x\tilde{w}' - 2\tilde{w})g_{\mathrm{L}} - 6L(L+1)\tilde{w}j_{\mathrm{L}}\right\}. \end{aligned} \tag{5.101}$$

The magnetic amplitudes for the relativistic correction are

$$\langle 00|\, M^{(\mathrm{L})}(\mathrm{RC}; O(m^{-2}))\,|{-1}\rangle = \frac{\beta\kappa_b^{(\mathrm{L})}}{4m^2}\int_0^\infty dx\, x^{-1}(xu' - u + 2x\tilde{w}' + 4\tilde{w})$$
$$\times j_{\mathrm{L}}\left\{-(L+1)F^{(\mathrm{L}\text{-}1)}_{(\mathrm{L}\text{-}1)00} + LF^{(\mathrm{L}+1)}_{(\mathrm{L}+1)00}\right\} \tag{5.102}$$

and

$$\langle 1, (m_d+1)|\, M^{(\mathrm{L})}(\mathrm{RC}; O(m^{-2}))\,|m_d\rangle = \frac{\beta\kappa_a^{(\mathrm{L})}}{4m^2}\int_0^\infty dx\, x^{-1} j_{\mathrm{L}} I^{(\mathrm{L})}_{m_d}, \tag{5.103}$$

where the functions $I^{(\mathrm{L})}$ are defined by

$$\begin{aligned} I^{(\mathrm{L})}_{-1} &= H^{(\mathrm{L})}_1 F^{(\mathrm{L})}_{(\mathrm{L}\text{-}1)10} + H^{(\mathrm{L})}_2 F^{(\mathrm{L})}_{(\mathrm{L}+1)10} \\ I^{(\mathrm{L})}_0 &= \frac{1}{L} H^{(\mathrm{L})}_1 F^{(\mathrm{L})}_{(\mathrm{L}\text{-}1)11} - \frac{1}{L+1} H L_2 F^{(\mathrm{L})}_{(\mathrm{L}+1)11} \\ &\quad - H^{(\mathrm{L})}_3 F^{(\mathrm{L}\text{-}1)}_{(\mathrm{L}\text{-}1)11} + H^{(\mathrm{L})}_4 F^{(\mathrm{L}+1)}_{(\mathrm{L}+1)11}, \end{aligned} \tag{5.104}$$

using

$$\begin{aligned} H^{(\mathrm{L})}_1 &= -(L+1)\left(xu' - u + \frac{2(L-2)}{L+1}x\tilde{w}' - 2\tilde{w}\right) \\ H^{(\mathrm{L})}_2 &= L\left(xu' - u + \frac{2(L+3)}{L}x\tilde{w}' - 2\tilde{w}\right) \\ H^{(\mathrm{L})}_3 &= \frac{(L-1)(L+1)}{L}(xu' - u - 4x\tilde{w}' - 2\tilde{w}) \\ H^{(\mathrm{L})}_4 &= \frac{L(L+2)}{L+1}(xu' - u - 4x\tilde{w}' - 2\tilde{w}). \end{aligned} \tag{5.105}$$

For the amplitudes of $O(m^{-3})$ included in the calculation, which derive from magnetic moment coupling, we have

$$\begin{aligned} &\langle 10|\, E^{(1)}(\mathrm{RC}; \mathrm{m.m.}, O(m^{-3}))\,|{-1}\rangle \\ &\quad = \frac{\beta\kappa_{\mathrm{V}}}{8m^3}\int_0^\infty dx\, x^{-2} j_1(xu' - u + 2x\tilde{w}' + 4\tilde{w})(2F^{(0)}_{110} + F^{(2)}_{110}), \\ &\langle 11|\, E^{(1)}(\mathrm{RC}; \mathrm{m.m.}, O(m^{-3}))\,|0\rangle \\ &\quad = \frac{\beta\kappa_{\mathrm{V}}}{8m^3}\int_0^\infty dx\, x^{-2} j_1(xu' - u + 2x\tilde{w}' + 4\tilde{w})\tfrac{3}{2}(F^{(1)}_{111} + F^{(2)}_{111}), \end{aligned} \tag{5.106}$$

and

$$\langle 00|\, M^{(1)}(\mathrm{RC}; \mathrm{m.m.}, O(m^{-3}))\,|{-1}\rangle = \frac{\beta\kappa_{\mathrm{V}}}{4q_0 m^3}\int_0^\infty dx\, x^{-3} I(x), \tag{5.107}$$

where

$$\begin{aligned} I(x) &= (xu' - u - 4x\tilde{w}' - 8\tilde{w})(2F^{(0)}_{000} - F^{(2)}_{200})g_1 \\ &\quad + 2(x^2u'' - 2xu' + 2u - 4x^2\tilde{w}'' - 4x\tilde{w}' + 16\tilde{w})(F^{(0)}_{000} + F^{(2)}_{200})j_1. \end{aligned} \tag{5.108}$$

5.3.3 One Pion Exchange Without a $\Delta(1232)$ Intermediate

To leading order, the amplitudes $E_1^{(\mathrm{L})}$ which arise from the $1\pi\mathrm{E}$ mismatch correction are (quoting equation (4.14) from Jaus *et al* [34])

$$\begin{aligned}\langle 00|\, E_1^{(\mathrm{L})}(1\pi\mathrm{E}; O(m^0))\,|-1\rangle &= 0\\ \langle 1,(m_d+1)|\, E_1^{(\mathrm{L})}(1\pi\mathrm{E}; O(m^0))\,|m_d\rangle &= \frac{\beta}{2q_0}\int_0^\infty dx\, g_{\mathrm{L}}(\tfrac{1}{2}q_0x)J_{m_d}^{(\mathrm{L})}(x),\end{aligned} \quad (5.109)$$

where $m_d = 0, -1$ and the functions $J_{m_d}^{(\mathrm{L})}$ are obtained from the functions $I_{m_d}^{(\mathrm{L})}$ by making the replacements

$$U^{(\mathrm{L})}(x) \to U(x), \quad \tilde{W}^{(\mathrm{L})}(x) \to \tilde{W}(x), \quad (5.110)$$

where $U(x)$ and $\tilde{W}(x)$ are defined in (5.59). Note that because of the factor $\exp(\frac{1}{2}i\boldsymbol{q}\cdot\boldsymbol{x}) - \exp(-\frac{1}{2}i\boldsymbol{q}\cdot\boldsymbol{x})$ appearing in (5.49) and (5.53) the amplitudes $E_1^{(\mathrm{L})}(1\pi\mathrm{E}; O(m^0))$ are nonzero only for L odd.

In leading order there is also a $1\pi\mathrm{E}$ contribution to the electric dipole amplitudes arising from the part of $\boldsymbol{j}(1\pi\mathrm{E})$ quadratic in $\boldsymbol{q}$, by means of the electric dipole operator

$$\boldsymbol{D} = \tfrac{1}{2}iq_0\boldsymbol{\nabla}_q(\boldsymbol{\nabla}_q\cdot\boldsymbol{j}(q_0,\boldsymbol{q};\boldsymbol{x},\boldsymbol{\nabla}_x))\Big|_{\mathbf{q}=\mathbf{0}}. \quad (5.111)$$

The electric dipole is expressed in terms of the functions defined in equation (4.7) of Jaus and Woolcock [42]; correcting the expression for G_{II} we have

$$\begin{aligned}G_{\mathrm{II}} &= \frac{f_{\pi\mathrm{NN}}^2}{4\pi}\frac{q_0}{6m_\pi}(1+\tfrac{1}{12}x_\pi^2)Y_0(x_\pi),\\ G_{\mathrm{III}} &= -\frac{f_{\pi\mathrm{NN}}^2}{4\pi}\frac{q_0}{24m_\pi}x_\pi Y_0(x_\pi)\\ G_{\mathrm{IV}} &= \frac{f_{\pi\mathrm{NN}}^2}{4\pi}\frac{q_0}{72m_\pi}x_\pi^2 Y_2(x_\pi),\end{aligned} \quad (5.112)$$

where

$$\begin{aligned}Y_0(t) &= t^{-1}e^{-t},\\ Y_1(t) &= (1+t^{-1})Y_0(t),\\ Y_2(t) &= (1+3t^{-1}+3t^{-2})Y_0(t).\end{aligned} \quad (5.113)$$

Continuing to follow Jaus and Woolcock [42], functions Φ_i are defined in terms of the functions G_i by

$$
\begin{aligned}
\Phi_{\rm I} &= xu'(G_{\rm IX} + \tfrac{2}{3}G_{\rm XI}) + u(G_{\rm II} - G_{\rm IX} - \tfrac{2}{3}G_{\rm XI}) \\
&\quad + x\tilde{w}'(8G_{\rm X} + \tfrac{16}{3}G_{\rm XI} - G_{\rm XII} + 6G_{\rm XIV} + 6G_{\rm XV}) \\
&\quad + \tilde{w}(6G_{\rm III} + 8G_{\rm IV} - 2G_{\rm V} - 2G_{\rm IX} - 6G_{\rm X} \\
&\qquad + \tfrac{32}{3}G_{\rm XI} + 2G_{\rm XIII} + 12G_{\rm XIV} - 6G_{\rm XV}), \\
\Phi_{\rm III} &= xu'(G_{\rm XIV} + G_{\rm XV}) + u(G_{\rm III} - G_{\rm XIV} - G_{\rm XV}) \\
&\quad + x\tilde{w}'(3G_{\rm XII} - G_{\rm XIV} - G_{\rm XV}) \\
&\quad + \tilde{w}(-G_{\rm III} + 3G_{\rm V} + 3G_{\rm IX} - 3G_{\rm X} - 3G_{\rm XIII} - 2G_{\rm XIV} + G_{\rm XV}), \\
\Phi_{\rm IV} &= xu'(G_{\rm X} + \tfrac{2}{3}G_{\rm XI}) + u(G_{\rm IV} - G_{\rm X} - \tfrac{2}{3}G_{\rm XI}) \\
&\quad + x\tilde{w}'(G_{\rm IX} - 2G_{\rm X} - \tfrac{2}{3}G_{\rm XI} - 2G_{\rm XII}) \\
&\quad + \tilde{w}(G_{\rm II} - G_{\rm IV} - 2G_{\rm V} - 3G_{\rm IX} + 4G_{\rm X} - \tfrac{4}{3}G_{\rm XI} + 6G_{\rm XII} + 2G_{\rm XIII}), \\
\Phi_{\rm V} &= xu'(G_{\rm XII}) + u(G_{\rm V} - G_{\rm XII}) + x\tilde{w}'(-G_{\rm XII} + 3G_{\rm XIV} + 3G_{\rm XV}) \\
&\quad + \tilde{w}(3G_{\rm III} - G_{\rm V} - 9G_{\rm X} - 2G_{\rm XII} + 3G_{\rm XIII} + 6G_{\rm XIV} - 3G_{\rm XV}), \\
\Phi_{\rm VII} &= (u + 2\tilde{w})G_{\rm VII}.
\end{aligned}
\tag{5.114}
$$

then the electric dipole amplitudes are obtained from the functions Φ_i by

$$
\begin{aligned}
\langle 00|\, E^{(1)}(1\pi{\rm E})\,|{-1}\rangle &= \beta I^{(1)}(F^{(1)}_{100}; -6\Phi_{\rm VII}) \\
\langle 10|\, E^{(1)}(1\pi{\rm E})\,|{-1}\rangle &= \beta\left[I^{(1)}(F^{(0)}_{110}; \tfrac{2}{3}(\Phi_{\rm I} - 6\Phi_{\rm III} - 4\Phi_{\rm IV} - 4\Phi_{\rm V}))\right. \\
&\quad \left. + I^{(1)}(F^{(2)}_{110}; \tfrac{2}{3}(-\Phi_{\rm I} + \tfrac{2}{5}\Phi_{\rm IV} - 2\Phi_{\rm V})) + I^{(1)}(F^{(2)}_{310}; -\tfrac{12}{5}\Phi_{\rm IV})\right], \\
\langle 11|\, E^{(1)}(1\pi{\rm E})\,|0\rangle &= \beta\left[I^{(1)}(F^{(1)}_{111}; \Phi_{\rm I} + 4\Phi_{\rm III} + 2\Phi_{\rm IV} - 2\Phi_{\rm V})\right. \\
&\quad \left. + I^{(1)}(F^{(2)}_{111}; -\Phi_{\rm I} + \tfrac{2}{5}\Phi_{\rm IV} - 2\Phi_{\rm V}) + I^{(1)}(F^{(2)}_{311}; \tfrac{12}{5}\Phi_{\rm IV})\right],
\end{aligned}
\tag{5.115}
$$

where

$$
I^{(n)}(F^{(j)}_{lsm_s}; \Phi) = \int_0^\infty dx\, x^n F^{(j)}_{lsm_s}(p_0 x)\Phi(x). \tag{5.116}
$$

The contribution to the amplitudes $E_1^{(L)}$ at $O(m^{-1})$ is obtained in a similar manner, using equations (5.114), (5.115), (5.113) and (5.116). Equation (5.112) is replaced by equation (4.3) of Jaus and Woolcock [42] with the terms in $G_{\rm II}$ and $G_{\rm IV}$ proportional to q_0 removed, that is

$$
\begin{aligned}
G_{\rm II} &= -\frac{f^2_{\pi{\rm NN}}}{4\pi}\frac{m_\pi}{4m}\frac{1}{12}Y_0(x_\pi), \\
G_{\rm III} &= \frac{f^2_{\pi{\rm NN}}}{4\pi}\frac{m_\pi}{4m}\frac{1}{2}\frac{1}{x_\pi}Y_1(x_\pi) \\
G_{\rm IV} &= -\frac{f^2_{\pi{\rm NN}}}{4\pi}\frac{m_\pi}{4m}\frac{1}{12}\frac{m_\pi}{4m}Y_2(x_\pi)
\end{aligned}
$$

$$
\begin{aligned}
G_{\rm VII} &= \frac{f^2_{\pi \rm NN}}{4\pi}\frac{m_\pi}{4m}\frac{Y_1(x_\pi)}{x_\pi},\\
G_{\rm IX} &= \frac{f^2_{\pi \rm NN}}{4\pi}\frac{m_\pi}{4m}\left[\frac{Y_0(x_\pi)}{x_\pi^2}-\frac{1}{3}\frac{Y_1(x_\pi)}{x_\pi}\right],\\
G_{\rm X} &= -\frac{f^2_{\pi \rm NN}}{4\pi}\frac{m_\pi}{4m}\frac{1}{3}\frac{Y_1(x_\pi)}{x_\pi},\\
G_{\rm XI} &= \frac{f^2_{\pi \rm NN}}{4\pi}\frac{m_\pi}{4m}\frac{Y_1(x_\pi)}{x_\pi}.
\end{aligned}
\tag{5.117}
$$

The magnetic dipole and quadrupole amplitudes are obtained from the 1πE contributions to the magnetic dipole moment operator (defined in (5.61))

$$
\begin{aligned}
\boldsymbol{M}(1\pi\mathrm{E};\boldsymbol{x}) &= i(\boldsymbol{\tau}_1\times\boldsymbol{\tau}_2)_z\frac{f^2_{\pi \rm NN}}{4\pi}\frac{1}{2m_\pi}\\
&\times\left[Y_0(x_\pi)i\boldsymbol{\sigma}_1\times\boldsymbol{\sigma}_2 - x_\pi Y_1(x_\pi)i(\boldsymbol{\sigma}_1\times\hat{\boldsymbol{x}}\boldsymbol{\sigma}_2\cdot\hat{\boldsymbol{x}}-\boldsymbol{\sigma}_1\cdot\hat{\boldsymbol{x}}\boldsymbol{\sigma}_2\times\hat{\boldsymbol{x}})\right]
\end{aligned}
\tag{5.118}
$$

and magnetic quadrupole moment operator

$$
\begin{aligned}
\boldsymbol{N}(1\pi\mathrm{E};\boldsymbol{x}) &= i(\boldsymbol{\tau}_1\times\boldsymbol{\tau}_2)_z\frac{f^2_{\pi \rm NN}}{4\pi}\frac{i}{4m_\pi}\\
&\times\left[Y_0(x_\pi)\left\{\boldsymbol{\sigma}_1\times\boldsymbol{x}\boldsymbol{\sigma}_{2z}+\boldsymbol{\sigma}_{1z}\boldsymbol{\sigma}_2\times\boldsymbol{x}+(\boldsymbol{\sigma}_1\times\boldsymbol{x})_z\boldsymbol{\sigma}_2+\boldsymbol{\sigma}_1(\boldsymbol{\sigma}_2\times\boldsymbol{x})_z\right\}\right.\\
&+x_\pi Y_1(x_\pi)\left\{(\boldsymbol{\sigma}_1\times\hat{\boldsymbol{x}}\boldsymbol{\sigma}_2\cdot\hat{\boldsymbol{x}}+\boldsymbol{\sigma}_1\cdot\hat{\boldsymbol{x}}\boldsymbol{\sigma}_2\times\hat{\boldsymbol{x}})z\right.\\
&\left.\left.+((\boldsymbol{\sigma}_1\times\hat{\boldsymbol{x}})_z\boldsymbol{\sigma}_2\cdot\hat{\boldsymbol{x}}+\boldsymbol{\sigma}_1\cdot\hat{\boldsymbol{x}}(\boldsymbol{\sigma}_2\times\hat{\boldsymbol{x}})_z)\boldsymbol{x}\right\}\right]
\end{aligned}
\tag{5.119}
$$

respectively. Following Jaus *et al* [34] they are

$$
\begin{aligned}
\langle 00|\,M^{(1)}(1\pi\mathrm{E})\,|-1\rangle &= \frac{f^2_{\pi \rm NN}}{4\pi}\frac{2\beta}{3m_\pi}\\
&\times\left[I^{(0)}(F^{(0)}_{000};(-3Y_0+2x_\pi Y_1)u+4\tilde{w}x_\pi Y_1)\right.\\
&\left.+I^{(0)}(F^{(2)}_{200};-x_\pi uY_1+2(3Y_0-x_\pi Y_1)\tilde{w})\right],\\
\langle 10|\,M^{(2)}(1\pi\mathrm{E})\,|-1\rangle &= \frac{f^2_{\pi \rm NN}}{4\pi}\frac{\beta q_0}{30m_\pi}\\
&\times\left[I^{(1)}(F^{(2)}_{110};(5Y_0+x_\pi Y_1)u+8(2Y_0+x_\pi Y_1)\tilde{w})\right.\\
&\left.+I^{(1)}(F^{(2)}_{310};(-4x_\pi Y_1)u+2(3Y_0-x_\pi Y_1)\tilde{w})\right],\\
\langle 11|\,M^{(2)}(1\pi\mathrm{E})\,|0\rangle &= \frac{f^2_{\pi \rm NN}}{4\pi}\frac{\beta q_0}{30m_\pi}\\
&\times\left[I^{(1)}(F^{(1)}_{111};-\tfrac{3}{2}(5Y_0+x_\pi Y_1)u+6(-Y_0+x_\pi Y_1)\tilde{w})\right.\\
&\quad I^{(1)}(F^{(2)}_{111};\tfrac{1}{2}(5Y_0+x_\pi Y_1)u+4(2Y_0+x_\pi Y_1)\tilde{w})\\
&\quad I^{(1)}(F^{(2)}_{311};\tfrac{4}{3}x_\pi Y_1u+2(-Y_0+\tfrac{1}{3}x_\pi Y_1)\tilde{w})\\
&\left.\quad I^{(1)}(F^{(3)}_{311};\tfrac{8}{3}x_\pi Y_1u+16(-Y_0-2x_\pi Y_1)\tilde{w})\right],
\end{aligned}
\tag{5.120}
$$

and

$$\langle 10|\, M^{(1)}\, |-1\rangle = \langle 11|\, M^{(1)}\, |0\rangle = \langle 00|\, M^{(2)}\, |-1\rangle = 0. \tag{5.121}$$

Note that we have corrected a printing error in Jaus *et al* [34] by making the replacement $6mm \rightarrow 6mm_\pi$ in the amplitude $\langle 00|\, M^{(1)}\, |-1\rangle$.

5.3.4 One Pion Exchange With a $\Delta(1232)$ Intermediate

The $E_1^{(1)}$ amplitudes for one pion exchange with a $\Delta(1232)$ intermediate are derived from the electric dipole operator $\boldsymbol{D}$ defined in (5.111). To leading order, they are given by the single function

$$G_{\rm III} = -\frac{q_0}{2m_\pi} F_\Delta (b+c) \frac{Y_1(x_\pi)}{x_\pi}, \tag{5.122}$$

with all the other functions G_i zero. The step from the functions G_i to the electric dipole amplitudes is identical to the simple one pion exchange case.

The magnetic dipole and quadrupole amplitudes arising from one pion exchange with a $\Delta(1232)$ intermediate are obtained from the $\Delta(1232)$ contribution to the magnetic dipole and quadrupole moment operators. These are given in equations (4.11) and (4.13) of Jaus and Woolcock [42] as

$$\begin{aligned}
\boldsymbol{M}(\Delta; q_0; \boldsymbol{x}) &\doteq (\boldsymbol{\tau}_1 - \boldsymbol{\tau}_2)_z \frac{iF_\Delta}{m_\pi} \left[\left\{ \frac{Y_1(x_\pi)}{x_\pi} (\boldsymbol{\sigma}_1 - \boldsymbol{\sigma}_2) - Y_2(x_\pi)(\boldsymbol{\sigma}_1 - \boldsymbol{\sigma}_2)\cdot\hat{\boldsymbol{x}}\hat{\boldsymbol{x}} \right\} \right. \\
&\quad \left. -b \left\{ 2\frac{Y_1(x_\pi)}{x_\pi} i\boldsymbol{\sigma}_1 \times \boldsymbol{\sigma}_2 - Y_2(x_\pi) i(\boldsymbol{\sigma}_1 \times \hat{\boldsymbol{x}}\boldsymbol{\sigma}_2 \cdot \hat{\boldsymbol{x}} - \boldsymbol{\sigma}_1 \cdot \hat{\boldsymbol{x}}\boldsymbol{\sigma}_2 \times \hat{\boldsymbol{x}}) \right\} \right] \\
\boldsymbol{N}(\Delta; q_0; \boldsymbol{x}) &= (\boldsymbol{\tau}_1 - \boldsymbol{\tau}_2)_z \frac{F_\Delta}{m_\pi} \\
&\quad \times \left[x_\pi (\boldsymbol{\sigma}_1 + \boldsymbol{\sigma}_2)\cdot\hat{\boldsymbol{x}}\hat{\boldsymbol{x}} z \right. \\
&\quad -\tfrac{3}{2} ia \frac{Y_1(x_\pi)}{x_\pi} \{(\boldsymbol{\sigma}_1 + \boldsymbol{\sigma}_2) z + (\boldsymbol{\sigma}_1 + \boldsymbol{\sigma}_2)_z \boldsymbol{x}\} \\
&\quad -\tfrac{3}{2} b Y_2(x_\pi) \{(\boldsymbol{\sigma}_1 \times \hat{\boldsymbol{x}}\boldsymbol{\sigma}_2 \cdot \hat{\boldsymbol{x}} + \boldsymbol{\sigma}_1 \cdot \hat{\boldsymbol{x}}\boldsymbol{\sigma}_2 \times \hat{\boldsymbol{x}}) z \\
&\quad \left. ((\boldsymbol{\sigma}_1 \times \hat{\boldsymbol{x}})_z \boldsymbol{\sigma}_2 \cdot \hat{\boldsymbol{x}} + \boldsymbol{\sigma}_1 \cdot \hat{\boldsymbol{x}} (\boldsymbol{\sigma}_2 \times \hat{\boldsymbol{x}})_z) \boldsymbol{x}\} \right]
\end{aligned} \tag{5.123}$$

respectively. Correcting an error in appendix D of Jaus and Woolcock [42], the magnetic dipole and quadrupole amplitudes are

$$\begin{aligned}
\langle 00|\, M^{(1)}(\Delta)\, |-1\rangle &= F_\Delta \frac{4\beta}{3m_\pi} \left[I^{(1)}(F^{(0)}_{000}; -(a+2b) u Y_0 + 4(a-b)\tilde{w} x_\pi Y_1) \right. \\
&\quad \left. + I^{(1)}(F^{(2)}_{200}; (-a+b) u Y_2 + 2\tilde{w}(-3(a+2b) x_\pi^{-1} Y_1 + (2a+b) Y_2)) \right],
\end{aligned}$$

$$\langle 10|\, M^{(2)}(\Delta)\,|-1\rangle\, F_\Delta \frac{\beta q_0}{10m_\pi}$$
$$\Big[I^{(1)}(F^{(2)}_{110}; 2u(-5ax_\pi^{-1}Y_1 + (2a-b)Y_2) + 8\tilde{w}(-ax_\pi^{-1}Y_1 + (a-2b)Y_2))$$
$$+I^{(1)}(F^{(2)}_{310}; 4(a+2b)uY_2 + 4\tilde{w}(3ax_\pi^{-1}Y_1 + (2a+b)Y_2))\Big]$$
$$\langle 11|\, M^{(2)}(\Delta)\,|0\rangle = F_\Delta \frac{\beta q_0}{10m_\pi}$$
$$\Big[I^{(1)}(F^{(1)}_{111}; u(-5ax_\pi^{-1}Y_1 + (2a+3b)Y_2) + 4\tilde{w}(2ax_\pi^{-1}Y_1 + (a-3b)Y_2))$$
$$+I^{(1)}(F^{(2)}_{111}; u(-5ax_\pi^{-1}Y_1 + (2a-b)Y_2) + 4\tilde{w}(-ax_\pi^{-1}Y_1 + (a-2b)Y_2))$$
$$+I^{(1)}(F^{(2)}_{311}; -\tfrac{4}{3}((a+2b)uY_2 + \tilde{w}(3ax_\pi^{-1}Y_1 + (2a+b)Y_2)$$
$$+I^{(1)}(F^{(3)}_{311}; \tfrac{16}{3}((a-b)uY_2 + \tfrac{2}{3}\tilde{w}(-3ax_\pi^{-1}Y_1 + (a+2b)Y_2)))\Big]. \qquad (5.124)$$

There are also amplitudes $E_2^{(1)}$ which derive from the terms in $\boldsymbol{j}(\Delta)$ quadratic in $\boldsymbol{q}$. Using (5.111), (5.114) and (5.115) these are given in terms of the functions

$$G_{\rm II} = G_{\rm IV} = -F_\Delta \frac{q_0}{6m_\pi} bY_2(x_\pi)$$
$$G_{\rm III} = F_\Delta \frac{q_0}{4m_\pi} bY_2(x_\pi)$$
$$G_{\rm V} = F_\Delta \frac{q_0}{4m_\pi} a\frac{Y_1(x_\pi)}{x_\pi}, \qquad (5.125)$$

where F_Δ is defined in (5.76), and the other functions G_i are zero.

For one pion exchange at $O(m^{-1})$, we consider only the amplitudes $E_1^{(1)}$. Removing a term from equation (4.4) of Jaus and Woolcock [42] we have

$$G_{\rm II} = F_\Delta \frac{m_\pi}{m} d\left[\tfrac{1}{3}\frac{Y_3(x_\pi)}{x_\pi} - \frac{Y_2(x_\pi)}{x_\pi^2}\right]$$
$$G_{\rm III} = F_\Delta \frac{m_\pi}{m}\left[e\frac{Y_1(x_\pi)}{x_\pi} - d\frac{Y_2(x_\pi)}{x_\pi^2}\right]$$
$$G_{\rm IV} = F_\Delta \frac{m_\pi}{m}\tfrac{1}{3} d\frac{Y_3(x_\pi)}{x_\pi}$$
$$G_{\rm XI} = F_\Delta \frac{m_\pi}{m} b\frac{Y_2(x_\pi)}{x_\pi^2}$$
$$G_{\rm XII} = F_\Delta \frac{m_\pi}{m} a\frac{Y_1(x_\pi)}{x_\pi^3}$$
$$G_{\rm XIII} = F_\Delta \frac{m_\pi}{m} a\frac{Y_2(x_\pi)}{x_\pi^2}$$
$$G_{\rm XIV} = F_\Delta \frac{m_\pi}{m}(b+c)\frac{Y_1(x_\pi)}{x_\pi^3}$$
$$G_{\rm XV} = F_\Delta \frac{m_\pi}{m} c\frac{Y_2(x_\pi)}{x_\pi^2}, \qquad (5.126)$$

where

$$Y_3(t) = Y_0(t)(1 + 6t^{-1} + 15t^{-2} + 15t^{-3}). \tag{5.127}$$

Then the electric dipole amplitudes can be obtained from these via (5.114) and (5.115).

5.3.5 Vector Meson Exchange

For vector meson exchange the only important contributions are to the magnetic dipole amplitudes. These may be obtained from the functions $H_{\rm I}$ and $H_{\rm II}$ defined in (5.81), (5.86) and (5.88) using

$$\begin{aligned}\langle 00|\, M^{(1)}\, |-1\rangle &= \frac{\beta}{3m} \\ &\times \left[I^{(0)}(F^{(0)}_{000}; 3H_{\rm I}u - 4H_{\rm II}\tilde{w}) + I^{(0)}(F^{(2)}_{200}; H_{\rm II}u - 2(3H_{\rm I} + H_{\rm II})\tilde{w})\right]. \end{aligned} \tag{5.128}$$

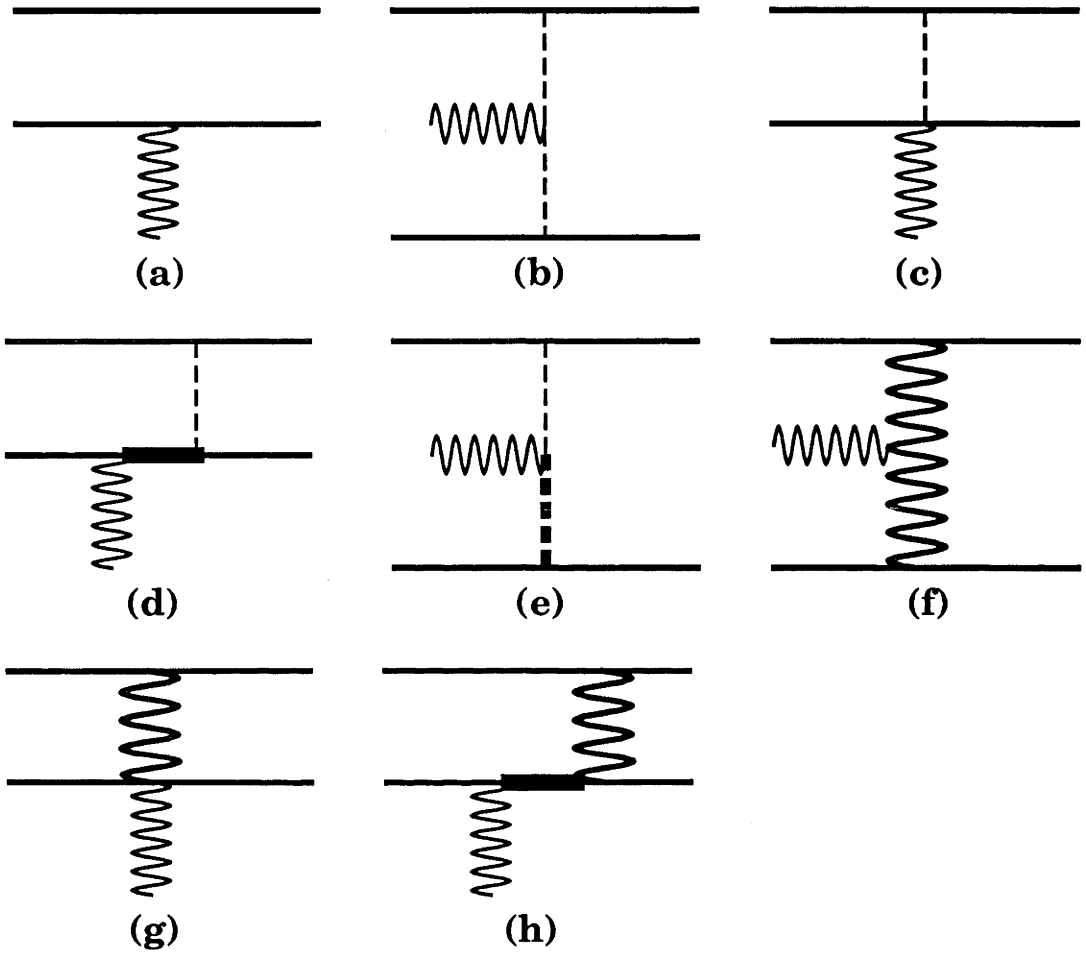

Figure 5: Irreducible diagrams included in this model which contribute to the electromagnetic current density. (a) impulse approximation, (b) pion current (c) pion exchange seagull diagram, (d) pion exchange with a $\Delta(1232)$ intermediate, (e) mixed $\gamma\omega\pi$ current, (f) $\rho(770)$ current, (g) $\rho(770)$ seagull diagram, (h) $\rho\Delta$ current.

Chapter 6

Comparison With Experiment

6.1 Fitting Procedure

In this chapter we describe the results of fitting the model described in chapter 5 to experimental data. We attempt to fit all the more recent data (roughly, post 1970) up to a laboratory photon energy of 200 MeV.

In order to extend the calculation past 200 MeV, we would be forced to operate in the region where the $\Delta(1232)$ resonance dominates. This would require us to include more terms in our multipole expansion, and the finite width of the $\Delta(1232)$ resonance, which we have neglected, would become more important. Also, whatever energy-dependent nucleon-nucleon potential we used would become less reliable. We have chosen to limit ourselves to obtaining the best fit we can to the data up to 200 MeV, using only a small number of adjustable parameters.

We have also chosen not to employ any formal fitting procedure, such as minimising the χ^2 statistic described in section 3.1. This was partly due to the difficulty of assigning uncertainties to the variety of data we are attempting to fit. Also, we will see later that certain combinations of parameters are very poorly determined, so a naive minimisation of the χ^2 statistic would be tend to settle on unrealistic values for these combinations. Instead, a heuristic procedure was used, which fitted to subsets of the available data to fix those combinations of parameters which could be determined with reasonable precision. In the course of this procedure, which we describe below, it was found that of the nucleon-nucleon potentials we tested, only with the Bonn 2 did parameter vectors exist which gave reasonable fits to all the data.

We have chosen to attempt fits using the Bonn 2, Paris 3 and Moscow 4 potentials, though as we shall see only with the Bonn potential do we find it possible

to obtain a reasonable fit. In the case of the Bonn potential several slightly differing versions are available. We have used the coordinate space described as B in Table A.3, appendix A.3 of reference [2], and the coordinate space wave functions described as A. Henceforth we shall refer to the combination as just the Bonn potential. This is slightly inconsistent, since the wave functions have not actually been obtained from the nucleon-nucleon potential we are using. However we can reasonably expect the error in this procedure to be small, and Jaus [58] has shown that this is indeed the case.

The Moscow potential consists of a central potential for $^1S_0$ and central and tensor potentials for $^3S_1$–$^3D_1$, from which the deuteron wave functions and the continuum $^1S_0$ and $^3S_1$-$^3D_1$ wave functions are generated. The central potentials have a deep attractive core which introduces a node at ≈ 0.6 fm into the S-wave functions. The other wave functions must be generated from a standard potential (we used the Bonn potential [2]).

The model was implemented in Fortran on DECStation 5000 and IBM RISC-6000 workstations. This was achieved by modifying a program by Jaus [59] which implemented the model described in Jaus and Woolcock [7] on an IBM mainframe. The appropriate changes were made to reflect the change in Fortran dialect and the corrections and improvements made to that model in evolving this one. The Bonn and Moscow potential potentials were also implemented in Fortran and the program modified to be able to use them.

For photons with a laboratory photon energy between 20 and 110 MeV, the forward and backward cross-sections are dominated by the 1πE mismatch correction contribution to the $E_1^{(L)}$ amplitudes, discussed in subsection 5.2.2. The other contributions which contain tunable parameters have almost no effect on $\sigma(0°)$ and $\sigma(180°)$ in this energy range. Since this is the energy range covered by the new very accurate measurements of the Gent-Mainz [60] group, we can use these data to constrain the 1πE parameters $f^2_{\pi NN}/4\pi$ and Λ_N.

We have therefore looked for values of the ordered pair $(f^2_{\pi NN}/4\pi, \Lambda_N)$ for which the theoretical predictions fit the experimental data on $\sigma(0°)$. Both experiment and theory show a maximum in $\sigma(0°)$ near a laboratory photon energy of 35 MeV, followed by a smooth monotonic decrease to a minimum near 200 MeV. The Gent-Mainz data determine the decrease $\sigma(0°; \text{maximum}) - \sigma(0°; 100\text{MeV})$ to be 1.36 ± 0.13 μb/sr.

With the Paris potential [3] it is possible to obtain a value for this quantity as high as 1.12 μb/sr by adopting $f^2_{\pi NN}/4\pi = 0.075$ and $\Lambda_N = 1300$ MeV. This is too low but perhaps acceptable. The 1πE mismatch correction has an effect on the decrease in $\sigma(0°)$ close to that produced by an *ad hoc* modification of the $T = 1$ Paris potential, which incorporates the difference between the charged and neutral pion masses. Inspection of Table 1 of Jaus and Woolcock [43] shows that the *ad hoc* modification reduces the decrease from 1.60 to 1.38 μb/sr. The further reduction to 1.12 μb/sr is the result of using the modified current conservation scheme to calculate the impulse approximation contribution. Thus the failure of the Paris potential to fit the data can be traced to the correct use of current conservation and the correct inclusion of the charged pion mass in $\boldsymbol{j}(1\pi E)$ in calculating the 1πE mismatch correction.

When calculations are performed using the Moscow potential [4] we find that the decrease $\sigma(0°; \text{maximum}) - \sigma(0°; 100\text{MeV})$ is approximately 0.8 μb/sr and quite insensitive to changes in $f^2_{\pi NN}/4\pi$ and Λ_N. It is therefore impossible to fit the low energy forward cross-section data using the Moscow potential.

When using the Bonn potential [2] the decrease in $\sigma(0°)$ hovers around 1.35 μb/sr for a range of reasonable choices of $(f^2_{\pi NN}/4\pi, \Lambda_N)$. Values close to (0.080, 1300 MeV), (0.079, 1600 MeV) or (0.078, 2000 MeV) give good fits to the Gent-Mainz data.

The next step is to choose a value for $(f^2_{\pi NN}/4\pi, \Lambda_N)$ which satisfies the large body of data for σ_t below 75 MeV. Increasing $f^2_{\pi NN}/4\pi$ and decreasing Λ_N increases the magnitude of the change in $\sigma(0°)$, but at the same time decreases σ_t. We find that the only value which satisfies the Gent-Mainz data using the Paris potential leads to a total cross-section which is unacceptably small for laboratory photon energies below 75 MeV. We are forced to conclude that the parameterised Paris potential is unable to fit the deuteron photodisintegration cross-section data.

A good fit to the total cross-section data below 75 MeV can be obtained by using the Bonn potential with $f^2_{\pi NN}/4\pi = 0.0785$ and $\Lambda_N = 1700$ MeV. As with the forward and backward cross-section data the other parameters g_Δ, Λ_Δ and F_ρ have a very small effect on the total cross-sectionin this energy region. The forward and total cross-section data thus provide a quite clean determination of the 1πE parameters when using the Bonn potential. Using the values of the parameters given above, the Bonn potential provides a good fit to the forward and backward

cross-sections up to 110 MeV and to the total cross-section, differential cross-section and γ-asymmetry up to 75 MeV.

In this way we see that our model of deuteron photodisintegration is indeed able to distinguish between various nucleon-nucleon potentials, as we originally hoped. In what follows we abandon the Paris and Moscow potentials and perform the remainder of the fits using the Bonn potential.

In order to fix the $\Delta(1232)$ and vector meson exchange parameters we fit to experimental data at higher energies. This consists of measurements of $\sigma(0°)$, $\sigma(180°)$ and σ_t at Frascati [61], of $d\sigma(\theta)/d\Omega$ at Indiana [62], TRIUMF [63, 64], Glasgow-Mainz [52], Bonn [65], Frascati [66], and MIT [67], of $A_y^{(n)}(\theta)$ at TRIUMF [63, 64] and of $\Sigma(\theta)$ at Tomsk [68] and Khar'kov [69]. The only significant effect of the $\Delta(1232)$ and vector meson contributions is via the $M^{(1)}$ amplitudes with a singlet final state. There already exists a large contribution to this amplitude from 1πE in leading order, and this is increased by the $\Delta(1232)$ contribution and decreased by vector meson exchange. Thus increasing g_Δ, increasing Λ_Δ and decreasing F_ρ all have similar effects. Although the energy dependence produced by a change in one of the parameters does vary between them somewhat, in practice the experimental data is not sufficient to separate them, and any ordered triple $(g_\Delta, \Lambda_\Delta, F_\rho)$ within a fairly large range gives an almost equally acceptable fit.

For the calculations we display in section 6.2 we adopt the parameter vector

$$\begin{aligned} \frac{f^2_{\pi NN}}{4\pi} &= 0.0785, \\ \Lambda_N &= 1700\text{MeV}, \\ g_\Delta &= 0.63, \\ \Lambda_\Delta &= 1100\text{MeV}, \\ F_\rho &= 2.03. \end{aligned} \tag{6.1}$$

The final equation in (6.1) could be interpreted as

$$\begin{aligned} \frac{g^2_{\rho NN}}{4\pi} &= 0.55, \\ K_\rho &= 2.0, \end{aligned} \tag{6.2}$$

however deuteron photodisintegration is not capable of distinguishing these parameters and in any case none of the last three parameter values in (6.1) has any particular significance on its own. The value of K_ρ suggested in (6.2) is much

smaller than the value of 6.1 obtained by Höhler and Pietarinen [70], however it is more consistent with values obtained from pion-nucleon scattering in chapter 3 or by Pearce and Jennings [30].

The values of Λ_N and, less seriously, Λ_Δ are substantially higher than is suggested by several other pieces of evidence. It is possible that the large value of Λ_N was forced upon us by the even larger value $\Lambda_N = 2000$MeV contained within the Bonn potential.

6.2 Results for Various Observables

The model through which we obtain theoretical predictions for the observables we wish to fit is given in chapter 5. The observables which we are interested in are the centre of mass differential cross-section $d\sigma(\theta)/d\Omega$, particularly for the special cases of forward ($\sigma(0°)$) and backward ($\sigma(180°)$) scattering, the total cross-section σ_t, the γ-asymmetry $\Sigma(\theta)$ and the neutron analysing power $A_y^{(n)}(\theta)$. As usual, the angle θ is measured between the incoming photon and outgoing proton in the centre of mass frame.

6.2.1 Forward Cross-Section

A comparison of experimental and theoretical results for $\sigma(0°)$ is shown in Table 2. As discussed in section 6.1 there is a distinct maximum at a laboratory photon energy of about 35 MeV, followed by a smooth decline to the limits of the data we have chosen to fit. There is also a deep minimum at 10 MeV; this is due to the interference of the rapidly increasing $E^{(1)}$ amplitude with the rapidly decreasing $M^{(1)}$ amplitude.

Since the data for $\sigma(0°)$ was used in fixing the 1πE parameters, it is not too surprising that the model fits it well. The accurate Gent-Mainz [60] data is very well fitted, except at 59.8 MeV. Their older data [74] is uniformly lower. In the region of the deep minimum near 10 MeV we have considerable difficulty in fitting the data of De Graeve *et al* [71, 72]; there is little freedom to adjust the theoretical results by varying parameters.

At laboratory photon energies above 100 MeV the most important data is that from Frascati [61]. The trend of the theoretical and experimental results is rather different. Theory lies above experiment up to about 143 MeV, and below it for

higher energies. The theoretical results have a minimum near 200 MeV, regardless of the value of the parameters, whereas the experimental results show a minimum near 150 MeV. However, considering the sparsity and imprecision of data points this cannot be considered to indicate a defect in the model. We conclude that the model fits the forward cross-section fairly well, for a range of values of $(f^2_{\pi NN}/4\pi, \Lambda_N)$.

6.2.2 Backward Cross-Section

A comparison of experimental and theoretical results for the backward cross-section is shown in Table 3 . By contrast with the forward cross-section, the backward cross-section is not used to determine the parameters $f^2_{\pi NN}/4\pi$ and Λ_N. It is therefore impressive that the model is able to fit these data so well. At higher energies the model does a very good job of fitting to the data from Frascati [61]. We conclude that the model fits the backward cross-section very well for a range of values of the parameters.

There are several experimental results which appear to be in error. In particular the three values of Althoff *et al* [78] are too high and the single value of Dupont *et al* [76] has $\sigma(180°)>\sigma(0°)$, in contradiction to theory and all the other experimental data.

6.2.3 Total Cross-Section

A comparison of theoretical and experimental results for the total cross-section is given in Table 4 . All of the experimental data are direct measurements, with the exception of the Debevec *et al* [87] data, which were obtained by integrating a very detailed measurement of the differential cross-section. Unfortunately, there are no measurements of σ_t between 75 and 200 MeV. If accurate measurements of σ_t are possible in this energy range they would be extremely valuable.

The variation of σ_t with energy is almost completely determined by the impulse approximation, and therefore by the potential. Varying parameters of the fit causes a uniform increase or decrease in the total cross-section without substantially affecting its energy variation.

We find that there does exist a choice of $(f^2_{\pi NN}/4\pi, \Lambda_N)$ for which the theoretical results are a reasonable fit to the experimental ones up to about 75 MeV. The theoretical predictions are uniformly below the Bernabei *et al* [81] data, however

there would be a good fit if the Bernabei *et al* data were reduced by 3%, which is well within the stated systematic error of 5-6%. The total cross-section in the vicinity of 30 MeV is approximately 4.6% lower than was the case in Jaus and Woolcock [43]; this is reflected (see subsection 6.2.4) in a lower value of the differential cross-section at this energy.

We found it impossible to simultaneously fit the result at 40.3 MeV and the results at 21.5 and 32.6 MeV, all from Wauters *et al* [86]; the data set is internally inconsistent. The Debevec *et al* [87] data suggest that the total cross-section should decline more rapidly from 64 to 70 MeV than the theoretical results suggest (by 16.1 ± 2.4 μb rather than by 11.8 μb). Otherwise the model fits the experimental data well.

6.2.4 Differential Cross-Section

In the energy range 3.5 to 18 MeV, Stephenson *et al* [88] have measured the ratios

$$R(\Theta) = \frac{\sigma^{\text{lab}}(\Theta)}{\sigma^{\text{lab}}(90°)}. \tag{6.3}$$

Here Θ is the angle between the incoming photon and the outgoing *neutron* in the *laboratory* frame, and σ^{lab} is the differetial cross-section measured in the *laboratory* frame. Stephenson *et al* measured this ratio for $\Theta = 45°, 135°$ and $155°$.

An earlier calculation by Schmitt *et al* [89] found that a serious discrepancy existed between theory and experiment. Hadjimichael *et al* [90] have speculated on possible missing effects, however deuteron photodisintegration at these energies is very well understood and there is no theoretical basis for any significant modification of the model. It is well known that the theoretical results for these ratios are almost independent of the potential. Our results are almost identical to those of Schmitt *et al*, and hence are also inconsistent with the results of Stephenson *et al*.

In the energy range 20 to 40 MeV, our results are very similar to and uniformly lower than those shown in Jaus and Woolcock [43]. The slight reduction improves the agreement with the experimental data.

At 66.9 MeV we have the very detailed experiment of Debevec *et al* [87], which largely supersedes older data in this energy range. The differential cross-section was measured at intervals of 3° between 22.5° and 160.5°. A comparison of the theoretical and experimental curves is shown in Figure 6. It can be seen that the

agreement is quite good. There is one obviously anomalous experimental result, and the theoretical curve is consistently below the experimental results for forward scattering and above it for backward scattering. However, for the special cases of forward and backward scattering we *know* that our results are consistent with those of the Gent-Mainz [60] group. It therefore appears that unknown systematic errors are affecting the measurement near $\theta = 0°$ and $\theta = 180°$.

We conclude that for laboratory photon energies up to 75 MeV deuteron photodisintegration is well-understood. The body of recent (post 1970) data in this region is quite large, and mostly internally consistent. Above 75 MeV the situation is less clear. All the data on $d\sigma(\theta)/d\Omega$ between 80 and 200 MeV have been published since 1984. A detailed comparison of this data with our results is given in Figures 6 through 13. Inspection of these figures shows that the experimental data contain numerous internal inconsistencies, and it is obviously impossible to fit all the data satisfactorily. We consider that the theoretical model and parameter vector used to generate Figures 6 through 13 to be a reasonably successful compromise attempt to fit these data.

Since the MIT [67] and Frascati [61, 66] data were used to determine the high energy parameters g_Δ, Λ_Δ and F_ρ, it is not surprising that our model provides a good fit to those experimental results. There is good agreement over the entire energy range, although it is impossible to draw any smooth curve with a reasonable χ^2 through the data points.

At 80 and 100 MeV most of the Frascati and MIT data points lie below the theoretical curves, while at 200 MeV most of them lie above the theoretical curve, particularly at backward angles. Between these energies (except perhaps at 140 MeV) agreement tends to be good. The obvious methods of correcting the trend of the theoretical curves are to either increase g_Δ or Λ_Δ (increasing the $\Delta(1232)$ contribution to the $M^{(1)}$ amplitude, see section 6.1), or to decrease F_ρ (decreasing the vector meson exchange contribution to $M^{(1)}$). Either method would improve the fit to the differential cross-section data at the expense of the forward and total cross-section data. Fundamentally the decline in the cross-section from 80 to 200 MeV mirrors an underlying decrease in the impulse approximation contribution, which is fixed once a potential is chosen. As we remarked in section 6.1, we expect our nucleon-nucleon potentials to become less reliable near the top of our energy range.

The remainder of the experimental data differ from each other and from the Frascati and MIT data to a distressing extent, considering that these are all recent experiments performed by experienced groups. The Indiana [62] data are in good agreement near forward scattering but fail to follow the strong rise as one moves away from the forward direction. The TRIUMF [63, 64] data are clearly too low at 100, 140 and 180 MeV, and the shape of the curve at 180 MeV is quite different. The Glasgow-Mainz [52] data agrees well for angles greater than about 120° as well as at the forward extreme of the measurement range, however the maximum at about 65° is much lower than that for the Frascati results. The Bonn [65] data are low compared with Frascati and MIT, but the shape is the same. Until the concensus of the experimental results improves, it is impossible to draw more than tentative conclusions from these fits.

6.2.5 Neutron Analysing Power

The polarisation of the outgoing neutron for deuteron photodisintegration is the same as the neutron analysing power for the radiative capture of neutrons by protons. Several measurements have been performed at low energies, and they are compared with our theoretical predictions in Table 6.2.4. The theory agrees well with experiment except at 5.23, 8.7, 11.1 and 13.5 MeV. These points are also obviously inconsistent with the remainder of the data, so the model is fitting the experimental results as well as possible. These results do nothing to dispel the conclusion that deuteron photodisintegration up to about 75 MeV is well understood.

At higher energies we have the measurements of TRIUMF near 100 and 140 MeV[63] and at 187.3 MeV[64]. Our results at 100 MeV differ little from those of Jaus and Woolcock [43], and agreement between theory and experiment remains excellent. At 140 MeV the agreement is considerably improved over that of Jaus and Woolcock, as shown in Figure 14. Although the curve is still consistently too low, it does not become negative near the backward direction, as did that of Jaus and Woolcock. This is due to the much larger strength in this work of the $\Delta(1232)$ contribution to the $M^{(1)}$ amplitudes with a singlet final state.

At 187.3 MeV the situation is similar and if anything slightly improved. The shape of the theoretical curve is very similar to that at 140 MeV and the agreement is somewhat better. The curve still lies somewhat below the experimental points, except possibly at the forward limit of measurement.

Neither meson exchange nor the details of the potential has much effect on the shape of the theoretical curve at these last two energies. We conclude that our model is providing a reasonable fit to the neutron analysing power over our energy range, and that the neutron analysing power is a poor probe of either potentials or meson-exchange effects.

6.2.6 γ-Asymmetry

Fairly complete angular distributions of the γ-asymmetry $\Sigma(\theta)$ are available at 30 and 60 MeV, and fits to them are shown in Figures 5 and 6 of Jaus and Woolcock [43]. Our theoretical results at 30 MeV are almost identical to theirs. At 60 MeV our results are slightly and uniformly lower, which improves the agreement with experiment. In addition there are data at various angles and at energies from 10 to 90 MeV. To the extent that these data are internally consistent the agreement is satisfactory. Again we find that up to a laboratory photon energy of 75 MeV our model has no difficulty fitting the results of deuteron photodisintegration experiments.

At higher energies we have the results of only two groups to draw upon. The Tomsk [68] data consist of only two data points at 100 MeV. Our main source of γ-asymmetry measurements is a series of measurements at intervals of 20 MeV from 100 to 200 MeV.

By contrast with the behaviour of the neutron analysing power (see subsection 6.2.5) the γ-asymmetry is strongly dependent on the $M^{(1)}$ amplitudes with a singlet final state; again the potential has only a small effect. Since the $\Delta(1232)$ and vector meson exchange contributions to this quantity are much larger in this model than in Jaus and Woolcock [43], the γ-asymmetry at these higher energies is dramatically altered. A comparison of our results with the experimental data is shown in Figures 16 and 17. Considering that the polarisation data were not used to fit any of the parameters, the agreement between theory and experiment is very good. This is extremely satisfying, and an immense improvement over the situation of Jaus and Woolcock [7], who were quite unable to fit either the data of the Tomsk [68] group at 100 MeV or that of the Khar'kov [69] group at 140 MeV. The only previous calculation that gave a reasonable fit to $\Sigma(\theta)$ in this energy range was that of Wilhelm *et al* [93]. This calculation was conducted using the Paris potential [3], however the choice of potential has no significant effect on $\Sigma(\theta)$ compared with the

effect of the $\Delta(1232)$ and $\rho(770)$ parameters.

We note that our results for $\Sigma(\theta)$ are if anything slightly too negative. This acts as an additional disincentive to the method we discussed in subsection 6.2.4 for improving our fit to the differential cross-section. We thus see that, even given the limited experimental data set available, the γ-asymmetry is acting as a very senitive probe of the $\Delta(1232)$ and $\rho(770)$ contributions to deuteron photodisintegration, and hence of the overall couplings g_Δ and F_ρ and the cutoff parameter Λ_Δ. Further measurements in this region would be of considerable value.

6.3 Conclusions

As described in section 6.1 and 6.2 a simple picture of deuteron photodisintegration for laboratory photon energies up to 200 MeV has emerged. Up to about 75 MeV deuteron photodisintegration is dominated by the impulse approximation and leading order 1πE, including the 1πE mismatch correction discussed in section 5.1. It is not possible to fit experimental results without using the 1πE mismatch correction.

Of the three potentials with which we performed fits, only the Bonn potential [2] allowed us to make a satisfactory fit to the forward and total cross-section in this energy range. Neither the Paris potential [3] nor the Moscow potential [4] were able to fit the recent Gent-Mainz [60] data on the forward cross-section between 20 and 100 MeV. Low energy deuteron photodisintegration has thus shown itself to be a sensitive probe of nucleon-nucleon potentials.

At higher energies the contributions of 1πE with a $\Delta(1232)$ intermediate and of 1ρE to the $M^{(1)}$ amplitudes with a singlet final state become important. The other meson exchange processes are of little importance compared with these major effects, which are now well understood. Any errors or omissions in the lesser effects will probably tend to be absorbed by small changes in the parameters affecting the principal contributions, so deuteron photodisintegration at these energies cannot be used to examine such processes.

We found it impossible to separate the effects of changes in the three parameters g_Δ, Λ_Δ and F_ρ. This is only partly due to the limitations of the experimental data available in the 80 to 200 MeV region. In this energy region the effect of changing any one of these parameters can be approximately duplicated by an appropriate

change to either of the others. The examination of deuteron photodisintegration at these energies is therefore a poor method for determining these parameters.

Several of the experimental observables have their underlying trend determined largely by the potential, and therefore act as tests of a nucleon-nucleon potential. Modification of the the meson exchange parameters is insufficient to allow us to fit the forward cross-section, for instance, using the Paris or Moscow potentials.

The Bonn potential was able to provide a reasonable fit to both the forward and total cross-section up to 75 MeV, however between 64 and 70 MeV there is a significant difference between the trends of our model and the result of Debevec *et al* [87]. Unless the measurements of Debevec *et al* are becoming unreliable at this upper end of their energy range, this suggests the Bonn potential [2] is beginning to fail for the higher energies we consider. Similarly our model suggests a noticeably sharper decrease in the differential cross-section between 100 and 200 MeV than do the experimental data [61–67, 87]: our curves are above the data at 80–100 MeV and below it at 180–200 MeV. It is possible that the experimental data are now becoming accurate enough to test the more subtle features of nucleon-nucleon potentials. Accurate measurements of the total cross-section between 80 and 200 MeV would be extremely valuable.

It is important to note that deuteron photodisintegration at these energies underdetermines our model. Even after fitting to all the available experimental data our model retains considerable flexibility in two degrees of freedom, since only one combination of the parameters g_Δ, Λ_Δ and F_ρ can be considered to be determined. Thus our results for these parameters are of very limited significance. Effectively, we are describing the entirety of the modern deuteron photodisintegration data with only three tunable degrees of freedom, which makes the general success of the model quite impressive.

The 1πE parameters $f^2_{\pi\mathrm{NN}}/4\pi$ and Λ_N, however, are well determined. The large value $\Lambda_\mathrm{N} = 1700$ MeV is a cause for concern, although it may be the result of our fit trying to match the value $\Lambda_\mathrm{N} = 2000$ MeV in the Bonn CSB potential. This might be tested by inserting alternative potentials into our model. A more serious worry is the very large size of the 1πE mismatch correction. This indicates that the parameters needed to fit deuteron photodisintegration are very different from those in the Bonn potential. The particular version of the Bonn coordinate space potential which we used contains a very large 1πE part, which is compensated for

by a very large 1ρE part. Both these contributions are substantially stronger than are needed to model deuteron photodisintegration. The size of the 1πE mismatch indicates that the Bonn CSB potential cannot be considered an entirely satisfactory nucleon-nucleon potential. Other forms of the Bonn potential, with smaller 1πE parts, do exist, and could be tested.

The model we have described provides a rather good global fit to the entire body of recent data, but is conceptually simple and contains only a few tunable parameters. We have shown that deuteron photodisintegration at low energies can be used as a quite harsh test of nucleon-nucleon potentials. Stronger conclusions might be drawn if more measurements were available in the energy range from 80 to 200 MeV, particularly for the total cross-section and for the γ-asymmetry. The $\Delta(1232)$ and vector meson exchange parameters are not easily fully determined by deuteron photodisintegration, which is therefore unsuitable for measuring them. We consider that this model represents a breakthrough in our theoretical understanding of deuteron photodisintegration.

Laboratory Photon Energy (MeV)	Reference	Experimental $\sigma(0°)(\mu b/sr)$		Theoretical $\sigma(0°)(\mu b/sr)$
7.17	[71]	6.14	(34)	5.59
8.49	[71]	5.48	(53)	5.11
9.98	[72]	5.38	(20)	4.92
10.74	[73]	4.70	(85)	4.89
14.71	[72]	6.11	(29)	5.07
22.7	[60]	5.63	(14)	5.60
24.5	[74]	5.17	(28)	5.67
28.1	[60]	5.71	(10)	5.78
31.7	[60]	5.83	(6)	5.84
32.8	[75]	4.72	(31)	5.85
33.0	[74]	5.66	(28)	5.85
38.2	[76]	5.10	(71)	5.85
40.5	[60]	5.75	(11)	5.83
43.0	[74]	4.81	(21)	5.80
48.9	[60]	5.55	(13)	5.69
59.8	[60]	5.15	(9)	5.42
64.0	[60]	5.44	(11)	5.30
68.3	[60]	5.09	(13)	5.19
74.2	[60]	5.07	(12)	5.03
78.5	[74]	4.43	(27)	4.92
79.5	[60]	5.15	(13)	4.89
85.7	[60]	4.82	(11)	4.74
93.1	[60]	4.61	(11)	4.57
99.1	[60]	4.47	(11)	4.44
100	[61]	4.06	(44)	4.42
104.5	[74]	4.15	(19)	4.33
106.1	[60]	4.33	(13)	4.30
109	[61]	3.84	(43)	4.25
118	[61]	3.93	(32)	4.09
124	[74]	3.72	(16)	4.00
130	[61]	3.63	(27)	3.92
143	[61]	3.53	(23)	3.78
159	[61]	4.00	(30)	3.65
175	[61]	3.96	(26)	3.58
191	[61]	4.63	(47)	3.57

Table 2: Experimental and theoretical results for the centre of mass differential cross-section for forward deuteron photodisintegration.

Laboratory Photon Energy (MeV)	Reference	Experimental $\sigma(180°)(\mu b/sr)$		Theoretical $\sigma(180°)(\mu b/sr)$
12.04	[77]	4.45	(39)	4.10
14.64	[77]	4.05	(41)	4.08
32.8	[75]	3.93	(43)	4.22
33.9	[60]	4.28	(9)	4.21
38.2	[76]	6.20	(78)	4.17
40.1	[60]	3.88	(16)	4.15
43.2	[60]	4.10	(16)	4.10
48.5	[60]	3.78	(11)	4.00
52.6	[60]	3.74	(12)	3.93
58.5	[60]	3.79	(10)	3.81
64.8	[60]	3.61	(25)	3.68
75.8	[60]	3.29	(15)	3.46
83.0	[60]	3.38	(17)	3.32
90.0	[60]	3.09	(9)	3.20
100.1	[60]	2.92	(14)	3.04
109.3	[60]	2.90	(17)	2.92
130	[61]	2.59	(16)	2.66
143	[61]	2.35	(13)	2.55
159	[61]	2.44	(16)	2.45
175	[61]	2.44	(17)	2.39
181	[78]	2.72	(6)	2.38
190	[78]	2.96	(5)	2.38
191	[61]	2.48	(33)	2.38
200	[78]	3.13	(6)	2.40

Table 3: Experimental and theoretical results for the centre of mass differential cross-section for backward deuteron photodisintegration.

Laboratory Photon Energy (MeV)	Reference	Experimental $\sigma_t(\mu b)$		Theoretical $\sigma_t(\mu b)$
2.754	[79]	1456	(45)	1484
5.97	[80]	2162	(99)	2211
7.25	[80]	1882	(11)	1902
7.60	[80]	1803	(16)	1824
7.64	[80]	1810	(28)	1816
8.80	[80]	1586	(11)	1585
9.00	[80]	1570	(36)	1549
11.39	[80]	1257	(36)	1191
14.70	[81]	925	(20)	873
14.76	[82]	970	(55)	868
15.00	[83]	867	(27)	851
15.03	[84]	870	(26)	849
19.3	[81]	617	(9)	610
20.0	[83]	585	(14)	581
20.8	[85]	582	(44)	551
21.5	[86]	550.3	(10.5)	526.6
23.4	[85]	511	(35)	469
25.0	[83]	428	(17)	427
25.9	[85]	385	(16)	407
28.5	[85]	367	(19)	356
28.9	[81]	361	(6)	349
31.0	[85]	306	(21)	316
32.6	[86]	307.0	(3.7)	294.2
33.5	[85]	264	(20)	283
38.2	[81]	249	(3)	236
38.6	[85]	234	(18)	232
40.3	[86]	215.8	(2.6)	218.5
47.5	[81]	177	(3)	174
57.5	[81]	139	(3)	135
64.0	[87]	122.3	(1.8)	117.9
65.8	[87]	117.7	(1.8)	114.0
67.8	[87]	112.5	(1.3)	110.1
70.0	[87]	106.2	(1.6)	106.1
74.0	[81]	97.6	(5.3)	99.6

Table 4: Experimental and theoretical results for the total cross-section for deuteron photodisintegration.

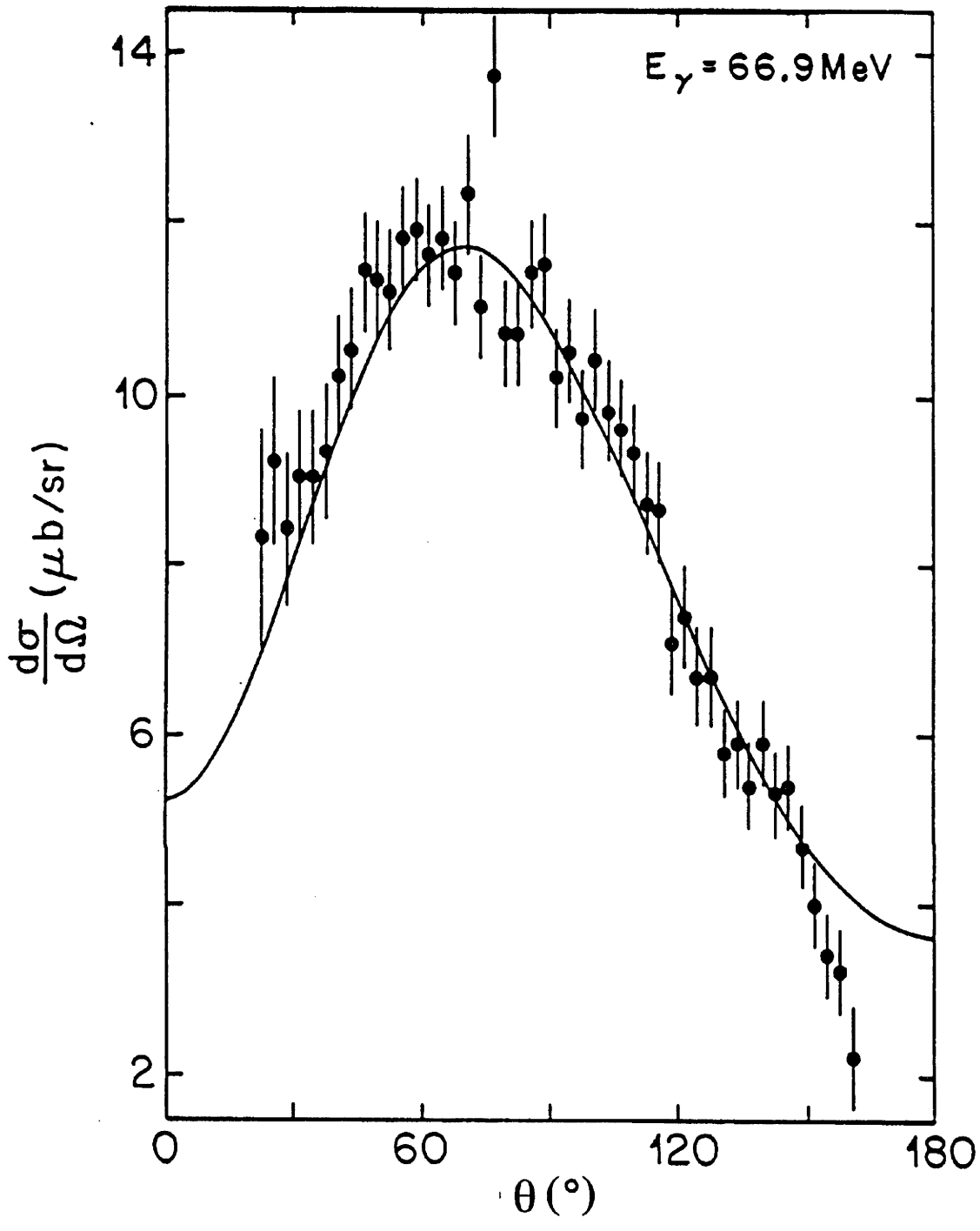

Figure 6: Unpolarised differential cross-section in the centre of mass frame for a laboratory photon energy of 66.9 MeV. Experimental results are from Debevec *et al* [87].

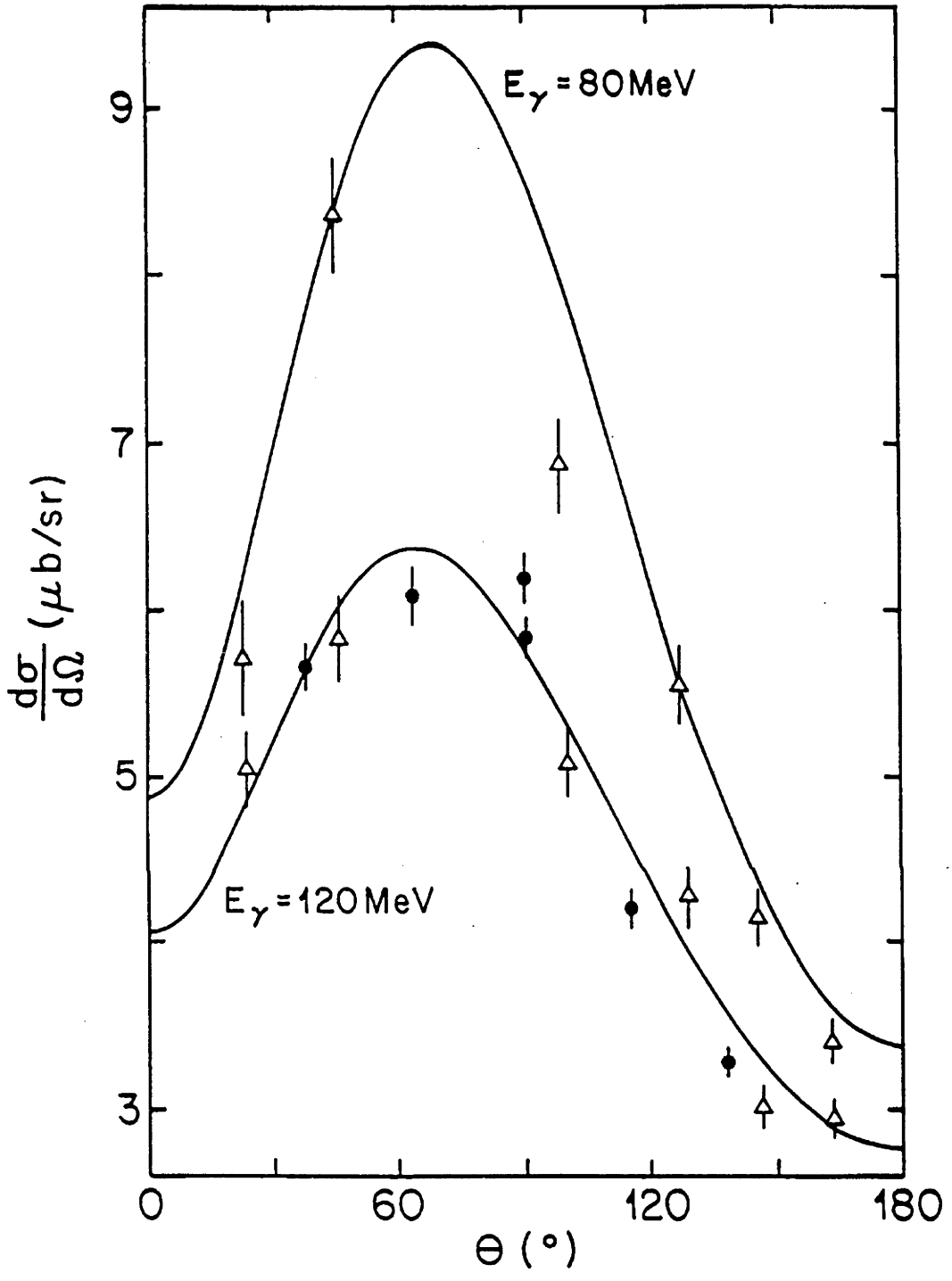

Figure 7: Unpolarised differential cross-section in the centre of mass frame for a laboratory photon energy of 80 and 120 MeV. Experimental results are from Frascati [61, 66] (solid circles) and from MIT [67] (open triangles).

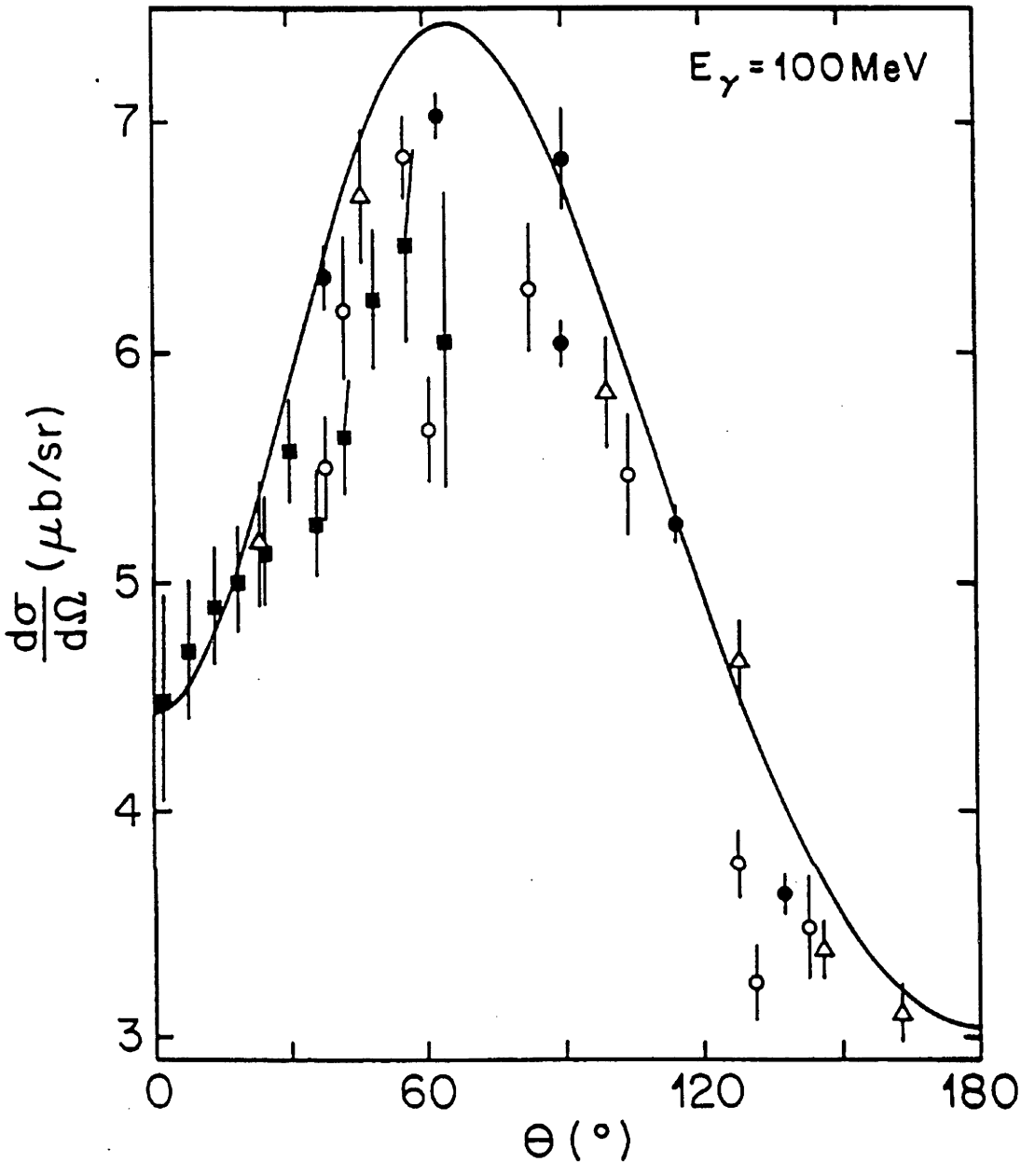

Figure 8: Unpolarised differential cross-section in the centre of mass frame for a laboratory photon energy of 100 MeV. Experimental results are from Frascati [61, 66] (solid circles), TRIUMF [63] (open circles), MIT [67] (open triangles) and Indiana [62] (solid squares).

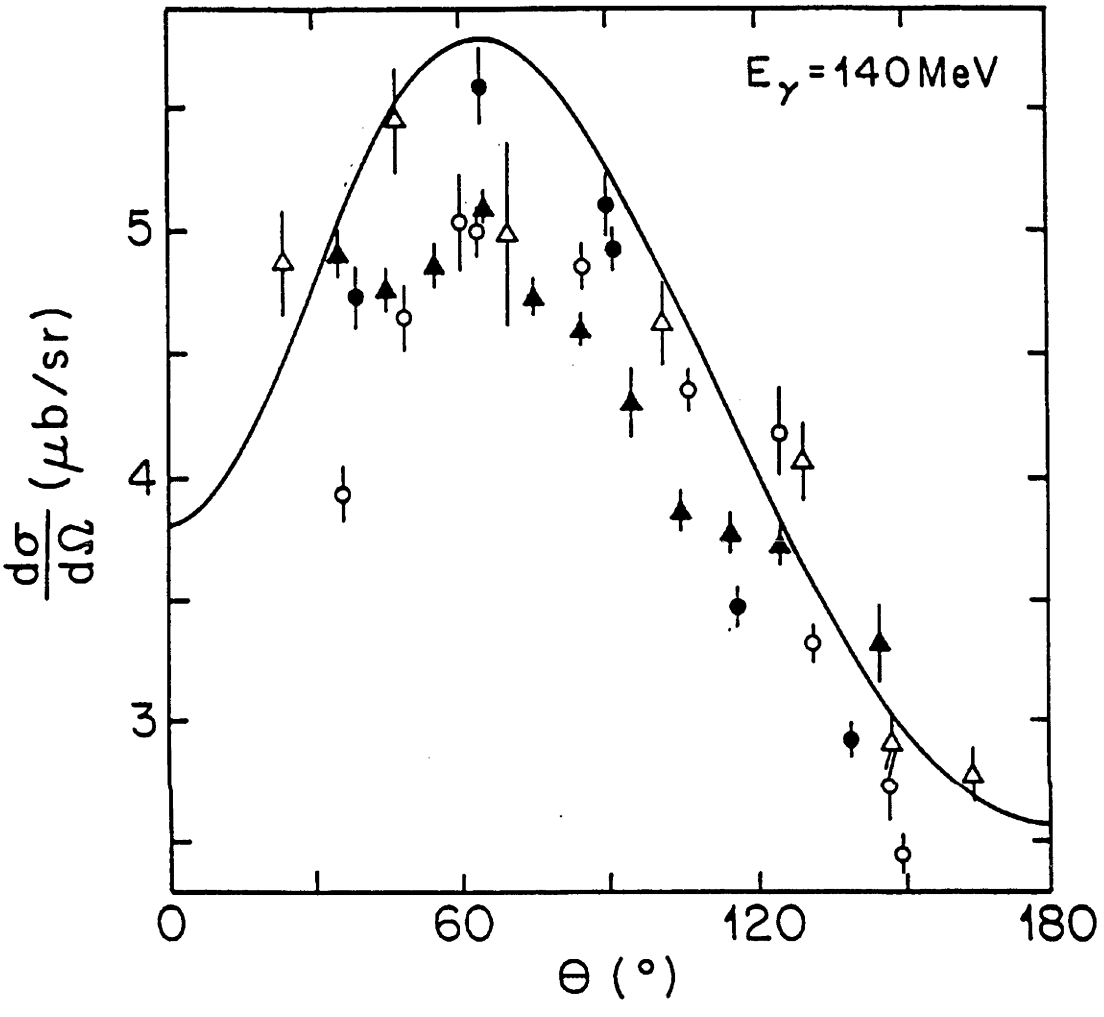

Figure 9: Unpolarised differential cross-section in the centre of mass frame for a laboratory photon energy of 140 MeV. Experimental results are from Frascati [61, 66] (solid circles), TRIUMF [63] (open circles), Glasgow-Mainz [52] (solid triangles) and MIT [67] (open triangles).

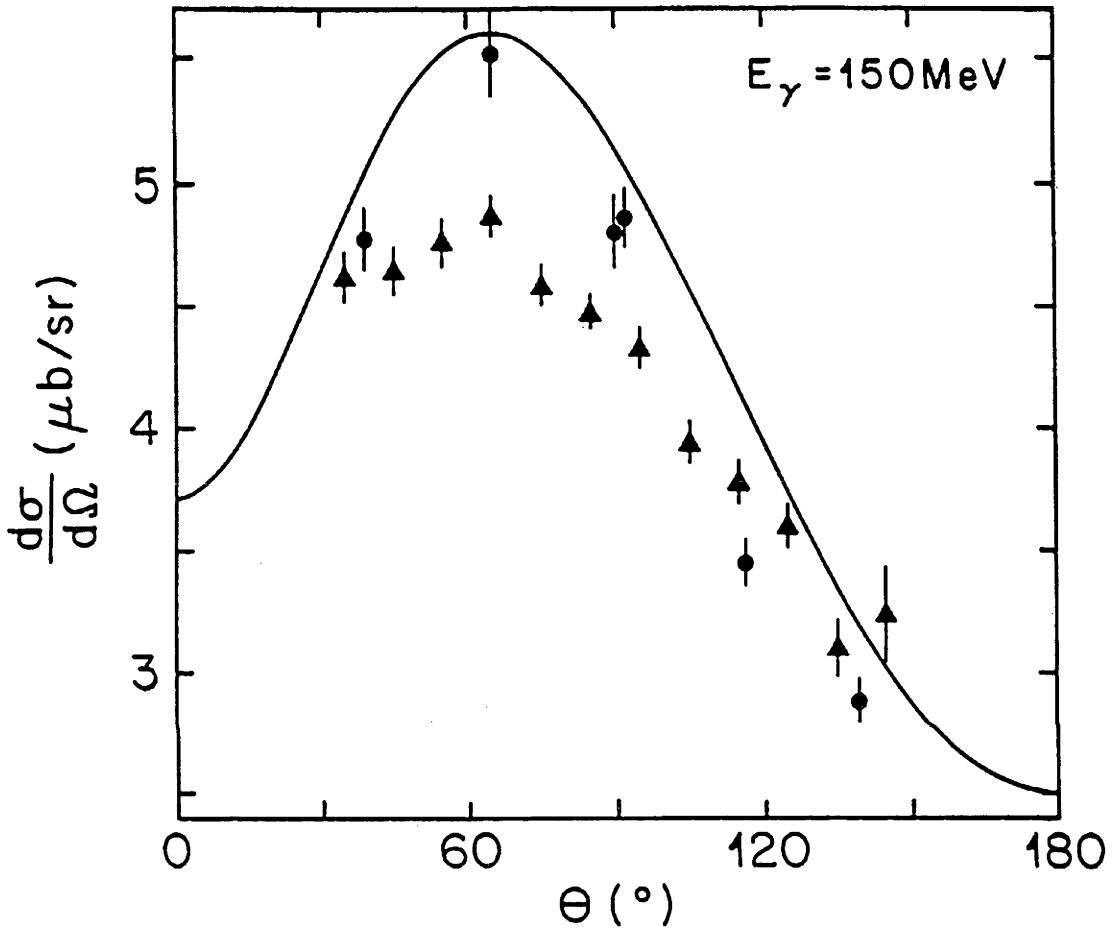

Figure 10: Unpolarised differential cross-section in the centre of mass frame for a laboratory photon energy of 150 MeV. Experimental results are from Frascati [61, 66] (solid circles) and Glasgow-Mainz [52] (solid triangles).

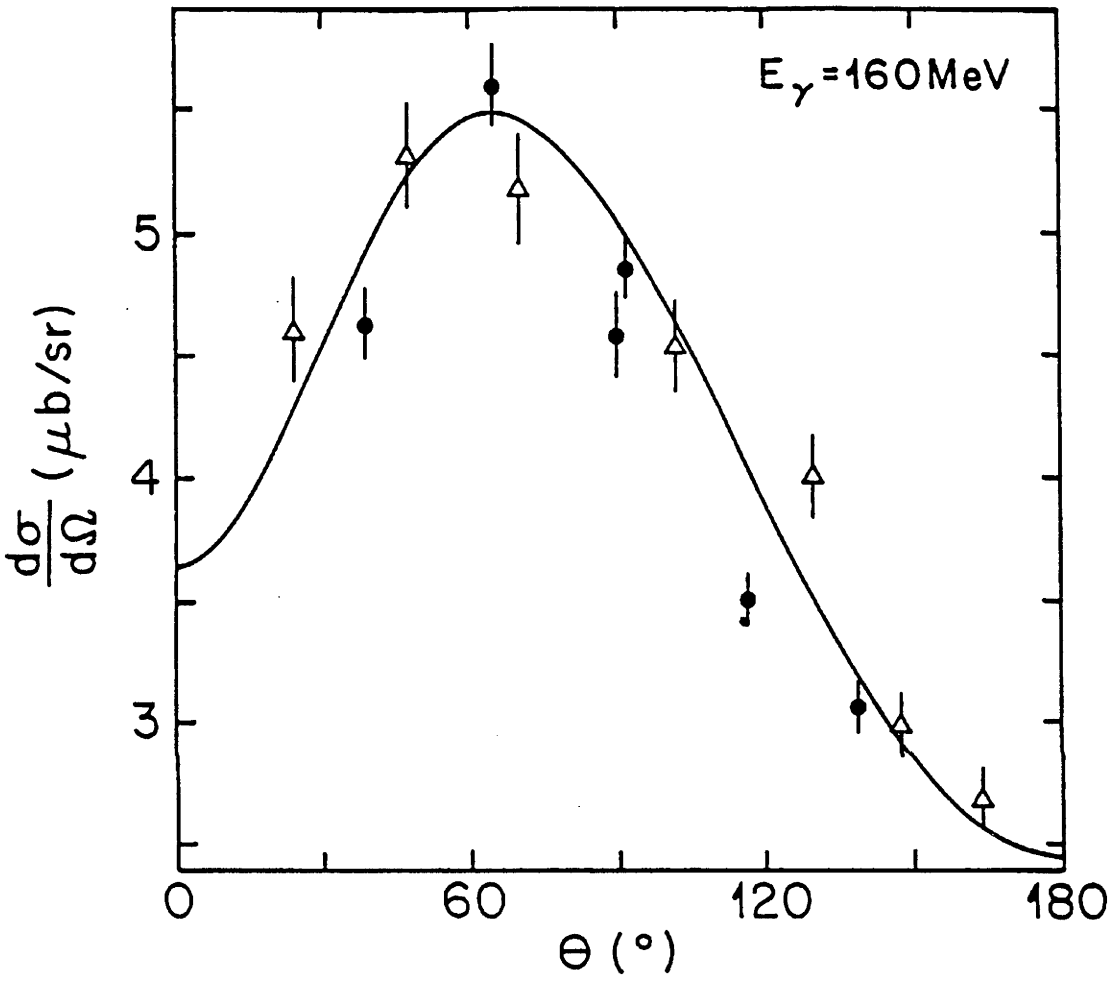

Figure 11: Unpolarised differential cross-section in the centre of mass frame for a laboratory photon energy of 160 MeV. Experimental results are from Frascati [61, 66] (solid circles) and MIT [67] (open triangles).

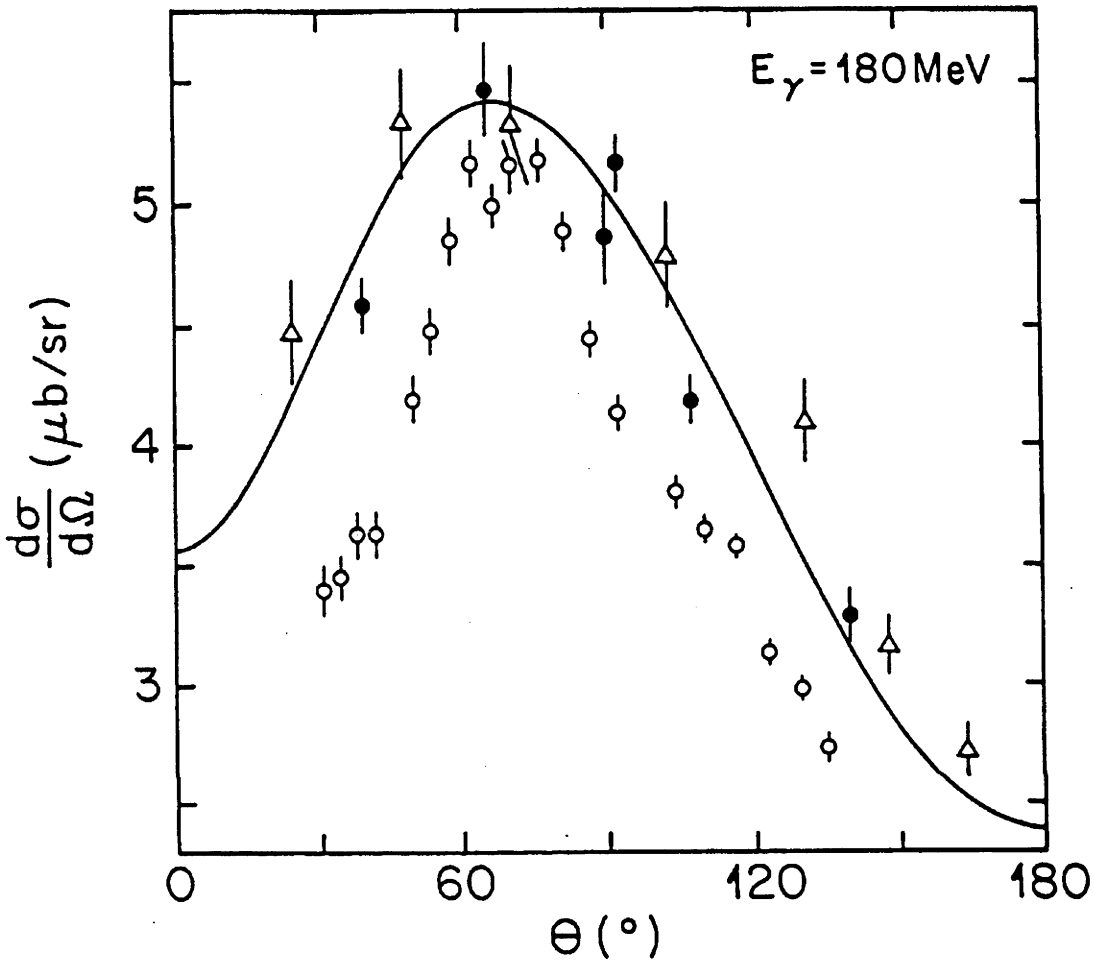

Figure 12: Unpolarised differential cross-section in the centre of mass frame for a laboratory photon energy of 180 MeV. Experimental results are from Frascati [61, 66] (solid circles), TRIUMF [64] (open circles) and MIT [67] (open triangles).

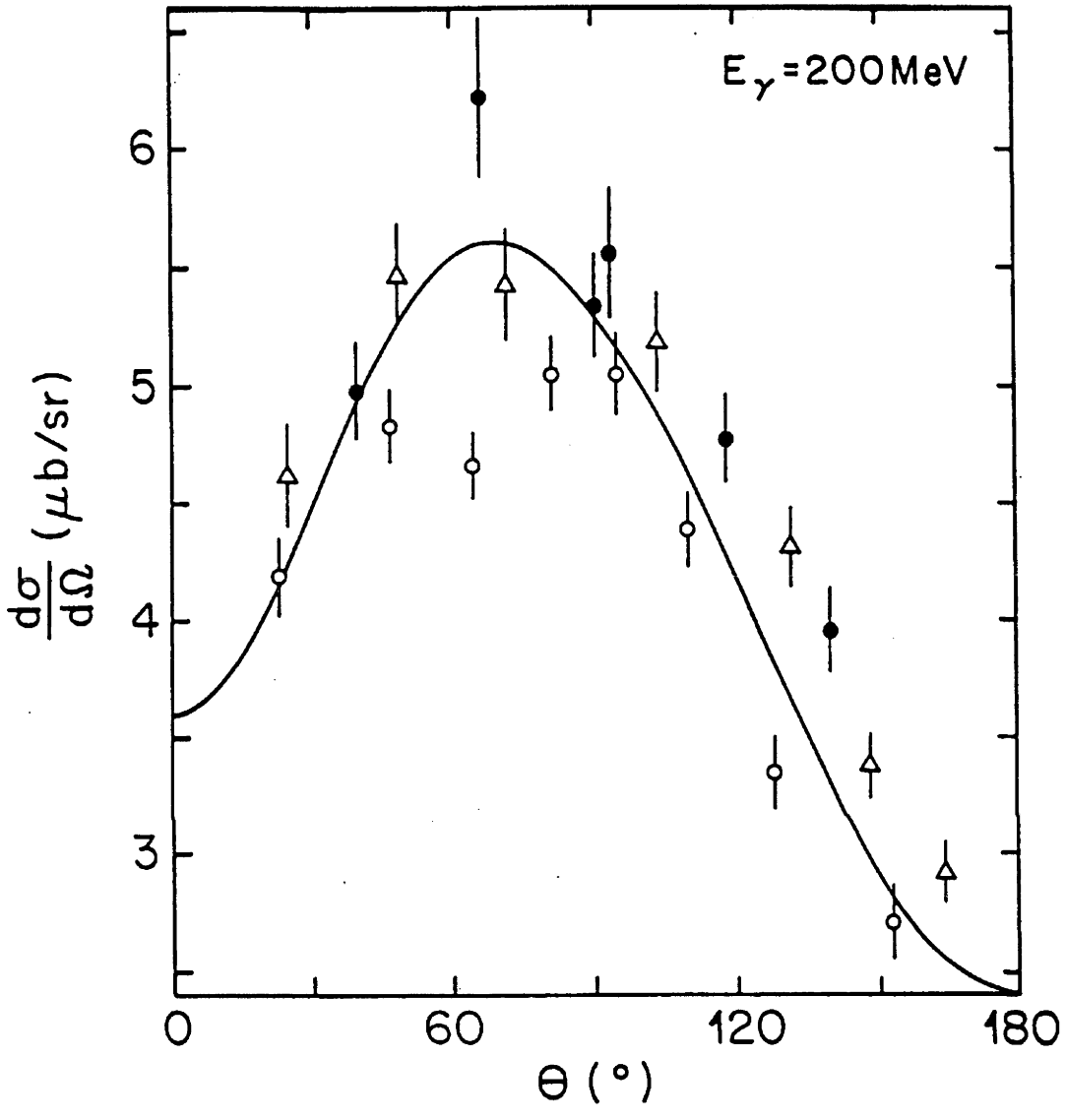

Figure 13: Unpolarised differential cross-section in the centre of mass frame for a laboratory photon energy of 200 MeV. Experimental results are from Frascati [61, 66] (solid circles), Bonn [65] (open circles) and MIT [67] (open triangles).

Laboratory Photon Energy (MeV)	Angle (°)	Reference	Experimental $A_y^{(n)}(\theta)$	Theoretical $A_y^{(n)}(\theta)$
5.23	86.8	[91]	0.068 (27)	0.121
5.85	87.1	[92]	0.105 (22)	0.112
7.0	87.0	[92]	0.096 (7)	0.103
7.6	86.9	[92]	0.104 (10)	0.101
8.7	86.8	[92]	0.061 (10)	0.099
8.94	85.2	[91]	0.095 (27)	0.099
11.1	86.5	[92]	0.051 (19)	0.097
13.15	86.3	[92]	0.072 (34)	0.096

Table 5: Experimental and theoretical results for the neutron polarisation $A_y^{(n)}(\theta)$ in low energy deuteron photodisintegration.

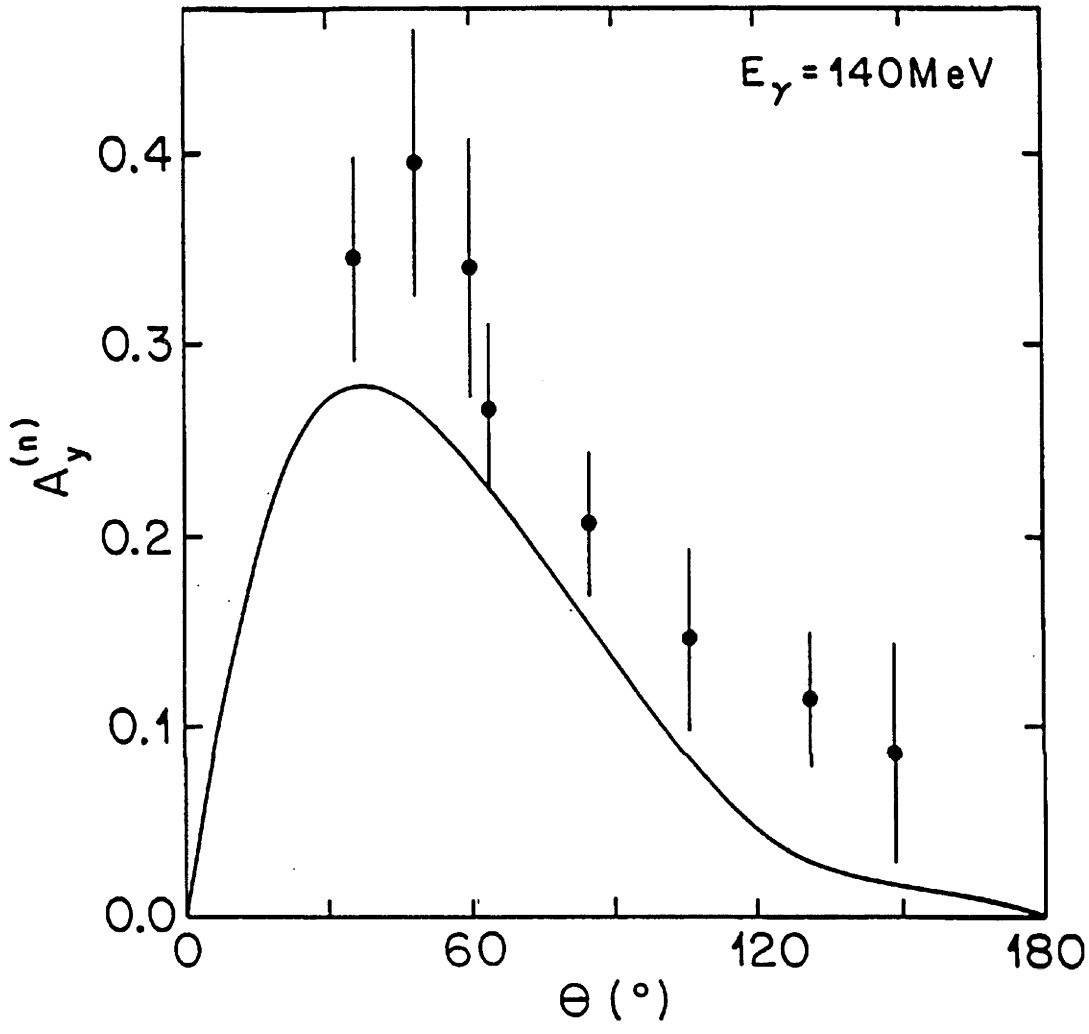

Figure 14: Neutron analysing power $A_y^{(n)}$ at an equivalent laboratory photon energy of 140 MeV. Experimental results are from TRIUMF [63].

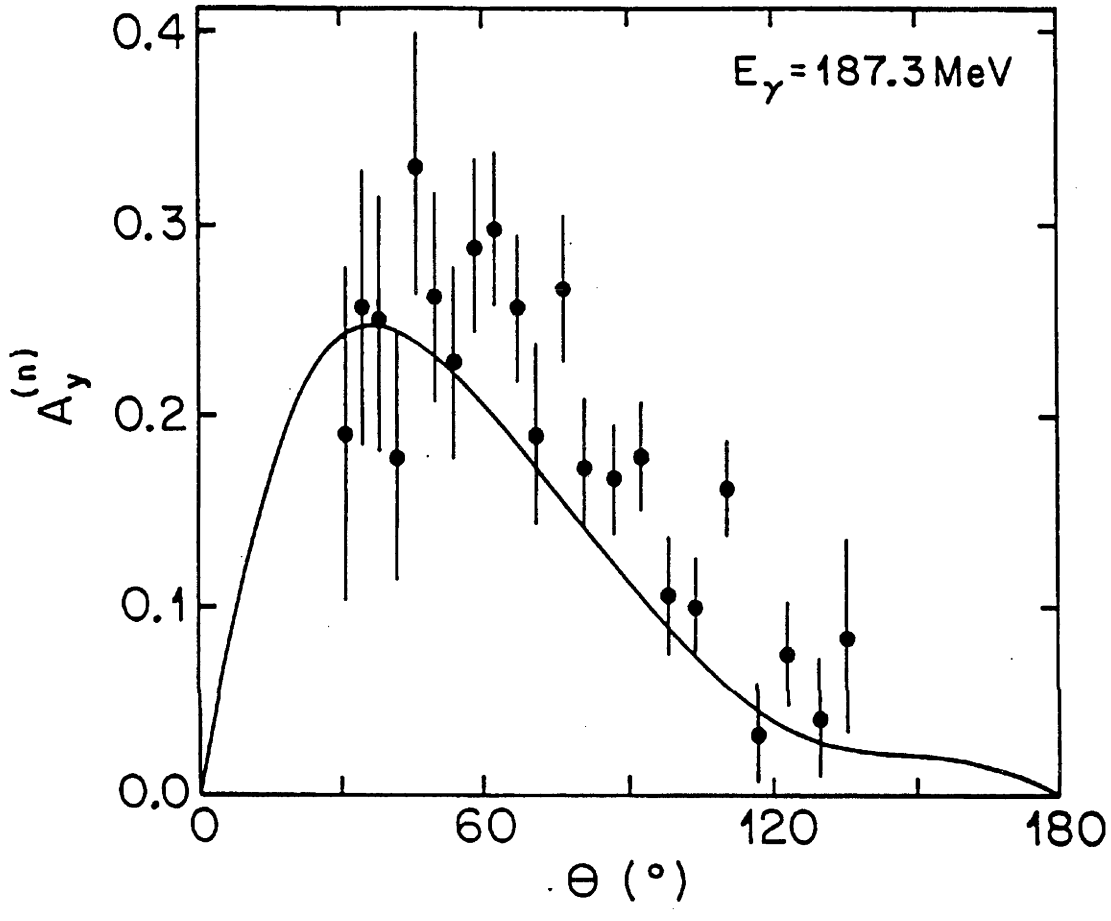

Figure 15: Neutron analysing power $A_y^{(n)}$ at an equivalent laboratory photon energy of 187.3 MeV. Experimental results are from TRIUMF [64].

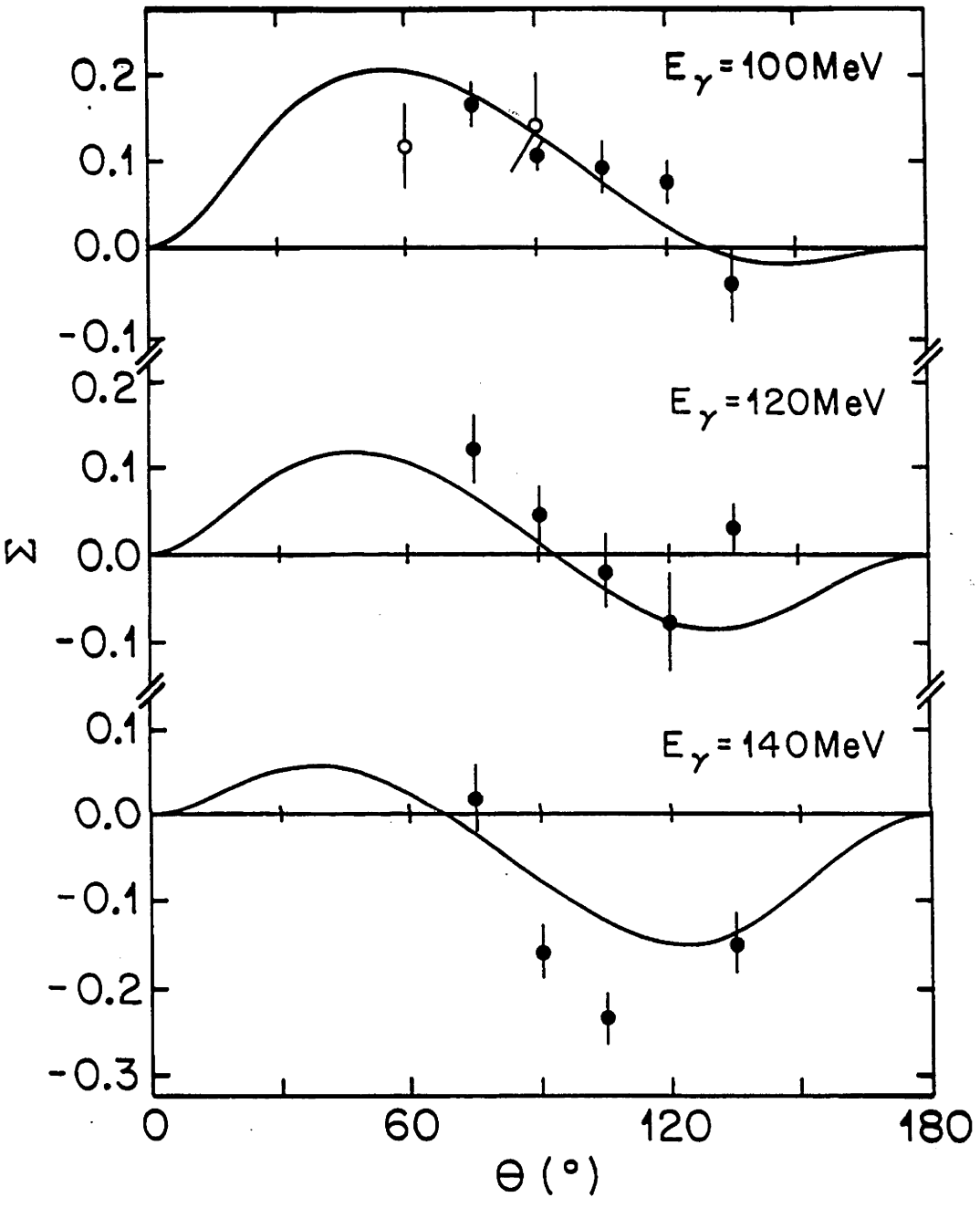

Figure 16: γ-asymmetry $\Sigma(\theta)$ at laboratory photon energies of 100, 120 and 140 MeV. Experimental results are from Tomsk [68] (open circles) and Khar'kov [69] (closed circles).

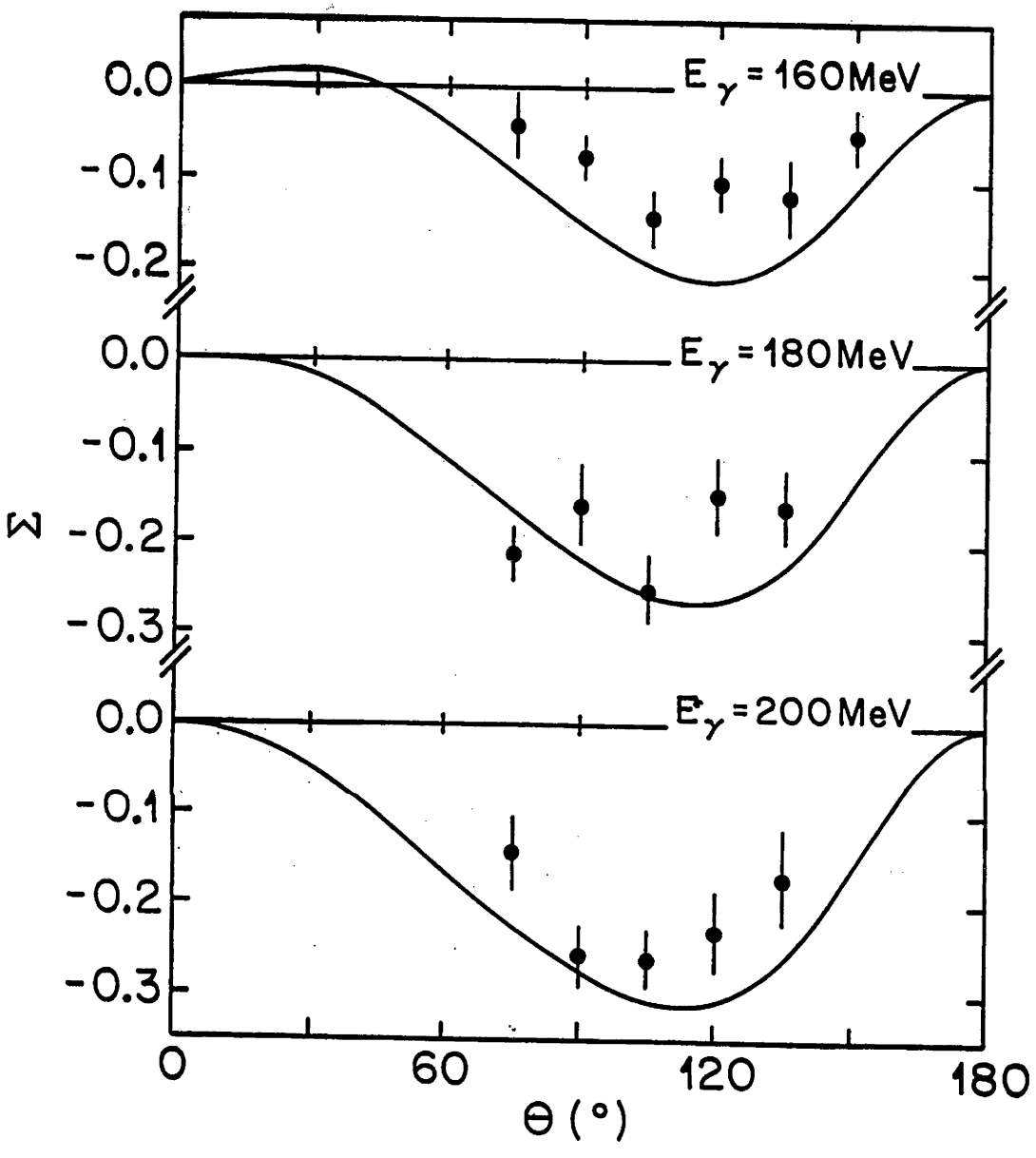

Figure 17: γ-asymmetry $\Sigma(\theta)$ at laboratory photon energies of 160, 180 and 200 MeV. Experimental results are from Khar'kov [69].

References

[1] H. T. Williams, *Phys. Rev.* **C31**, 2297 (1985).

[2] R. Machleidt, *Adv. Nucl. Phys.* **19**, 189 (1989).

[3] M. Lacombe, B. Loiseau, J. M. Richard, R. Vinh Mau, J. Côté, P. Pirés and R. de Tourreil, *Phys. Rev.* **C21**, 861 (1980).

[4] V. I. Kukulin, private communication. The parameters for the Moscow potential were provided by Professor Kukulin.

[5] D. Bofinger and W. S. Woolcock, *Il Nuovo Cimento* **104**, 1489 (1991).

[6] M. G. Olsson and E. T. Osypowski, *Phys. Rev.* **B101**, 136 (1975).

[7] W. Jaus and W. S. Woolcock, *Nucl. Phys.* **A473**, 667 (1987).

[8] H. M. Pilkuhn, *Relativistic Particle Physics*, Springer-Verlag 1979.

[9] B. H. Bransden and R. G. Moorhouse, *The Pion-Nucleon System*, Princeton University Press 1973.

[10] J. Hamilton and W. S. Woolcock, *Rev. Mod. Phys.* **35**, 737 (1963).

[11] Numerical Algorithms Group, FORTRAN Library Subroutine E04FCF; P. E. Gill and W. Murray, *SIAM Journal on Numerical Analysis* **15**, 977 (1978).

[12] B. Moussallam and V. Soni, *Phys. Rev.* **D39**, 1883 (1989).

[13] P. van Nieuwenhuizen, *Phys. Rep.* **68**, 189 (1980).

[14] M. W. Guidry, *Gauge Field Theories: An Introduction With Applications*, Wiley (1991).

[15] C. Fronsdal, *Supplemento del Nuovo Cimento* **2**, 416 (1957).

[16] A. Aurilia and H. Umezawa, *Phys. Rev.* **182**, 1682 (1969).

[17] R. E. Behrends and C. Fronsdal, *Phys. Rev.* **106**, 345 (1957).

[18] M. Benmerrouche, R. M. Davidson and N. C. Mukhopadhyay, *Phys. Rev.* **C39**, 2339 (1989).

[19] W. Jaus and W. S. Woolcock, *Nucl. Phys.* **A365**, 477 (1981).

[20] E. D. Cooper, A. O. Gattone and M. H. MacFarlane, *Phys. Lett.* **130B**, 359 (1983).

[21] O. Dumbrajs, R. Koch, H. Pilkuhn, G. C. Oades, H. Behrens, J. J. de Swart and P. Kroll, *Nucl. Phys.* **B216**, 277 (1983).

[22] T. E. O. Ericson and W. Weise, *Pions and Nuclei*, Clarendon Press, Oxford.

[23] Particle Data Table, *Phys. Lett.* **204B**, 1 (1988).

[24] R. D. Peccei, *Phys. Rev.* **176**, 1812 (1968).

[25] F. E. Close, *An Introduction to Quarks and Partons*, (Academic Press, New York, 1979).

[26] J. Bernstein, *Elementary Particles and Their Currents*, (Freeman, San Francisco, 1968).

[27] J. Gasser, H. Leutwyler, M. P. Locher and M. E. Sainio, *Phys. Lett.* **B213**, 85 (1988).

[28] M. G. Olsson, *Nucl. Phys.* **B78**, 55 (1974).

[29] P. Noelle, *Prog. Theor. Phys.* **60**, 778 (1978).

[30] B. C. Pearce and B. K. Jennings, Nucl. Phys. A528, 655(1991).

[31] G. Höhler, H. P. Jakob and R. Strauss, *Nucl. Phys.* **B39**, 232 (1972).

[32] R. A. Arndt, J. M. Ford and L. D. Roper, *Phys. Rev.* **D32**, 1085 (1985); J. C. Alder, C. Joseph, J. P. Perroud, M. Tran, G. H. Eaton, R. Frosch, H. Hirschmann, S. Mango, J. W. McCulloch, P. Shrager, G. Strassner, P. Truöl, P. Weymuth and P. Weiderkehr, *Phys. Rev.* **D27**, 1040 (1983); M. Salomon, D. F. Measday, J-M. Poutissou and B. C. Robertson, *Nucl. Phys.*, **A414**, 493 (1984); A. Bagheri, K. A. Aniol, F. Entezami, M. D. Hasinoff, D. F. Measday, J-M. Poutissou, M. Salomon and B. C. Robertson, *Phys. Rev.* **C38**, 885 (1988).

[33] R. Koch and E. Pietarinen, *Nucl. Phys.* **A336**, 331 (1980).

[34] W. Jaus, D. Bofinger and W. S. Woolcock, *Nucl. Phys.* **A562**, 477 (1993).

[35] W. Jaus, D. Bofinger and W. S. Woolcock, *Nucl. Phys.* **A562**, 500 (1993).

[36] H. Arenhövel and M. Sanzone, "Photodisintegration of the Deuteron", *Few Body Syst. Suppl.* **3**, 1991.

[37] F. Partovi, *Ann. Phys.* **27**, 79 (1964).

[38] T. Hamada and I. D. Johnson, *Nucl. Phys.* **34**, 382 (1962).

[39] H. Arenhövel and W. Fabian, *Nucl. Phys.* **A282**, 397 (1977).

[40] W. Jaus and W. S. Woolcock, *Helv. Phys. Acta* **57**, 644 (1984).

[41] A. Cambi, B. Mosconi and P. Ricci *Phys. Rev. Lett.* **48**, 462 (1982).

[42] W. Jaus and W. S. Woolcock, *Nucl. Phys.* **A431**, 669 (1984).

[43] W. Jaus and W. S. Woolcock, *Nucl. Phys.* **A473**, 685 (1987).

[44] H. Arenhövel, Preprint MKPH-T-88-3, Institute for Nuclear Physics, University of Mainz

[45] W. Jaus and W. S. Woolcock, *Il Nuovo Cimento* **103A**, 587 (1990).

[46] R. Blankenbecler and R. Sugar, *Phys. Rev.* **142**, 1051 (1966).

[47] R. M. Woloshyn and A. D. Jackson, *Nucl. Phys.* **B64**, 269 (1973).

[48] J. Haidenbauer, K. Holinde and A. W. Thomas, *Phys. Rev.* **C45**, 952 (1992).

[49] R. M. Davidson, N. C. Mukhopadhyay and R. S. Wittman, *Phys. Rev.* **D43**, 71 (1991).

[50] M. Dillig and M. Brack, *J. Phys.* **G5**, 223 (1979).

[51] J. F. Mathiot, Chr. Bargholtz and G. E. Brown, *Nucl. Phys.* **A397**, 365 (1983).

[52] P. A. Wallace, J. R. M. Annand, I. Anthony, G. I. Crawford, S. N. Dancer, S. M. Doran, S. J. Hall, J. D, Kellie, J. C. McGeorge, I. J. D. MacGregor, G. J. Miller, R. O. Owens, J. Vogt, B. Scoch and D. Branford, *Nucl. Phys.* **A532**, 617 (1991).

[53] M. G. Olsson and E. T. Osypowski, *Phys. Rev.* **D17**, 174 (1978).

[54] M. Chemtob and M. Rho, *Nucl. Phys.* **A163**, 1 (1971)

[55] T. D. Lee and C. N. Yang, *Phys. Rev.* **128**, 885 (1962).

[56] D. O. Riska, *Nucl. Phys.* **A402**, 377 (1983).

[57] M. Gari and W. Krümpelmann, supplement to the proceedings of the Third International Symposium on Mesons and Light Nuclei, May 27 – June 1, 1985, p. 78 (Prague, February 1986).

[58] W. Jaus, private communication (1994).

[59] W. Jaus, private communication.

[60] A. Zeiger, A. De Graeve, D. Christmann, R. van de Vyver and B. Ziegler, *Phys. Lett.* **B285**, 1 (1992).

[61] P. Levi Sandri, M. Arghinolfi, N. Bianchi, G. P. Capitani, P. Corvisiero, E. De Sanctis, C. Guaraldo, V. Lucherini, V. Muccifora, E. Polli, A. R. Reolon, G. Ricco, P. Rossi, M. Sanzone and M. Tauiti, *Phys. Rev.* **C39**, 1701 (1989).

[62] H. O. Meyer, J. R. Hall, H. Hugi, H. J. Karwowski, R. E. Pollock and P. Schwandt, *Phys. Rev.* **C31**, 309 (1985).

[63] J. M. Cameron, C. A. Davis, H. Fielding, P. Kitching, J. Pasos, J. Soukup, J. Uegaki, J. Wesick, H. S. Wilson, R. Abegg, D. A. Hutcheon, C. A. Miller, A. W. Steitz and I. J. van Heerden, *Nucl. Phys.* **A458**, 637 (1986).

[64] M. Hugi, J. M. Cameron, M. Ahmed, J. Collot, G. Gaillard, J. S. Wesick, G. W. R. Edwards, H. Fielding, D. A. Hutcheon, R. Abegg, C. A. Miller, P. Kitching, N. E. Davison, N. R. Stevenson and I. J. van Heerden, *Nucl. Phys.* **A472**, 71 (1987).

[65] J. Arends, H. J. Gassen, A. Hegerath, B. Mecking, G. Nöldecke, P. Prenzel, T. Reichelt and A. Voswinkel, *Nucl. Phys* **A412**, 509 (1984).

[66] E. De Sanctis, M. Anghinolfi, G. P. Capitani, P. Corvisiero, P. Di Giacomo, C. Guaraldo, V. Lucherini, E. Polli, A. R. Reolon, G. Ricco, M. Sanzone and A. Zucchiatti, *Phys. Rev.* **C34**, 413 (1986).

[67] T. Soos *et al*, to be published; J. L. Matthews, private communication.

[68] I. E. Vnukov, I. V. Glavanakov, Yu. F. Krechetov, A. P. Potylitsyn, G. A. Suarev, V. N. Stibunov and P. V. Sorokin, *Sov. J. Nucl. Phys.* **47**, 581 (1988).

[69] V. G. Gorbenko, Yu, V. Zhebrovsk˘ıı, L. Ya. Koleshnikov, A. L. Rubasckin and P. V. Sorokin, *Sov. J. Nucl. Phys.* **35**, 627 (1982).

[70] G. Höhler and E. Pietarinen, *Nucl. Phys.* **B95**, 210 (1975); E. Pietarinen, Helsinki University HU-TFT-17-77 (1977)

[71] A. De Graeve *et al*, *Few-Body Systems* **10**, 37 (1991).

[72] A. De Graeve, A. Zieger, R. van de Vyver, H. Ferdinande, L. van Hoorebecke, D. Ryckbosch, P. van Otten, B. Ziegler, *Phys. Lett.* **B227**, 321 (1989).

[73] A. Zieger, P. Grewer and B. Ziegler, *Few-Body Systems* **1**, 135 (1986).

[74] R. J. Hughes, A. Zieger, H. Wäffler and B. Ziegler, *Nucl. Phys.* **A267**, 329 (1976).

[75] A. Ninane, C. Dupont, P. Leleux, P. Lipnik and P. Macq, *Phys. Rev.* **C35**, 402 (1987).

[76] C. Dupont, P. Leleux, P. Lipnik, P. Macq and A. Ninane, *Nucl. Phys.* **A445**, 13 (1985).

[77] A. De Graeve, Ph.D. Thesis, University of Gent (1988).

[78] K. H. Althoff, G. Anton, D. Bour, B. Bock, W. Ferber, H. W. Gelhausen, N. Horikawa, Th. Jahnen, O. Kaul, W. König, K. C. Königsmann, D. Menze, W. Meyer, Th. Miczaika, E. Roderburg, W. Ruhm, E. P. Schilling, W. Schwille, D. Sundermann and K. Wagener, *Z. Phys.* **C21**, 149 (1983).

[79] R. Moreh, T. J. Kennett and W. V. Prestwich, *Phys. Rev.* **C39**, 1247 (1989).

[80] Y. Birenbaum, S. Kahane and R. Moreh, *Phys. Rev.* **C32**, 1825 (1985).

[81] R. Bernabei, A. Incicchitti, M. Mattioli, P. Picoza, D. Prosperi, L. Casano, S. d'Angelo, M. P. De Pascale, C. Schaerf, G. Giordano, G. Matone, S. Frullani and B. Girolami, *Phys. Rev. Lett.* **57**, 1542 (1986).

[82] T. Stiehler, B. Kühn, K. Möller, J. Mösner, W. Neubert, W. Pilz and G. Schmidt, *Phys. Lett.* **B151**, 185 (1985).

[83] J. Ahrens, H. B. Eppler, H. Gimm, M. Kröning, P. Riehn, H. Wäffler, A. Zieger and B. Ziegler, *Phys. Lett.* **52B**, 49 (1974).

[84] P. Michel, K. Möller, J. Mösner and G. Schmidt, *J. Phys.* **G15**, 1025 (1989).

[85] M. Bosman, A. Bol, J. F. Gilot, P. Leleux, P. Lipnik and P. Macq, *Phys. Lett.* **B82**, 212 (1979).

[86] P. Wauters, P. Dupont, P. Leleux, P. Lipnik, P. Macq, A. Ninane and Sindano Wa Kitwanga, *Few-Body Systems* **8**, 1 (1990).

[87] P. T. Debevec, P. D. Harty, J. E. Knott, D. A. Jenkins and R. T. Jones, *Phys. Rev.* **C45**, 904 (1992).

[88] K. E. Stephenson, R. J. Holt, R. D. McKeown and J. R, Specht, *Phys. Rev.* **C35**, 2023 (1987).

[89] K.-M. Schmitt, P. Wilhelm and H. Arenhövel, *Few-Body Systems* **10**, 105 (1991).

[90] E. Hadjimichael, E. Rutstgi and L. N. Pandey, *Phys. Rev.* **C36**, 44 (1987).

[91] J. P. Soderstrum and L. D. Knutson, *Phys. Rev.* **C35**, 1246 (1987).

[92] R. J. Holt, K. E. Stephenson and J. R. Specht, *Phys. Rev. Lett.* **50**, 577 (1983).

[93] P. Wilhelm, W. Leidemann and H. Arenhövel, *Few-Body Systems* **3**, 111 (1988).